Regulation of synaptic adhesion molecules by RNA processing

Inauguraldissertation
zur
Erlangung der Würde eines Doktors der Philosophie
vorgelegt der
Philosophisch-Naturwissenschaftlichen Fakultät
der Universität Basel

von

David Hauser

2021

Genehmigt von der Philosophisch-Naturwissenschaftlichen Fakultät

auf Antrag von:

Prof. Dr. Peter Scheiffele

Prof. Dr. Markus Rüegg

Prof. Dr. Gerhard Schratt

Basel, 22. Juni 2021

Prof. Dr. Marcel Mayor

The Dean of Faculty

Table of Contents

Summary

The highly specialized neuronal cells and their complex connectivity pattern is the hallmark of central nervous system organization. Synapse formation and specification are crucial steps in generating this complex wiring and proper establishment of functional synapses is essential for correct brain function. Cell adhesion molecules are key mediators in synapse specificity and moreover in generating functional synapses. Their diversification by alternative mRNA splicing, which can amplify the gene pool, is proposed to underlie molecular codes for synapse formation (Gomez et al., 2021). Additionally, alternative splicing is thought to be a stronger driver for synapse diversification than differential gene expression, as determined by transcriptomic approaches (Furlanis et al., 2019). However, due to mechanisms influencing translation of transcripts on multiple levels, it is hard to predict the proteome only based on transcriptome studies. Moreover, the expression, localization and function of individual protein isoforms, or “proteoforms”, generated by alternative splicing remains enigmatic.

In this thesis, I combine multiple approaches to highlight the importance of probing individual proteoforms to study the generation of a molecular code underlying synapse specification. By combining targeted proteomics with the analysis of specific knock-in and knock-out mice, I could characterize a non-canonical proteoform of the synaptic adhesion molecule family of Neurexins. Alternative splicing and inclusion of an alternative exon at the splice segment 5 (AS5) of Neurexin 3 (*Nrxn3*) leads to specific expression of this proteoform in GABAergic interneurons and at pre-synaptic GABAergic terminals. Strikingly, this stands in contrast to the abundance of *Nrxn3-AS5+* transcripts and could be determined to depend on translational repression elements in the 3’ untranslated region of *Nrxn3.* Aberrant splicing at AS5 and altered incorporation of repression elements leads to a drastic drop in NRXN3 protein levels while mRNA levels of *Nrxn3* are unaltered.

Moreover, NRXN3 AS5+ protein isoforms change their membrane association from a transmembrane to a GPI-anchored form. Deletion of this novel GPI-anchored NRXN3 protein isoform leads to an impairment of synaptic transmission in a subset of CCK positive GABAergic synapses in the dentate gyrus.

Thus, my thesis supports the use of more refined proteomic approaches to study the pleiotropy of synaptic molecules shaping synapse diversity. Finally, and to promote and collect already validated and successfully used targeted mass-spectronomy assays, we develop a database (https://scheiffele-SYNCODE.scicore.unibas.ch/) to strengthen the efforts of studying synaptic function on the proteome level.

1. Introduction

1.1 General Introduction

The brain is one of the most complex organs in the body. Studies done by pioneers of the field started to characterize the brain and its individual cell types over 100 years ago. Research studying the brain accelerated over the past decades, but still a lot of mysteries remain elusive. We know that the correct function of this highly organized organ relies on the proper wiring and connectivity of all the specialized cells within. This precise network and circuitry organization originates during development in a well-orchestrated manner including the specification and migration of individual neurons to and within their brain region. It further relies on the formation and later elimination or remodeling of individual synapses.

While these mechanisms to some extents are based on spontaneous network activity and on inputs from sensory stimuli, underlying neuronal morphological development is segregated from neurotransmission. Loss of neurotransmitter secretion during development thereby does not prevent proper assembly of the brain and individual synapses for both excitatory and inhibitory synapses (Chen et al., 2013; Verhage et al., 2000). Presynaptic terminals, dendrites and functional spines are further properly assembled and also maintained in the absence of synaptic transmission (Lu et al., 2013; Sando et al., 2017; Sigler et al., 2017). All these studies underscore the importance of intrinsic factors which instruct the development and function of synapses. Activity-dependent spine formation, remodeling and elimination (Hofer et al., 2009; Kwon and Sabatini, 2011; Trachtenberg et al., 2002), is further thought to be instructed by these genetically encoded programs. These programs are thought to be directed by terminal selector transcription factors. Thereby defined groups of genes, or gene batteries, orchestrate important aspects of development and maintenance of synapses. They not only define different neuronal cell types, but also the timing of neuronal contact establishment and the plastic nature of the nervous system (Hobert, 2016; Sanes and Zipursky, 2020).

Synaptic molecules including cell adhesion molecules, receptors, ion-channels, signaling molecules and proteins part of the synaptic release machinery play an important role in these gene batteries. They define neuronal cell types and are more importantly considerable contributors to synaptic development and maintenance (Sudhof, 2017, 2018). Hence, transcriptomic studies suggested that the combinatorial use of these gene categories is the determining factor for the assembly of the synaptic architecture. These tailored pre- and post-synaptic molecular scaffolds are the basis for correct brain function (Paul et al., 2017).

The accelerating progress in transcriptomic studies further helped in understanding not only cell-type specific molecular repertoires or gene batteries, but also synapse specific molecule pools (Sanes and Zipursky, 2020; Shigeoka et al., 2016). Intrinsically specified gene expression patterns not only determine to which neuron a selected cell has to connect, but its molecular program also defines where on the target cell (Favuzzi et al., 2019). The precise targeting on the soma, axon initial segment or the position on the dendritic tree of the target cell further adds to the complex genetically encoded blueprint. The proper expression of synaptic molecules is therefore crucial, as studies investigating mutations in genes that are responsible for diseases like Alzheimer's or Autism have found a wide variety of synaptic risk genes (Autism Genome Project et al., 2007; Geschwind and State, 2015). Mutations in synaptic genes can thus be linked to these neurological diseases and highlight the importance of understanding the precise patterning and connectivity of neuronal circuits in relation to the expression of synaptic molecules. Transcriptomic studies further highlighted the impact of amplifying the limited gene pool by mechanisms as alternative mRNA splicing. Alternative splicing, a process in which multiple mRNA isoforms can be produced from a single gene, is thereby even a stronger driver of synaptic specificity when compared to the overall gene expression levels (Furlanis et al., 2019). Altering single exons in different studies showed that alternative splicing is contributing to the diversity of synaptic molecules and their function (Gomez et al., 2021). Even though a lot of effort was put into these characterizations, there is a substantial gap of studies linking the transcriptome to the proteome. To investigate synapse specificity, the analysis of the translated pool of synaptic proteins would be essential, as studies showed that only 40% of steady-state protein level variance can be explained by mRNA levels (Liu et al., 2016; Vogel and Marcotte, 2012). The underlying mechanisms, which include in addition to translation the regulation of mRNA stability, transport and degradation, are widely used in the nervous system (Holt and Schuman, 2013). Even though this is a well-known and characterized phenomena, the synaptic proteome and the contribution of individual protein isoforms or proteoforms to synaptic function remains a big question.

In my work I will show one example on how individual proteoforms can be specifically expressed at a subset of synapses, adding one puzzle piece to better understand synaptic diversity. For this I will introduce the principle of individual cell classes and the logic of their specific connectivity by a trans-synaptic adhesion code. I will further discuss the role of co- and post-transcriptional mechanisms in generating this trans-synaptic code. In a last step I will introduce the model protein which I characterized in this work, the pre-synaptic adhesion molecule family of Neurexin and will discuss the topic of generating synaptic specification through Neurexins.

1.2 Neuronal and synaptic diversity

The highly organized and meticulously controlled nervous system relies on a plethora of specialized cells. These cells need to establish proper connections to eventually form functional neuronal networks. Connectivity originates during development and is based on the specification of individual cells and their proper migration in combination with the growth of their processes. In a final step, neurons form functional synapses. Molecular intrinsic factors are the basis of all these steps. They are responsible for segregating neuronal cell types and in shaping individual synapses by encoding molecular scaffolds. These molecular repertoires are pivotal for the specification of neuronal synapses (Gomez et al., 2021; Hassan and Hiesinger, 2015; Sanes and Zipursky, 2020; Sudhof, 2017).

I will introduce this specification of neuronal cell types, their connectivity and the mechanisms behind these molecular repertoires in the context of the hippocampus, a brain region responsible for memory formation and learning. The spatial organization of its neurons, well-characterized synapses and the clear flow of information makes it a prime candidate to study neuronal connectivity and changes thereof. Informational flow or neuronal signals into the hippocampus arrive in the dentate gyrus with input from entorhinal cortex through the perforant path. Via the trisynaptic pathway information arrives at CA1 pyramidal cells (cornu ammonis) as the major output neurons of the hippocampus. The trisynaptic pathway consists of excitatory input onto granule cells in the dentate gyrus and further glutamatergic connections to CA3 (mossy fiber pathway) and then to CA1 (Schaffer collateral pathway)(Andersen, 2007)(Figure 1).

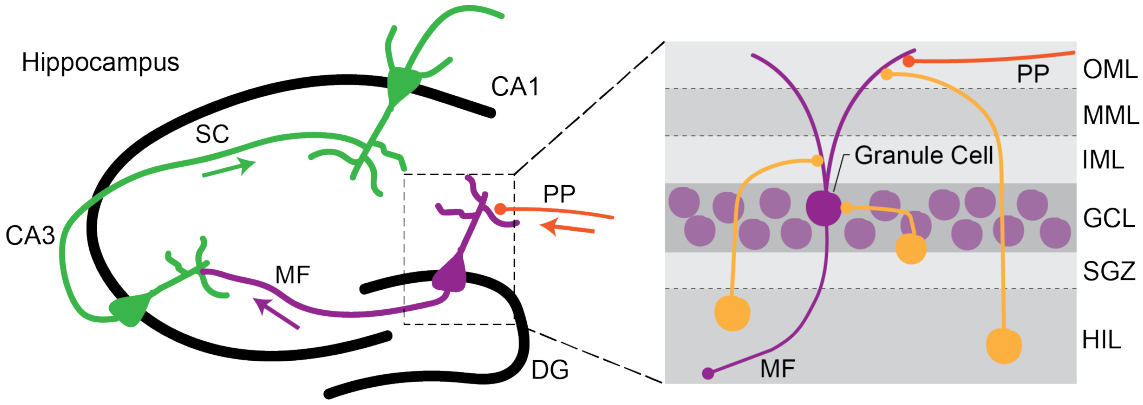

Figure 1. Schematic view of the hippocampus
Drawing of the schematic view of the hippocampus including flow of information and local inhibitory networks. Flow of information (arrows) via perforant path (PP) to dentate gyrus (DG), mossy fiber pathway (MF) to CA3 and Schaffer collaterals (SF) to CA1. Dashed box: Blow up of dentate gyrus showing targeting of different interneurons (in yellow) residing in different sublayers of the dentate gyrus (OML/MML/IML: Outer-/Middle-/Inner-molecular layer, GCL: granule cell layer, SGZ: Sub-granular zone, HIL: Hilus). (Adapted from (Andersen, 2007; Scharfman, 2016))

At each step of the pathway information flow is tightly regulated by local interneurons, which mediate signal propagation through this brain region. For example, inhibitory cells in the CA1 region of the hippocampus are responsible to tune the input and output of CA1 pyramidal cells in a precise spatial and temporal patterned way (Klausberger and Somogyi, 2008). This basic circuitry, and the shape and size of its diverse synapses, is hardwired and not dependent on neuronal transmission (Sando et al., 2017; Sigler et al., 2017). Individual neuronal cell classes therefore need to be able to form these connections through intrinsic programs, which will be discussed in the following chapter.

1.2.1 Neuronal cell types

Proper network function as in the tripartite circuit of the hippocampus is relying on well balanced synaptic excitation and inhibition. In general, and based on their neurotransmitters, neurons can be classed in excitatory or glutamatergic and inhibitory or GABAergic neurons, using glutamate or GABA as a neurotransmitter, respectively. Flow of information as information coming from granule cells to CA3 pyramidal cells is generally based on glutamatergic transmission, the fine-tuned inhibition and regulation of these signals by GABAergic signals. Since the initial studies of Ramón y Cajal and his pioneer work in characterizing neuronal cell classes based on their morphology, additional characterization criteria include the expression of genes, intrinsic properties and where on a target cell synapses are formed (Kepecs and Fishell, 2014; Zeng and Sanes, 2017).

Fine tuning inhibitory cells thereby contribute to only 15% of neuronal cells, while glutamatergic cells represent more than 80% of neurons (Meyer et al., 2011). Interneurons show a wide variety of connectivity and subcellular targeting domains, therefore requiring a precise establishment of synaptic connectivity. After their initial classification based on those targeting domains, their morphology, specific molecules and firing properties into Somatostatin (SST), Parvalbumin (PV), Cholecystokinin (CCK), Vasoactive intestinal peptide (VIP) or calretinin (CR) positive interneurons, recent studies proposed up to 23 different GABAergic cell classes (Kepecs and Fishell, 2014; Tasic et al., 2016). Those results come from single-cell sequencing studies looking at individual transcriptomes of hundreds of cells. They further demonstrated a clear connection between previously defined cell classes and their transcriptome data, thereby laying the ground for molecular defined characterization of neuronal cells classes (Tasic et al., 2016; Tasic et al., 2018).

Looking at the development of interneurons added additional evidence for the intrinsically determined fate of neuronal cells. In brief, neocortical interneurons originate from two progenitor zones termed caudal and medial ganglionic eminences (CGE and MGE)(Kepecs and Fishell, 2014). Neurons entering their migration pathway to their final localization are thereby thought to already express genetic markers which define them molecularly (Brown et al., 2011; Mayer et al., 2018; Mi et al., 2018).

One class of molecular markers, genes encoding for proteins expressed at the synapse, is thereby the biggest driver of segregating neuronal cell classes (Paul et al., 2017). This means that next to shape, localization and target cells, synaptic molecules are important contributors in generating neuronal identity and furthermore in establishing specific synaptic connections.

1.2.2 Specification of synaptic connectivity

After individual neurons reach their destination due to migration, an elaborate network of neuronal connections is formed. The second step of synapse specification, next to initial axon guidance and in the end synaptogenesis or the forming of functional synapses, is thought to be the most complex (Sanes and Zipursky, 2020). This is nicely illustrated in a study that characterized and reconstructed a part of the mouse barrel cortex with the help of three-dimensional electron microscopy (Motta et al., 2019). They not only reconstructed the cell bodies and their dendritic trees (Left Panel, Figure 2), but also all axons innervating this dense structure (Right Panel, Figure 2).

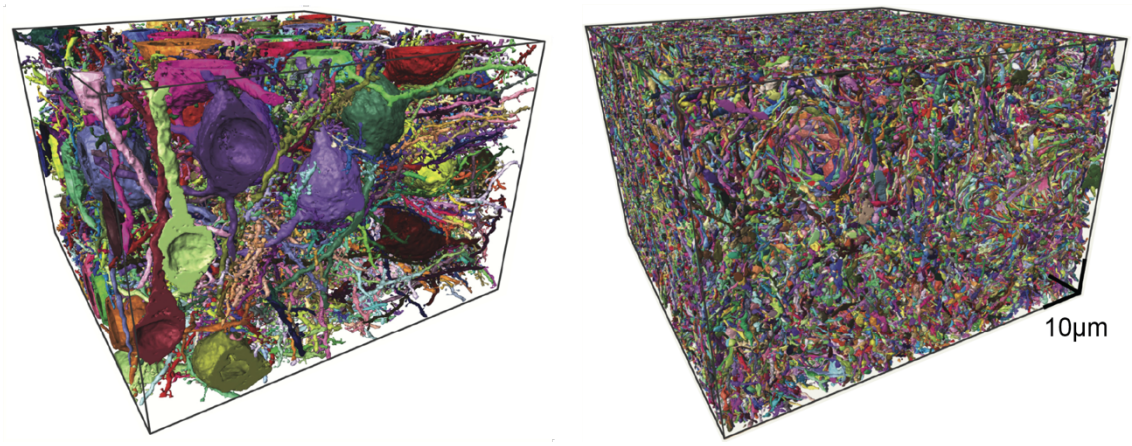

Figure 2. EM reconstruction of individual neurons
Left: Visualization of individual cell bodies and their dendrites, each color represents one neuron.
Right: Axonal innervations in the same region, same scale (adapted from (Motta et al., 2019))

Synaptic molecules and therein especially cell adhesion molecules (CAMs) and signaling molecules are key determinants in governing synapse specification. They are crucial for initiating contact of pre- and post-synapse in close proximity and guiding the correct choice of the synaptic partner cell (Sanes and Zipursky, 2020; Sudhof, 2018).

Technical advances led to the discovery and characterization of multiple families of proteins responsible for synaptic specificity. Those protein families thereby exhibit variable binding affinities to their evolutionary conserved molecular partners. As those binding properties are precisely controlled, they can instruct the targeted formation of specific cell interactions (Honig and Shapiro, 2020).

Next to their ability to act in binding *trans*-synaptically, they need to be expressed in defined cell populations and moreover to be expressed in a sufficient variety. It is thereby thought that the differential and combinatorial usage of these receptor families leads to molecular specification through molecular diversity (de Wit and Ghosh, 2016). This molecular code and its coding power are based on the availability of pre- and post-synaptic modules of biochemical interaction partners. Different modules can thereby be present at individual synapses and their members can overlap between modules (Gomez et al., 2021; Schroeder et al., 2018; Shen and Scheiffele, 2010).

Next to the process of synapse specification by a cue-driven molecular code, the presence or absence of specific adhesion molecules can facilitate unique synaptic properties in terms of release probabilities and receptor composition, together mediating plasticity (de Wit and Ghosh, 2016). One example thereof comes from mis-expression experiments of an alternative protein isoform of Neurexin, a pre-synaptic adhesion molecule, which can alter post-synaptic AMPA-receptor levels and therefore instruct regulation of glutamate receptors (Aoto et al., 2013). Neurexins are widely studied in being an essential part of the pre-synaptic molecular scaffold and are key mediators of the synaptic molecular code by binding to several extracellular and intracellular binding partners. They can fulfill this role by extensive alternative splicing and are expressed in a cell type specific way (Gomez et al., 2021; Sudhof, 2017). Neurexins are the model protein of my PhD Thesis and will therefore be introduced in detail after exploring the mechanisms behind the generation of molecular repertoires including the essential mechanism of alternative splicing.

1.2.3 Cell type specific molecular repertoires

Molecular repertoires within a cell are maintained by the mechanism of transmitting information from DNA via RNA to proteins. During transcription mRNAs undergo a series of modifications including the capping of pre-mRNA, alternative splicing of individual exonic regions, editing and the terminal step of polyadenylation. At each step the processed RNA interacts with a subset of binding partners like RNA-binding proteins (RBPs) among others, which are responsible in regulating and coupling individual processes (Ule and Darnell, 2006).

While there are many processes involved in the generation of mRNAs, splicing of pre-mRNA to mature transcripts by excising intronic sequences and combining exonic sequences is one critical step in their maturation process. The alternative usage of single exons therein is termed alternative splicing, which was predicted to occur in more than 95% of all genes (Pan et al., 2008; Wang et al., 2008) and which is now thought to occur in nearly all genes in human (Barbosa-Morais et al., 2012; Merkin et al., 2012). Alternative splicing is hereby thought to be an important driving force in evolution by expanding the proteome massively. This expansion of the proteome is evident if we compare the number of genes and the respective proteome, which is for invertebrates as the worm a relative increase of 2.5-fold, in mammals as the mouse 4.5-fold and in human 10-fold (Lee and Rio, 2015). Alternative splicing is thereby a bigger driver of phenotypic diversity than differential gene expression, as analysis of differentially expressed genes shows the clustering of genes by organs and not species, while analysis of alternative splice events leads to a segregation of species (Barbosa-Morais et al., 2012; Merkin et al., 2012). Alternative splice events are therefore more similar between individual organs of one species and will be introduced in the following paragraph as an important contributor not only for phenotypic diversity but also cell identity.

Splicing and therefore intron removal is mediated by a reoccurring assembly and disassembly of a highly dynamic and large complex consisting of five ribonucleoproteins, termed U1, U2, U4/6 and U5. Detailed genome-wide studies have shown how these subunits can bind different regions of a pre-mRNA, including the branch point and 5’ or 3’ splice sites. Additional elements include either positive or negative regulators of intronic or exonic sequences, which are termed exonic splice enhancers/silencers (ESE/ESS) or intronic enhancers/silencers (ISE/ISS)(Chen and Manley, 2009; Licatalosi and Darnell, 2010). Mutations in those cis-acting elements are often at the base of disease states and the importance of correct alternative splicing guided by these cis-acting elements is evident if we look at splicing defects. Pathways involved in alternative splicing are frequently hijacked by altered trans-acting factors in tumor cells (David and Manley, 2010)

and aberrant splicing is often associated with neurological disorders like autism spectrum disorder (Parikshak et al., 2016; Quesnel-Vallieres et al., 2016).

Correct splicing is a meticulous task, as splicing can be quite complex. Individual alternative splicing events can be grouped in different classes, ranging from single cassette exon in- or exclusions to complex splicing patterns involving multiple different acceptor and donor splice sites. Next to alternative cassette exons, mutually exclusive exons or alternative 3' and 5' splice sites, the usage of different promoters and alternative 3' exons can further augment the coding power of individual genes (Figure 3).

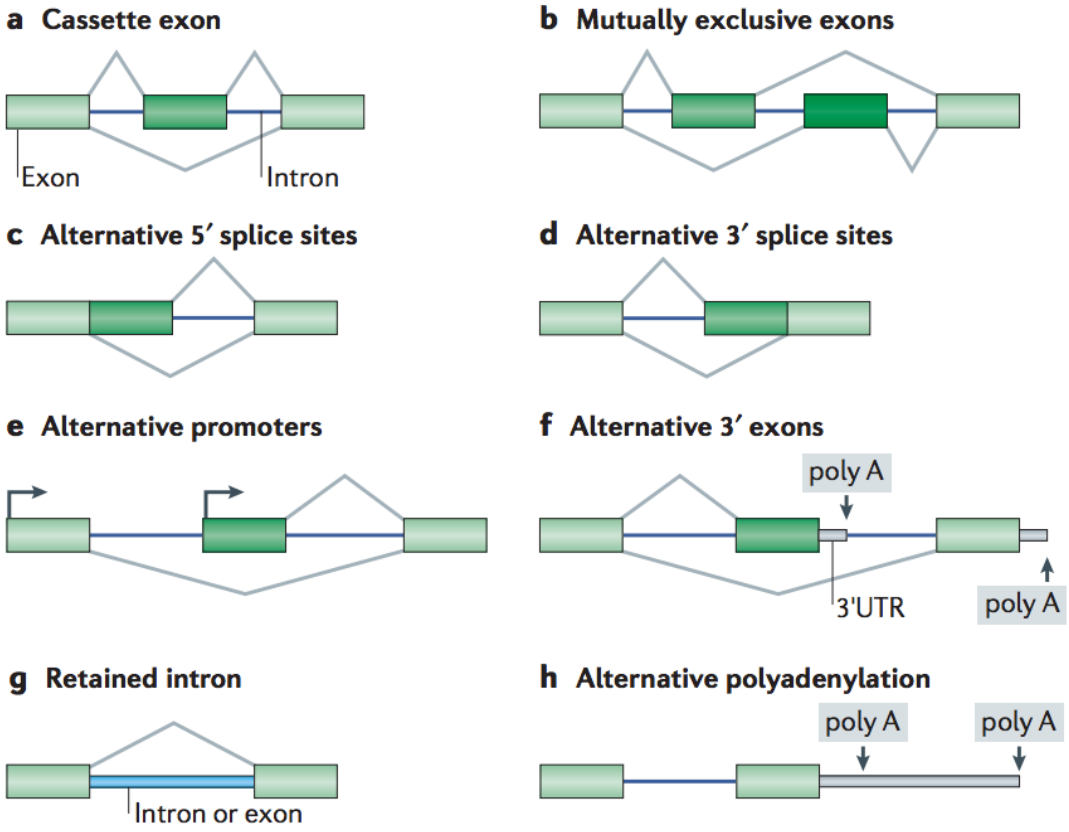

Figure 3. Alternative splicing patterns
Splicing can be classified into three groups: In- or exclusion of internal exons (**a**,**b**), alternative acceptor or donor sites (**c**,**d**) and alternative 5' or 3' exons (**e**,**f**). Retaining introns or using different polyadenylation sites can generate additional differential pre-mature/mature transcripts (**g**,**h**)(Vuong et al., 2016)

The combinatorial use of alternative exons and alternative acceptor- and donor-sites in multiple regions can amplify the coding power tremendously, going from a few isoforms of one gene up to producing thousands of different protein isoforms like in the Drosophila gene *DSCAM* which can generate up to 38'000 proteoforms (Schmucker et al., 2000).

Control of splicing patterns is mediated by different RNA-binding proteins. General splicing regulators include the family of SR proteins (Ser-Arg) as well studied mediators of ESEs

and heterogeneous nuclear RNPs (hnRNPs) which bind to ISSs and ESSs (Chen and Manley, 2009; Smith and Valcarcel, 2000). These splicing regulators can act ubiquitously, while others act on specific transcripts in a cell-type dependent manner. In the combination with ubiquitously expressed regulators and depending on their concentration they have an important role in generating tissue-specificity and cell-type identity during development (Black, 2003; Zhang et al., 2008).

Interestingly, the occurrence of alternative splice events in neuronal tissue is highest when compared to other tissues and further demonstrates the need for a bigger variety of protein isoforms in the mammalian brain (Castle et al., 2008).

One prominent example of RNA-binding proteins that help to fine-tune splicing choices in neurons is Nova, which is responsible for splicing choices of synaptic proteins (Ule et al., 2005). RBPs can act on different *cis*-elements, as *Nova1* is able to either act on ISEs, promoting inclusion of certain exons, or on ESEs, promoting skipping of certain exons (Dredge and Darnell, 2003; Dredge et al., 2005). The expression of *Nova1* and *Nova2* was further validated in knock-out studies as a tissue specific and to some extents even brain region specific splicing factor (Ule et al., 2005).

RNA-binding proteins regulating alternative splicing were additionally reported to act in a cell-type dependent manner. One example is the activity dependent splicing regulator *Rbfox1,* which is a crucial factor in guiding the connectivity of SST+ and PV+ interneurons in the developing cortex by alternative splice programs (Wamsley et al., 2018).

Another example comes from members of the STAR (signal transduction activators of RNA) protein family, which are defined by a conserved RNA-binding domain (Vernet and Artzt, 1997). The expression pattern of individual members of this family, *SLM1* and *SLM2* (SAM68-like mammalian protein 1 and 2), thereby shows further evidence that RBPs are not only segregated between different neurotransmitter-expressing cell types but also within individual glutamatergic and GABAergic cell classes. While *SLM1* is highly expressed in VIP+ interneurons and excitatory dentate granule cells, *SLM2* is mostly expressed in SST+ interneurons and pyramidal cells in CA (Iijima et al., 2014; Nguyen et al., 2016; Traunmuller et al., 2014).

A recent transcriptomic study further highlighted this phenomenon by showing that these are not rare events, but that the differential expression of individual exons between cell classes and even within cell classes segregated by tissues can control synaptic protein pools. Alternative splicing of genes related to synaptic genes is therefore more associated with synapse diversification when compared to the overall gene expression of those genes (Furlanis et al., 2019). In combination with studies deciphering steady-state transcriptomes of individual cell classes, recent studies further pushed gene expression analysis looking

at activity dependent transcripts in different cell populations and at their sub-cellular localization (Hrvatin et al., 2018; Tushev et al., 2018).

Transcriptomic studies are thus an important tool to assess molecular repertoires at synapses and helped to better understand how neuronal cell classes and synaptic diversity are shaped by transcript diversification.

1.3 Transcriptome to proteome divergence

Transcriptome studies can give us a detailed insight into the pool of mature transcripts within individual cells. However, studies comparing the transcriptome to the translated proteins or proteome revealed that only about 40% of the proteome can be predicted by looking at mRNA levels (Liu et al., 2016; Vogel and Marcotte, 2012). Underlying this striking difference are post-transcriptional mechanisms taking place after maturation of transcripts, when mRNA is exported to the cytoplasm. There it is further regulated in terms of translation rates, transported to sub-cellular locations and finally degraded. This is the basis for the spatial and temporal regulation of single mRNAs and their rapid and controlled translation in specific subcellular localizations (Jereb et al., 2018; Taliaferro et al., 2016; Tushev et al., 2018). The non-coding and untranslated regions (UTRs) up- and down-stream of the coding sequence (CDS) can thereby act as hubs for binding a variety of co-factors responsible for this spatial and temporal control. Alternate UTRs are further known to not only regulate the stability but also the sub-cellular localization of mRNA transcripts (Tushev et al., 2018). Differential 3'UTR expression driving the generation of a hub for multiple binding partners responsible for post-transcriptional modifications will be introduced in the following chapters.

1.3.1 Differential 3'UTR expression

In addition to alternative coding sequences generated by alternative splicing, alterations in the non-coding parts or UTRs have a profound impact on protein expression. Next to alternate 5'UTRs and their influence on translation initiation 3'UTRs show a high potential for translational control. Differential usage of 3'UTRs can have a high influence on translation as longer 3'UTRs and thereby bigger "platforms" for *trans*-acting regulators lead to regulation of transcript stability and sub-cellular localization (Miura et al., 2014).
3'UTR length or choice of variable poly(A)-sites is regulated by alternative polyadenylation (APA). Alternative polyadenylation can thereby either change the length of the 3'UTR or in other cases, and when coupled to splicing, alter the CDS (Tian and Manley, 2017). Sequencing studies in mice revealed that nearly 80% of mRNA coding genes have more than one polyadenylation site (Elkon et al., 2013). The process of polyadenylation is further linked to alternative splicing through splice factors that interact with downstream polyadenylation factors and plays an important role in generating transcript diversity (Danckwardt et al., 2008; Danckwardt et al., 2007).

The attachment of the poly(A)-tail is a two-step process including endonucleolytic cleavage and the addition of a stretch of Adenosines, which in humans normally consists of 250-300 basepairs (Elkon et al., 2013). It is mediated by *cis*-acting RNA elements and proteins that bind to the pre-mature RNA. The most important *cis*-element is a 6-nucleotide long motif, which can have different variants; the canonical variant is defined as AAUAAA. It is located 15-30 nucleotides (nt) upstream of the cleavage site and is recognized by cleavage and polyadenylation specificity factor (CPSF) which in combination with the cleavage stimulation factor (CSTF) promotes the cleavage between these two multi-polypeptide complexes. CSTF binds to U- or GU-rich downstream sequence elements (DSEs) that mediate together with upstream sequence elements (USEs) the cleavage efficiency (Mandel et al., 2008). Recognition of alternative poly(A)-sites is differently regulated during development and across different tissues, dependent on the concentration of polyadenylation factors like CSTF and on the strength of the poly(A)-site (Colgan and Manley, 1997).

Changes in alternative polyadenylation are important for proper development with the usage of proximal poly(A)-sites before and usage of distal poly(A)-sites after maturation (Ji et al., 2009; Wang et al., 2013). APA changes were also found to be regulated by neuronal activity (Flavell et al., 2008). The usage of longer 3'UTRs and thereby more possibilities for regulation in general is facilitated in neuronal tissue and like alternative splicing thought to help the functional and anatomical more complex neuronal cells to fulfill their tasks (Miura et al., 2013; Zhang et al., 2005). In addition to alternative 3'UTRs, alternative terminal exons were also reported to promote differential regulation by *trans*-acting factors (Taliaferro et al., 2016). In this case, APA occurs upstream of the 3'UTR, leading to the expression of alternative terminal exons (Tian and Manley, 2017). One classic example thereof is the production of two proteins, calcitonin and calcitonin gene-related peptide 1, by either skipping or including an alternative terminal exon (Amara et al., 1982). This regulation is tissue specific and together with a study investigating the switch of IgM heavy chain mRNA during B-Cell activation from distal to proximal poly(A)-site usage the first evidence of this mechanism (Alt et al., 1980). APA can additionally generate dominant negative counterparts of specific proteins, by generating truncated isoforms that compete with the full length proteoform (Di Giammartino et al., 2014).

This mechanism of not only changing the non-coding but also the coding sequence is widespread and occurs in more than 40% of transcripts (Hoque et al., 2013). Altering the coding sequences have a profound impact on the protein identity. This includes changes in membrane association shifting transmembrane protein isoforms to secreted isoforms, which was found in at least 376 mouse genes (Davis et al., 2006). This termed upstream-APA is more prominent in cells that are proliferating, adding evidence that APA in non-

terminal and terminal exons may be linked (Elkon et al., 2012; Hoque et al., 2013; Taliaferro et al., 2016; Tian and Manley, 2017).

1.3.2 Post-transcriptional regulatory mechanisms

Regulatory mechanisms that act on differential 3'UTRs are mediated by *trans*-acting factors which guide translational control, and which influence the divergence between transcriptome and proteome. They predominantly regulate stability, translation rates and localization of transcripts (Tian and Manley, 2017).

Trans-acting factors like micro RNAs (miRNAs) and RNA-binding proteins (RBPs) are known to influence the stability of transcripts by binding sequence elements in their 3'UTR. miRNAs are small RNAs (~23nt), which after processing and loading into the silencing complex, pair with mRNA in a repressive manner, normally leading to endonucleolytic cleavage and degradation of target mRNAs (Bartel, 2009). Stability of mRNA molecules is thereby greatly influenced by 3'UTR length in having more accessible binding sites, either leading to degradation of transcripts when harboring destabilizing elements or stabilizing them by incorporation of elements recruiting stabilizing RBPs (Hogg and Goff, 2010; Tian and Manley, 2017).

Degradation of mRNAs is canonically either regulated by 5' to 3' or by 3' to 5' decay after mRNAs are deadenylated (Garneau et al., 2007; Houseley et al., 2006; Sheth and Parker, 2003). Next to the degradation of properly processed transcripts, mechanisms as non-sense mediated mRNA decay (NMD) are responsible to degrade aberrant transcripts. One way of NMD function is its ability to recognize premature translation termination codons (PTCs), which can be the consequence of genetic mutations, imprecise transcription or faulty pre-mRNA splicing (Conti and Izaurralde, 2005). If NMD only has a function in detecting aberrant transcripts or if it is more general involved in the degradation of mRNAs is still unclear, but core features of its machinery are ubiquitously expressed and well characterized (Brogna et al., 2016; Garneau et al., 2007; He and Jacobson, 2015). Core proteins include UPF1, UPF2 and UPF3, which bind to exon junction complexes (EJC), a complex which is placed at spliced exon junctions (Conti and Izaurralde, 2005; Le Hir et al., 2000). EJCs are normally removed by translating ribosomes, but in cases where the translating ribosome encounters a PTC upstream of an EJC they trigger NMD (Conti and Izaurralde, 2005; Garneau et al., 2007).

Brogna and co-workers additionally proposed a model called "The Ribosome release model", which would be caused by ribosomes falling off after encountering a PTC on mRNAs due to non-efficient binding after a stop codon, leaving more mRNA sequences

“unprotected” from ribosomes (Brogna et al., 2016). NMD might further play a crucial role in regulating storage of mRNAs at a distinct cellular location, adding support to the high need of temporal and spatial control of neuronal gene expression (Giorgi et al., 2007).

Neurons are in high need of controlled translation of mRNAs, as they need to be able to quickly react to stimuli in adapting and changing local protein pools (Holt et al., 2019). Evidence for local translation in response to stimuli comes from early studies showing localized transcripts by using *in situ* hybridization, which in more recent years and by the usage of more advanced techniques went first to 100-200 and more recently to over 2500 localized transcripts in the CA1 neuropil (Cajigas et al., 2012; Kleiman et al., 1990; Poon et al., 2006; Zhong et al., 2006).

Localization of transcripts is thereby guided by RBPs binding to 3’UTRs, and with neurons tending to use longer 3’UTRs and the inclusion of localization elements led to the hypothesis that differential localization in neurons is a widely used mechanism (Zhang et al., 2005). Brain-derived neurotrophic factor (BDNF) is a good example of this mechanism, as short 3’UTR isoforms restrict expression to the cell body and long isoforms locate the mRNA to dendrites. Truncating long isoforms thereby leads to defects in spine density and long-term potentiation (LTP) impairment in hippocampal dendrites (An et al., 2008).

Local signaling in dendrites is further thought to change regulation of transcripts by *trans*-acting factors, leading to translation, degradation or altered translational efficiency (Glock et al., 2017). Recent studies also started to characterize the local translatome of axonal compartments by adapting the Ribo-Trap Method to different cellular compartments in the mouse visual system. The ribosome is thereby tagged in a Cre-mediated way and together with bound mRNA isolated from complex samples (Sanz et al., 2009). These isolated axonal translatomes showed common regulators and interestingly shared sequence elements generated by alternative splicing (Shigeoka et al., 2016).

All these mechanisms influence the process of generating cell identity to form specific synapses in an intrinsically defined way. To better understand how processes including co- and post-transcriptional regulatory mechanisms shape synaptic diversity a profound analysis on the transcriptome, local translatome and proteome needs to be integrated. In my dissertation I will illustrate this by showing one example of a synaptic adhesion molecule of the Neurexin gene family involved in shaping the synapse in previously unknown fashion. Before introducing the project, I will therefore discuss the terms of synaptic specification as well as co- and post-transcriptional mechanisms in relation to Neurexins.

1.4 Neurexins

The gene family of Neurexins (*Nrxn*) encode for important pre-synaptic signaling molecules with a high diversity of proteoforms, which can be expressed in a cell-type specific manner. Multiple NRXN loss-of-function models have highlighted the important role of distinct NRXN protein isoforms for synaptic function. However, due to the lack of tools, this class of adhesion molecules is hardly studied at the protein level.

Neurexins are synaptogenic proteins, first identified as receptors for alpha-latroxin and with a suggested role in cell recognition (Ushkaryov et al., 1992). Synaptogenic proteins thereby have the ability to trigger pre- or postsynaptic functional assemblies, as shown for both Neurexins and their best studied postsynaptic binding partners Neuroligin (*Nlgn*)(Chih et al., 2006; Dean et al., 2003; Graf et al., 2004; Scheiffele et al., 2000). In addition to their role in synaptic development and maintenance, numerous studies in the last 30 years attributed Neurexins further roles in synaptic transmission in both glutamatergic and GABAergic synapses (Etherton et al., 2009; Missler et al., 2003; Zhang et al., 2010), whose disruption leads to severe phenotypes (Sudhof, 2008, 2017).

Neurexins represent a highly efficient hub for the organization of the synapse. Thanks to their specific domain composition, Nrxns have the power to recruit distinct types of post-synaptic molecules, and therefore *trans*-synaptically influence the post-synaptic composition and properties. In addition to the well-characterized post-synaptic partners Nlgns (Chih et al., 2005; Ichtchenko et al., 1995; Scheiffele et al., 2000), Neurexins can efficiently recruit leucine-rich repeat transmembrane proteins (LRRTMs)(de Wit et al., 2009; Ko et al., 2009; Siddiqui et al., 2010), GABA-A receptors (Zhang et al., 2010) and α-Dystroglycans (Sugita et al., 2001). They were further characterized to bind to soluble proteins such as C1ql proteins and Cerebellins (*Cbln*), which have the power to couple kainate and glutamate receptors to Neurexins respectively (Matsuda et al., 2016; Matsuda and Yuzaki, 2011; Uemura et al., 2010), and to the family of neurexophilin (Missler et al., 1998; Petrenko et al., 1996).

1.4.1 Neurexin molecular diversity

Genomic variability, coupled with post-transcriptional and post-translational modifications of Neurexins, can generate protein isoforms with multiple structural motifs responsible for the specific *trans*-synaptic recruitment. Variability of NRXNs arise from the presence of three different genes in the mammalian genome (*Nrxn1, Nrxn2, Nrxn3*) and the usage of three (α, β, γ) or two (α, β) alternative promoters for *Nrxn1* or *Nrxn2* and *Nrxn3,*

respectively. They are very large genes with up to 1.8Mb in humans for *Nrxn3* (Reissner et al., 2013; Tabuchi and Sudhof, 2002; Yan et al., 2015). Beside their genomic variability, multiple NRXN isoforms can result from co-transcriptional processing. In particular, alternative splicing of their pre-mRNAs have the potential to generate hundreds of different transcripts by combinatorial usage of six alternative splice segments (AS1-6), which are conserved across mouse and human (Flaherty et al., 2019; Schreiner et al., 2014; Treutlein et al., 2014). Longer α-NRXNs (~1500 amino acids) contain all six splice segments while β-NRXNs (~450 amino acids) contain only AS4 and AS5 (Figure 4).

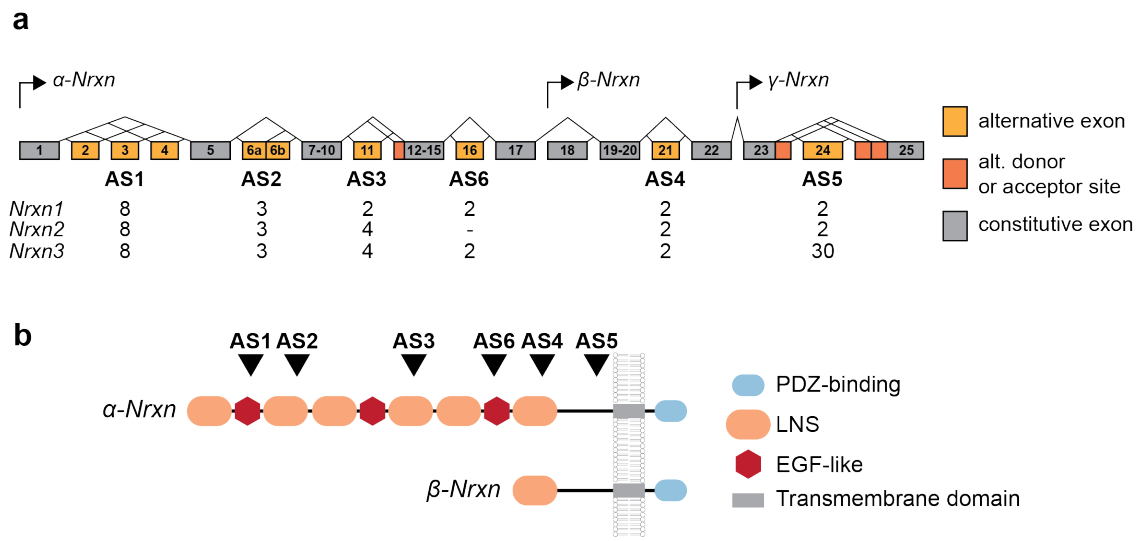

Figure 4. Neurexin splice site and molecular diversity
a, Schematic view of alternative splice segments in Nrxn pre-mRNA. Splicing patterns shown by lines, possible splice combinations indicated below; promoters (arrows), splice sites (AS1-6) and exon numbers (exons 1-25) labelled (Adapted from (Schreiner et al., 2014)). Yellow: Alternative Exon, Orange: Alternative donor or acceptor site, Grey: Constitutive exon. **b**, Domain organization of NRXN proteins with location of splice sites indicated; extracellular domains left, intracellular domains right from the lipid bilayer, domains indicated on the right (Adapted from (Ushkaryov et al., 1992)).

Alternative exon usage within *Nrxn* transcripts can highly influence the extracellular protein domains and their interactive potential to binding partners. NRXN proteins consist of six Laminin-Neurexin-Sex hormone binding globulin (LNS) domains, which are interspersed by epidermal growth factor (EGF) domains. AS2, AS3 and AS4 are located in the extracellular LNS domains, and their inclusion or exclusion thereby directly alters the binding specificity and the degree of affinity with post-synaptic partners (Figure 4b)(Gomez et al., 2021; Sheckler et al., 2006). For example, the formation of the tripartite synaptic complex composed of glutamate receptors, Cerebellins and Neurexins depends on the inclusion of AS4 within *Nrxn* transcripts (AS4+) (Matsuda and Yuzaki, 2011). Moreover, AS2 insertions are known to guide the binding of α-Dystroglycan (DAG1) and also

Neurexophilin 1 (Nxph1). DAG1 binding is further dependent on AS4 and both are competing with Nlgn binding to Nrxns. This not only demonstrates how splicing modulates small structural changes and in consequence leads to different binding partners but also the dependence of a combinatorial use of splice sites (Reissner et al., 2014; Sugita et al., 2001; Wilson et al., 2019).

AS1, AS6 and AS5 on the other hand are thought to have direct influence on the sterical flexibility of Nrxn proteins, as they influence the length between LNS domains (AS1, AS6) or the length of the stalk region situated in the juxtamembrane region before the transmembrane domain (AS5, Figure 4b)(Miller et al., 2011; Schreiner et al., 2014).

Intracellularly, NRXNs are linked to the cytoskeleton by binding scaffolding proteins. At the carboxy-terminus they contain a PDZ-binding motif, which is binding to CASK, together with protein 4.1 nucleating assemblies of actin filaments and furthermore linking NRXNs to pre-synaptic clusters of Ca^{2+} and K^{+} channels (Biederer and Sudhof, 2001; Hata et al., 1996; Leonoudakis et al., 2004; Maximov et al., 1999).

1.4.2 Role of Neurexin in determining a molecular code

The astonishing diversity in Neurexin composition and its combinatorial use has the potential to generate cell type- or even single synapse-specific molecular codes. Supporting this hypothesis, recent studies show the selective expression of proteoform subsets in defined neuronal cell populations. This diversity in expression can be observed at different levels. First, there is a clear relation of the variety of transcript isoforms to tissue heterogeneity, as shown by a study using single molecule long-read PacBio RNA-sequencing. *Nrxn1* transcripts are more diverse in overall brain tissue when compared to isolated cell populations, where a more defined subset of transcripts is expressed. This holds true when comparing brain regions as Cortex and Cerebellum, which differ in complexity (Schreiner et al., 2014). Second, there is as cell type specific expression of alternatively spliced exons of Neurexins as determined by single-cell mRNA profiling and by translatome studies (Fuccillo et al., 2015; Furlanis et al., 2019; Lukacsovich et al., 2019). Finally, alternative splicing also correlates with interneuron development, as there are distinct splicing profiles for interneurons emigrating from either medial or caudal ganglionic eminence (Lukacsovich et al., 2019).

Two other mechanisms could alter the role of Neurexins in shaping a synaptic molecular code. First, post-translational modifications, here the attachment of heparan sulfate (HS) in the stalk region of NRXNs, was shown to enhance NRXN binding to NLGNs and LRRTMs. NRXN itself can thereby by classified as a heparan sulfate glycoprotein (HSGP),

with the loss of its HS-modification leading to impairments in synaptic transmission and development. Next to the previously described protein-protein interactions this raises the question of an additional glycan-code next to a splicing code (Roppongi et al., 2020; Zhang et al., 2018). Second, proteolytic cleavage of NRXNs, which results in ectopic shedding, might amplify the function of Neurexin at the synapse. It was shown that the clearance of C-terminal fragments of shedded NRXNs is required for proper neurotransmitter release (Saura et al., 2011; Servián-Morilla et al., 2018).

Impairments in synaptic transmission were also shown in conditional triple knock-out (KO) mice, where all α- and β-Neurexins are deleted in a Cre-dependent manner after development, as constitutional KOs are lethal (Missler et al., 2003). Interestingly, conditional KOs exhibited different phenotypes in different cell classes, as PV+ cells show a decrease in synapse numbers while SST+ interneurons display altered pre-synaptic Ca^{2+} transients, both leading to a decrease in synaptic strength (Chen et al., 2017).

Cell type specific expression of Neurexin isoforms is closely linked to the expression of RBPs responsible for the regulation of Neurexin splicing. In addition to more general RBPs like *Nova2* and *Rbfox1* identified in genetic screens as splicing regulators of *Nrxns* (Saito et al., 2019; Wamsley et al., 2018), members of the STAR protein family are well characterized Neurexin regulators, in particular for their role in promoting skipping of AS4. Thus, high levels of *SLM2* in pyramidal cells in CA1/CA3-regions of the hippocampus lead to selective expression of NRXN-AS4- proteins, while low levels of *SLM2* in PV+ interneurons guide the expression of AS4+ isoforms. Furthermore, *SLM2*-loss in pyramidal cells leads to loss of AS4- splice isoforms and mis-expression of *SLM2* in cells that do not express it leads to the production of AS4- isoforms (Nguyen et al., 2016; Traunmuller et al., 2016).

Alternative splice segment 4 was further shown to have possible differential function when comparing *Nrxn1* and *Nrxn3.* Overexpression of either *Nrxn1-AS4+* or *Nrxn3-AS4+* leads to changes in the post-synaptic recruitment of NMDA or AMPA receptors, therefore highly influencing the post-synaptic responses. On the other hand, overexpression of *Nrxn2-AS4+* had no effect on the recruitment of ionotropic glutamate receptors and on synaptic properties (Dai et al., 2019).

The alternative splice site 5, which could be involved in regulating length and sterical variability of the stalk region and furthermore membrane attachment is not well studied, although it has the highest potential for transcript diversification with theoretical 30 different splice variants in *Nrxn3* (Figure 4a)(Schreiner et al., 2014). As this splice site is analyzed in detail in my work, I will introduce it in the following paragraph.

1.4.3 Alternative splice segment 5 of Neurexin 3

Although *Nrxn3-AS5* has the highest potential for protein diversification, its impact on the functional role of Neurexins in generating synaptic specificity remains elusive. Alternative splicing at AS5 of *Nrxn3* can lead to the inclusion or exclusion of the alternative exon (exon 24). Exon 24 is flanked by two alternative donor sites (exon 23a/23b) and three downstream alternative acceptor sites (exon 25a/25b/25c), with theoretical four alternative acceptor sides in exon 24 (Figure 5)(Schreiner et al., 2014). NRXN-AS5- isoforms (i.e., isoforms that skip alternative exon 24) which include the alternative acceptor site 25b are known to bind to C1ql2/3 proteins. This coupling thereby generates a tripartite trans-synaptic complex with kainate receptors at hippocampal mossy fibers, which disruption leads to reduced network activity in the hippocampus (Matsuda et al., 2016).

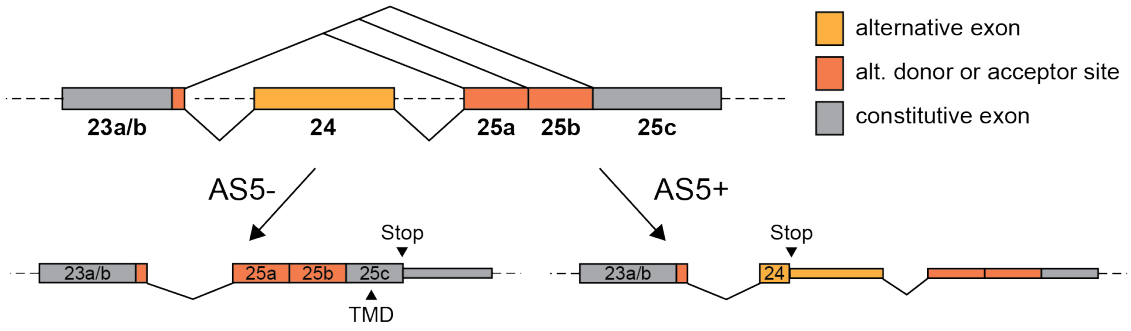

Figure 5. Alternative splice segment 5 of Nrxn3
Top: Alternative splice segment 5 within *Nrxn3* pre-mRNA, with exons indicated, Yellow: Alternative cassette exon, Orange: Alternative acceptor and donor sites, Grey: Constitutive exon; Bottom: Main isoforms generated by AS5 splicing, with translational Stop-Codons and transmembrane domain (TMD) annotated.

Inclusion of the alternative exon 24 results in the generation of NRXN3-AS5+ isoforms. So far, only a limited number of studies thoroughly investigated the functional implication of this transcript isoform. In a first study, *Nrxn3-AS5+* was reported to encode for a secreted protein by inclusion of an in-frame premature stop codon before the canonical transmembrane domain, encoded by exon 25c (Ushkaryov and Sudhof, 1993). As inclusion of a PTS upstream of the exon 24-25 boundary would lead to NMD, it has been hypothesized that the inclusion of AS5 would result in the loss of NRXN3 protein (Giorgi et al., 2007). Another hypothesis highlighted the possibility that $AS5^{+}$ might encode for a GPI-anchored protein, as NRXN3-AS5+ was shown to be tethered to membranes in heterologous cells and furthermore can be released by adding phosphatidylinositol-specific phospholipase C (PI-PLC), an enzyme that specifically cleaves GPI-anchors

(Schreiner 2014). When looking at the alternative acceptor sites in exon 24, only the usage of acceptor site 24a could be detected by sequencing. Thus, splicing at AS5 can either generate secreted/GPI-anchored NRXN3-AS5+ or transmembrane NRXN3-AS5- isoforms and as there is no evidence for multiple acceptor sites in exon 24 it will be treated as an alternative cassette exon (Figure 5)(Schreiner et al., 2014). The expression of this splice site on the protein level and its functional impact on synaptic formation or synaptic properties remain unclear. The expression on the protein level, its functional impact and the representation of *Nrxn3-AS5+* in shaping a molecular code underlying synaptic diversity therefore remain unclear.

1.5 The dissertation project

To understand how the specificity of synapses is generated a lot of effort was put into a wide variety of studies as introduced. These studies tried to decipher the fundamental molecular logic underlying synapse complexity and further how synapse diversity shapes the complexity of the brain. Synaptic adhesion molecules were thus prime candidates to investigate. With the help of transcriptomic studies identifying gene families or classes, and follow-up work looking at those families with biochemistry methods, the ground was lied for a better understanding of the molecular scaffold at the synapse.

However, due to the lack of tools the characterization of not only overall gene expression but also the characterization of individual transcript isoforms and their respective proteome lags behind. Additionally, transcriptome studies can give us no insight into the subcellular localization of individual proteins. To therefore better understand the molecular scaffold generating synapse specificity we need to apply more sophisticated tools to examine the proteome of individual neuronal cell classes to overcome the divergence of proteome predictions in relation to the transcriptome.

In this work I applied refined methods to study an endogenous alternative splice form of Neurexin 3. As introduced, mutations in different variants of *Nrxn3* are disease associated and alternative splice isoforms of a pool of over 1000 transcripts generated by the Nrxn gene family show phenotypes in glutamatergic and GABAergic transmission. The alternative splice segment 5 of *Nrxn3* thereby shows the greatest potential for synaptic diversification, as it consists of multiple evolutionary conserved alternative acceptor- and donor-sites up- and down-stream of the cassette exon. As the incorporation of the alternative exon leads to the inclusion of a pre-mature stop codon, AS5+ transcripts were predicted to undergo NMD and would therefore not contribute to the molecular repertoire at the synapse. As NRXN3-AS5+ was further predicted to be either a secreted or GPI-anchored protein, it might significantly change its role in forming a trans-synaptic code shaping synaptic identity.

The aim of my thesis project is to characterize how non-canonical NRXN3-AS5+ proteoforms contribute to synaptic function. To achieve this, I applied a combination of proteome driven methods by specifically tagging NRXN3-AS5+ proteoforms and performing targeted proteomics to study the influence of NRXN3-AS5+ in shaping a molecular code. The results, which highlight a specific example of molecular complexity underlying synaptic diversity, are included here in form of a manuscript, and will be discussed separately afterwards.

2. Results

2.1 Preface

The following result chapter in form of a manuscript represents the work of my PhD, carried out in close collaboration with several people. Below I will illustrate the individual contributions of each person involved in the project investigated during my PhD thesis. Supplementary experiments that are not represented in the manuscript will be mentioned and put into perspective in the discussion part.

The project was supervised by Peter Scheiffele who was involved in writing the manuscript. The work was supported by and the manuscript prepared in collaboration with Katharina Behr, Dietmar Schreiner and Alexander Schmidt.

Proteoform mapping uncovers cell- and synapse-specific forms of Neurexin 3
David Hauser, Katharina Behr, Dietmar Schreiner, Alexander Schmidt, Josef Bischofberger and Peter Scheiffele
in preparation

For this project, I generated and validated the knock-out and knock-in mouse lines. Biochemistry experiments in characterizing the mouse lines and further characterizing Nrxn splice isoforms were done by me, for pull-downs I had help from Dietmar Schreiner. All stainings, quantifications and data analyses were performed by me, including preparation of neuronal cell cultures and mouse brain sections. I performed RNA isolation and RT-qPCR analysis as well as semi-quantitative PCR assays which I optimized and designed.

All samples for Mass-Spec analysis were prepared and submitted by me, design of heavy peptides for PRM was done by Alexander Schmidt, who also ran and analyzed all Mass-Spec experiments.

Katharina Behr was critically involved in characterizing knock-out mice with electrophysiological recordings, which were performed by her and in which design Josef Bischofberger was involved.

Pawel Pelczar from the Center for Transgenic Models (CTM, Basel) was involved in the generation of the *Nrxn3-AS5* knock-out and the *Nrxn3-AS5*^{HA} knock-in mouse line. Caroline Bornmann and Laetitia Hatstatt-Burkle gave technical support with perfusion of animals for cryo-sectioning.

2.2 Proteoform mapping uncovers cell- and synapse-specific forms of Neurexin 3

David Hauser[1], Katharina Behr[2], Dietmar Schreiner[1], Alexander Schmidt[1], Josef Bischofberger[2], Peter Scheiffele[1]

[1]Biozentrum of the University of Basel, Klingelbergstrasse 50-70, CH-4056 Basel, Switzerland

[2]Department of Biomedicine, University of Basel, Pestalozzistrasse 20, 4056 Basel, Switzerland

Correspondence: peter.scheiffele@unibas.ch

Abstract

The diversification of cell adhesion molecules by alternative splicing is proposed to underlie molecular codes for synapse formation and specification in the nervous system. Transcriptomic approaches uncovered detailed cell type-specific mRNA splicing programs and genetic studies support a key role for alternative splicing in functional synapse specification. However, due to technical limitations, it has been hard to probe synapse-specific localization and function of the resulting protein splice isoforms, or “proteoforms”, in vivo. We here apply a proteoform-centric workflow in mice to test synapse-specific functions of splice isoforms of the synaptic adhesion molecule Neurexin-3 (NRXN3). Combination of splice isoform-specific knock-in, knock-out and targeted proteomics uncovers a major non-canonical proteoform, NRXN3 AS5, that is selectively expressed in GABAergic interneurons and presynaptic GABAergic terminals. NRXN3 AS5 protein abundance significantly diverges from the broad distribution of the mRNA transcript isoform and is gated by translation-repressive elements in the 3’ untranslated region of the

mRNA. Deletion of NRXN3 AS5 isoforms results in a >60% decrease of total NRXN3 protein expression without modifying the total *Nrxn3* mRNA level. This loss-of-function is accompanied by an impairment of synaptic transmission at CCK interneuron synapses in the dentate gyrus. Finally, we develop a database (https://scheiffele-SYNCODE.scicore.unibas.ch/) of validated targeted mass-spectrometry assays to facilitate the dissection of synaptic connectivity and function at the proteome level.

Introduction

The formation and functional specification of neuronal synapses are fundamental for neuronal circuit operation. During development, molecular programs play a central role in shaping synapse formation and function [1-7]. Terminal gene batteries direct the cell type-specific expression of key molecular constituents that encode components of neurotransmitter synthesis, release, neurotransmitter receptors, and synaptic adhesion molecules [8]. Major advances in transcriptomic and proteomic approaches have advanced our understanding of cell type- and synapse-specific molecular repertoires that contribute to the specification of synaptic connectivity and function [9-18].

Recent work highlighted that regulators of neuronal wiring are extensively modified at the level of alternative mRNA splicing, producing distinct cellular transcript isoform repertoires [19-26]. Evolutionary comparisons of alternative splicing across species highlighted a massive expansion of alternative exon usage from invertebrates to mammals, non-human primates and humans [27,28]. Thus, the increased molecular diversification by alternative splicing was proposed to be a major driver of phenotypic diversity. Targeted manipulation of specific alternative exons in individual genes demonstrated that alternative splicing provides a fundamental mechanism for functional regulation [29-39]. Thus, alternative splice variants of synaptic proteins are thought to underlie a cell and synapse-specific code for neuronal wiring.

While methodologies for deep profiling of transcript isoforms continue to rapidly advance, there are major limitations in probing to what extent such transcript isoforms actually contribute to functionally relevant proteoform diversity in vivo. Quantitative transcriptome – proteome correlations have led to the conclusion that only 40% of protein level variance can be explained by mRNA levels [40-43]. Non-coding, 5' and 3' untranslated regions are major regulators of translation, protein localization, protein-protein interactions [44]. Such post-transcriptional regulation is particularly prevalent in the nervous system [45,46]. Moreover, transcriptomic analyses cannot uncover subcellular allocation of protein splice variants which is central for the hypothesis of a splice-code dependent specification of neuronal connectivity. Given these limitations, it remains a major question how mRNA splice isoforms contribute to functionally distinct synaptic proteoforms and a functional code for cell type-specific synapse properties.

We here combined selective genetic tagging of an endogenous splice isoform, selective ablation, and splice isoform-specific targeted proteomic approaches to test synapse-specific recruitment and function of splice isoforms of the synaptic adhesion molecule Neurexin-3 (NRXN3). *Nrxn3* sequence variants and mutations have been linked to alterations in emotional behavior, drug abuse, and autism [47,48]. Alternative splicing at up to six segments (AS1-6) results in the generation of thousands of *Nrxn3* mRNA isoforms in the mammalian brain [25,49,50]. Mouse knock-out models for *Nrxn3* and mis-expression of the mRNA encoding mRNA isoforms containing or lacking an alternative exon at AS4 uncovered phenotypes in glutamatergic transmission, as well as GABAergic alterations [30,31,47]. Moreover, sequences encoded by an alternative splice acceptor site at AS5 interact with C1q-like proteins in vitro [26]. The *Nrxn3* AS5 segment (here designated as exon 23-24-25, with exon 24 encoding the alternative exon, Fig.1a) consists of multiple, evolutionarily conserved alternative splice donor and acceptor sites, and thus, has been proposed to be the biggest contributor to *Nrxn3* mRNA isoform diversification. However,

AS5-containing mRNAs are predicted to encode secreted Neurexin-3 proteins that lack function [30,51]. Thus, representation and function of NRXN3 proteoforms has remained enigmatic.

Results

Splice proteoform-specific tagging of Nrxn3 in vivo

mRNAs containing exon insertions at the alternatively spliced segment AS5 are widely detected in the mouse nervous system. Using Sashimi-plots to visualize exon-exon junctions from deep RNA sequencing data [19], we observed that in mouse hippocampus AS5+ mRNA isoforms mostly contain exon 23-24 and the downstream alternative acceptor side 25a (Fig.1a). By contrast, AS5- variants skip exon 24 and mostly join exon 23 into downstream acceptor sites 25b and 25c. Importantly, the alternative exon 24 contains a premature translational stop codon and exon 24-containing *Nrxn3*^{AS5} mRNAs were hypothesized to be targeted by nonsense-mediated decay [52]. However, we did not observe translation-dependent mRNA decay of endogenous *Nrxn3*^{AS5} isoforms *in vitro* (Fig.S1a). Thus, it has remained unclear to what extent AS5+ proteoforms are expressed *in vivo*.

We used homology-directed genome editing with CRISPR-Cas9 and asymmetric donor DNA [53] to directly probe NRXN3 AS5 variants on the protein level. We generated knock-in mice where a double HA epitope was inserted into the coding sequence of *Nrxn3* exon 24 (Fig.1b, S1b). Hetero- and homozygous *Nrxn3*^{AS5HA} mice were viable and fertile and did not show any visible abnormalities. *Nrxn3*α and *Nrxn3*β mRNA levels were unaltered (Fig.S1c). There was a slight increase in exon 24 containing *Nrxn3* mRNAs, indicating that the sequence alterations in the alternative exon slightly increased its incorporation into the mature transcripts (Fig.S1c). The endogenous epitope-tagged NRXN3α and NRXN3β AS5^{HA} proteins were readily detected by Western blot in neocortical, hippocampal and cerebellar tissue, demonstrating that these non-canonical NRXN3 proteins are highly expressed in vivo (Fig.1c).

Biochemical fractionation experiments demonstrated that the endogenous NRXN3α AS5^{HA} and NRXN3β AS5^{HA} proteins were tightly membrane associated (Fig.1c). When examining the sequence of AS5^{+} variants, we observed that exon 24 encodes evolutionarily conserved amino acids that resemble GPI-anchor attachment sites (Fig.1b, S1d). When expressed in HEK293T cells in vitro, NRXN3 AS5 proteins incorporated ^{3}H-ethanolamine, one of the key building blocks of GPI-anchors (Fig.1e). Transfer of the exon 24-encoded amino acids to a heterologous protein was sufficient to confer membrane anchoring (Fig.S1e,f). Thus, AS5+ mRNAs encode non-canonical, membrane-anchored proteoforms of NRXN3 that are significantly expressed in the mouse hippocampus.

Cell type-specific expression of Nrxn3AS5 splice forms

Differential alternative splicing of *Nrxns* at AS4 across neuronal cell populations underlies cell type-specific functions [22,29,31,49,54,55]. When examining AS5 incorporation across CA1, CA3, and SST interneurons of the mouse hippocampus, we noted high levels of exon 24 incorporation levels in all cells, albeit slightly elevated incorporation in GABAergic SST interneurons (Fig.S2a). This is similar to previous conclusions from neocortical single cell sequencing analysis [55]. Remarkably, the endogenous AS5+ protein in *Nrxn3*^{AS5HA} mice was almost exclusively detected in GABAergic neurons of the hippocampus, indicating a strong cell class selectivity of this splice isoform at the protein level (Fig.2a-e). Co-labeling for NRXN3 AS5^{HA} and markers of interneuron subclasses suggests that NRXN3 AS5 protein is commonly expressed in multiple interneuron classes of the hippocampus (Fig.2e). Similar selective expression was detected in other brain areas (Fig.S2b). While a pool of NRXN3 AS5^{HA} was localized to a peri-nuclear compartment, higher magnification analysis uncovered a substantial concentration at GABAergic synapses (Fig.2 and S2). In cultured hippocampal neurons, punctate NRXN3 AS5^{HA} labeling closely co-localized with GABAergic synapse markers vGAT and gephyrin whereas immune-reactivity was absent from sites containing glutamatergic markers (Fig.S2c-d). One particularly notable site of

NRXN3 AS5 localization in the hippocampus is the inner molecular layer (IML) of the dentate gyrus, the site were axons of cholecystokinin (CCK)-expressing interneurons arborise (also referred to as “hilar cells with axon terminals in the commissural and association pathway termination field”, HICAP) [56-58]. Detailed examination of NRXN3 AS5^{HA} protein localization in the IML revealed co-localization with the presynaptic cannabinoid receptor 1 (CB1R). Thus, the selective tagging of the NRXN3 AS5 proteoform uncovered an unexpected cell type-specific localization.

Isolation of native Nrxn3AS5 protein complexes

We took advantage of the tagged splice proteoform for affinity isolation of native neurexin-ligand complexes. Shotgun mass-spectrometry of anti-HA immunoprecipitates from detergent-solubilized hippocampus of *Nrxn3 AS5$^{HA/HA}$* mice and comparison to negative control precipitates from wild type mice, identified 8 proteins as candidate NRXN3 AS5 interactors (Fig.3a, Table S1). These interactors encompass a discrete sub-set of known Neurexin ligands, including FAM19A1, FAM19A2, Dystroglycan 1 (DAG1), and Neurexophilin-1 (NXPH1) (Fig.3a) [59-62]. Interestingly, these native NRXN3 AS5 complexes differed significantly from complexes recovered by affinity isolation with anti-NRXN1 antibodies that recover trans-membrane forms of endogenous NRXN1, 2, and 3. Thus, Neuroligins and LRRTMs, two major classes of NRXN1 ligands [1,63,64] were not recovered as native NRXN3 AS5 interactors by shotgun mass-spectrometry (Fig.3b) or Western blotting (Fig.3c, Tables S2, S3).

We hypothesized that this selective recruitment of interactors by the native NRXN3 AS5 protein might be due to alternative splice insertions at additional alternative segments that gate these ligand interactions. To test this, we developed and optimized splice isoform-specific targeted parallel reaction monitoring (PRM) assays [65,66]. Conventional shotgun proteomics stochastically samples a random portion of the proteome. By contrast, PRM assays use optimized separation and detection for a subset of pre-selected proteotypic

peptides (PTPs) that are specific to a protein or proteoform of interest. PTPs are detected based on their chromatographic retention time and mass to charge ratio of pre-selected fragments (transitions) with an isotopically labeled reference peptide serving an internal standard for quantification. Remarkably, NRXN3AS5 proteins immunoprecipitated from mouse hippocampal tissue contained almost exclusively alternative insertions at AS3 and AS4 with partial use of insertions at AS6 (Fig.3d, S3a,b). Notably, AS4 insertions significantly reduce affinity for interaction with neuroligins and LRRTMs, thus, providing a potential mechanism for the observed ligand selectivity of native NRXN3AS5. In sum, this analysis uncovers a selective synaptic splice code for hippocampal GABAergic neurons at the protein level.

Deletion of a single alternative exon at AS5 results in the loss of NRXN3 protein

To explore the functional relevance of NRXN3 AS5 proteoforms, we generated AS5 knock-out mice by Crispr/Cas9-mediated genome editing with two guide RNAs targeting sequences flanking exon 24. Non-homologous end joining resulted in a 1,309 bp deletion which removed the entire alternative exon 24 (*Nrxn3*$^{\Delta Ex24}$ mice, Fig.4a). Heterozygous and homozygous *Nrxn3*$^{\Delta Ex24}$ mice were born at Mendelian frequencies and were fertile. However, mice exhibited significantly reduced weight (Fig.S4a,b). The mRNA levels of the primary Neurexin transcripts (*Nrxn1,2,3* α and β) were unchanged in the hippocampus of *Nrxn3*$^{\Delta Ex24}$ mice (Fig.4b). Given the presence of multiple downstream acceptor sites in exon 25 (25a, 25b, 25c) we examined which of these sites would be incorporated in *Nrxn3* mRNA lacking the alternative exon at AS5. Semi-quantitative and quantitative PCR confirmed the loss of exon 24 and uncovered a significant increase in exon 25a, whereas (the constitutive) exon 25c was unaltered (Fig.4c). This suggests that in the absence of exon 24, the majority of pre-mRNAs in cells that previously produced AS5+ isoforms, now splice into the downstream 25a acceptor (Fig.4d). This interpretation was further supported by semi-quantitative PCR with oligonucleotide primers flanking AS5 which identified as the

dominant mRNA isoforms in mouse hippocampus the exon 23 - exon 24 - exon 25a containing mRNA isoforms in wild-type and exon 23 - 25a containing mRNA isoforms in *Nrxn3*$^{\Delta Ex24}$, respectively (Fig.4d). This mRNA isoform pattern predicts that the GPI-anchored NRXN3 AS5 proteoform is highly abundant in wild-type mice and is converted into transmembrane NRXN3 proteoforms containing sequences encoded by the longest form of exon 25 (using the alternative acceptor site 25a) in *Nrxn3*$^{\Delta Ex24}$ mice. We then applied targeted proteomics (PRM) to directly quantify Neurexin proteoforms in the mutant mice. Surprisingly, peptides encoded by exon 25a were not detectable in wild-type or *Nrxn3*$^{\Delta Ex24}$ mice, despite sensitive detection of recombinant proteins in the same assay (Fig.4f and S3c). The canonical transmembrane NRXN3 proteoforms (detected based on 25b and 25c-encoded peptide sequences) were slightly increased (Fig.4f). This suggests that in *Nrxn3*$^{\Delta Ex24}$ mice the exon 25a containing, highly abundant *Nrxn3* mRNA isoform either does not produce protein or that the resulting protein is instable. Consistent with this observation, the total NRXN3 protein level (assessed with pan-NRXN3 PRM assays detecting α and β isoforms) was reduced by 61$\pm$3 % in the hippocampus of *Nrxn3*$^{\Delta Ex24}$ mice (Fig.4g, similar observations in neocortex, and cerebellum, Fig.S3d). Considering this surprising mis-match between *Nrxn3* mRNA and protein output we hypothesized that exon 25a might confer translational silencing of the resulting mRNAs. To test this, we examined translational output from luciferase reporters containing as 3'UTR the various exon 25 sequences including or lacking 25a in Neuro2A cells. Indeed, we observed a strong exon 25a-dependent repression of mRNA translation (Fig.4h, no alteration in mRNA abundance for the reporters of various Nrxn3 isoforms). Collectively, this data demonstrates that upon deletion of *Nrxn3* Exon 24, the *Nrxn3* mRNAs incorporate Exon 25a which results in a loss of NRXN3 protein through translational repression.

Loss of NRXN3 AS5 results in impaired synaptic transmission at CCK interneuron synapses

To uncover the consequences of loss of GPI-anchored NRXN3 AS5 in the *Nrxn3*$^{\Delta Ex24}$ mice we examined synaptic transmission in the dentate gyrus, a region where the endogenous NRXN3AS5 protein is highly concentrated at CCK interneuron synapses in the IML (see Fig.2). Recording of spontaneous inhibitory postsynaptic currents from dentate granule cells uncovered a significant reduction in amplitudes (Fig.5a-c; 59.60 vs 48.08 pA, p=0.0008, n=35, N=12-16 mice/genotype), without detectable alterations in the frequency and kinetics (Fig.5d). Immunohistochemical assessment revealed no significant alterations in the density of VGAT or gephyrin-positive puncta in the dentate gyrus (Fig.S4c-e). However, there was a trend towards a reduction in VGAT/gephyrin double-positive punctate structures in the IML, suggesting a potential impairment in the development of CCK interneuron synapses onto dentate granule cells (Fig.S4f). To obtain further insight in to the source of this alteration in spontaneous postsynaptic currents, we selectively evoked synaptic currents by stimulation of axons in the IML and GCL. While evoked transmission in the GCL was unchanged, there was a significant reduction of postsynaptic currents evoked by IML stimulation (Fig.5e-h). Paired-pulse and stimulation intensities used to evoke these currents were comparable between genotypes. Notably, evoked glutamatergic transmission was unchanged. These experiments demonstrate that the loss of NRXN3 protein resulting from AS5 ablation is accompanied by a highly selective impairment of GABAergic transmission in the dentate gyrus.

Discussion

The Neurexin family of adhesion molecules are critical regulators of synapse formation and function, and, mutation in human *NRXN* genes predispose to neurodevelopmental disorders [1,3]. Transcriptomic mapping supports broad expression of a large number of distinct Neurexin mRNA splice isoforms. However, due to the major challenge of detecting

corresponding neurexin proteoforms, the localization and function of the resulting proteins has remained largely unclear. Appending epitope-tags that visualize all proteoforms derived from the *Nrxn1* gene has uncovered important new insights into the transport and sub-cellular localization of the NRXN1 protein [10,67]. In the present study, we developed and applied quantitative approaches for the analysis of individual proteoforms defined by specific alternative splicing events in *Nrxn3*. We find that in the hippocampus, AS5-containing non-canonical NRXN3 proteoforms are GPI-anchored and almost exclusively expressed in GABAergic interneurons. NRXN3 AS5+ forms concentrate at GABAergic synapses and interact with a distinct sub-set of endogenous Neurexin ligands. We further demonstrate that the alternative *Nrxn3* exon 25a imposes powerful translational silencing and, thus, gates NRXN3 protein expression in vivo. Remarkably, ablation of the NRXN3 AS5 alternative exon results in a major loss of NRXN3 protein in the absence of changes in overall *Nrxn3* transcript levels. This severe loss of the NRXN3 protein is accompanied by defects in synaptic transmission at GABAergic CCK interneuron synapses of the dentate gyrus.

The significant dissociation between NRXN3 proteoform and transcript expression highlights the value and importance of proteoform-centric investigation in studies of neuronal wiring.

Previous work on transcript isoforms containing or lacking an alternative exon at AS4 support cell type-specific function of AS4+ and AS4- isoforms [22,29-31,49,54]. Here, *Nrxn3* AS4+ and AS4- transcript isoforms exhibit highly differential expression in parvalbumin interneurons versus *cornu ammonis* pyramidal cells of the mouse hippocampus [29,54] and manipulation of the AS4 mRNA isoforms impairs glutamatergic transmission and plasticity in the hippocampus isoforms [22,29-31]. By contrast, *Nrxn3* AS5+ and AS5- transcript isoforms do not exhibit dramatically divergent expression across cell types investigated to date. However, the resulting NRXN3 AS5 proteoforms exhibit selective expression in GABAergic neurons and synapses and their ablation produces synapse-specific

phenotypes. Thus, the targeted, proteoform-centric workflow established here provides an important complement to the recently developed approaches for local shotgun proteomics [12,17,68]. Databases documenting validated targeted proteomic assays have been instrumental in accelerating their use, in particular in clinical settings for human pathologies [69-71]. To enable the broader application of such assay for studies on neuronal wiring we created a public database with validated targeted proteomic assays of synaptic proteins and specific proteoforms (SYNCODE).

Methods

Animals

All procedures involving animals were approved by and performed in accordance with the guidelines of the Kantonales Veterinäramt Basel-Stadt. All lines were maintained on a C57Bl6/J background. Mice generated for this study were backcrossed to Bl6 mice for > 8 generations.

Generation of Nrxn3$^{\Delta Ex24}$ mice

Nrxn3 AS5 knock-out mice were generated by Cas9/CRISPR embryo microinjection. gRNAs targeting sequences in intron 23 (INT23) gcagtagtacaaatcatggg(tgg) and intron 24 (INT24) gagagcaaataataccaata(agg) (PAM sequence in brackets) of the Nrxn3 gene were selected with the help of CRISPOR software (http://crispor.tefor.net/). ssDNA oligonucleotides for LoxP_INT_23 (tggaacaacttcagctgcaggacctcacatcctcacctttcagatgagct agtctcattggcagtagtacaaatcatt**ataacttcgtataatgtatgctatacgaagttat**gggtggcttatgcaaggtgga tgatgtcatttggaatataccatttctctacagaggactcaatagcatcctggtatgtggactctgc) and LoxP_INT_24 (tagcttctatattgttatttctctttgtttgtgttcttatattgtgaatgccttattggtattatttgctctccttctt**ataacttcgtataatgt atgctatacgaagttat**ggtatcatttgctatcttctgcttaatttgttttggctatgatgttggttttatttttcttctatctgtatgattttga aaactata) were designed to insert LoxP sites (in bold) into the Cas9-genereted DSBs by homologous recombination with the help of 5' and 3' homology arms.

Insertion of LoxP sites was carried out using Cas9/CRISPR directly in fertilized mouse oocytes. C57BL/6J female mice underwent ovulation induction by i.p. injection of 5 IU equine chorionic gonadotrophin (PMSG; Folligon–InterVet), followed by i.p. injection of 5 IU human chorionic gonadotropin (Pregnyl–Essex Chemie) 48 h later. For the recovery of zygotes, C57BL/6J females were mated with males of the same strain immediately after the administration of human chorionic gonadotropin. All zygotes were collected from oviducts 24 h after the human chorionic gonadotropin injection and were then freed from any remaining cumulus cells by a 1–2 min treatment of 0.1% hyaluronidase (Sigma-Aldrich) dissolved in M2 medium (Sigma-Aldrich). Mouse embryos were cultured in M16 (Sigma-Aldrich) medium at 37°C and 5% CO_2. For micromanipulation, embryos were transferred into M2 medium. All microinjections were performed using a microinjection system comprised of an inverted microscope equipped with Nomarski optics (Nikon), a set of micromanipulators (Narashige), and a FemtoJet microinjection unit (Eppendorf). Injection solution containing: Cas9 protein (IDT) 100ng/ul (60uM), cr:trcrRNA INT23 (IDT) 50uM, cr:trcrRNA INT24 (IDT) 50uM, LoxP_INT_23 oligo 10ng/ul, LoxP_INT_24 oligo 10ng/ul was microinjected into the male pronuclei of fertilized mouse oocytes until 20-30% distension of the organelle was observed.

Embryos that survived the microinjection were transferred on the same day into the oviducts of 8–16-wk-old pseudopregnant Crl:CD1 (ICR) females (0.5 d used after coitus) that had been mated with sterile genetically vasectomized males the day before embryo transfer [72]. Pregnant females were allowed to deliver and raise their pups until weaning age.

In total 510 embryos were microinjected and 372 surviving embryos were transferred into 18 foster mothers. 16 foster mothers produced live litters with a total of 65 viable F0 pups. Five F0 pups carried a deletion for Exon 24. Selected founder animals were bred to C57BL/6J partner to establish the *Nrxn3*$^{\Delta Ex24}$ mouse line.

Generation of Nrxn3-AS5^{HA} mice

The Nrx3-HA allele was obtained by Cas9/CRISPR embryo electroporation. The HA tag was added to the splice site 5 of Nrx3 thereby tagging all alternatively spliced Nrx3 transcripts. The Cas9/CRISPR target sequence atgtccatgtaagggcggca(cgg) (PAM sequence in brackets) was selected with the help of CRISPOR software (http://crispor.tefor.net/). ssDNA oligonucleotide cttccttacagccagaagctctattgcagct**tacccat acgatgttcctgactatgcg**ggc**tatccctatgacgtcccggactatgca**ggaacagccagaagctctaacgcggc gagatcactacgtgccgcccttacatggacatggcgactcacttacacact was designed to insert a double HA tag (in bold) into the Cas9-genereted DSB by homologous recombination with the help of 5' and 3' homology arms (underlined). C57BL/6J female mice underwent ovulation induction by i.p. injection of 5 IU equine chorionic gonadotrophin (PMSG; Folligon–InterVet), followed by i.p. injection of 5 IU human chorionic gonadotropin (Pregnyl–Essex Chemie) 48 h later. For the recovery of embryos, C57BL/6J females were mated with males of the same strain immediately after the administration of human chorionic gonadotropin. Embryos were collected from oviducts 24 h after the human chorionic gonadotropin injection, and were then freed from any remaining cumulus cells by a 1–2 min treatment of 0.1% hyaluronidase (Sigma-Aldrich) dissolved in M2 medium (Sigma). Prior to electroporation, the zona pellucida was partially removed by brief treatment with acid Tyrode's solution and the embryos were washed and briefly cultured in M16 (Sigma) medium at 37°C and 5% CO_2. Electroporation with a mixture of ssDNA oligonucleotide targeting template, 16uM cr:trcrRNA hybrid targeting Nrx3 and 16uM Cas9 protein (all reagents from IDT) was carried out using 1mm gap electroporation cuvette and the ECM830 electroporator (BTX Harvard Apparatus). Two square 3 ms pulses of 30V with 100 ms interval were applied as previously described [73]. Surviving embryos were washed with M16 medium and transferred immediately into the oviducts of 8–16-wk-old pseudopregnant Crl:CD1(ICR) females that had been mated with sterile genetically vasectomized males [72] the day before embryo transfer (0.5 dpc). Pregnant females were allowed to deliver and raise their pups until weaning age.

In total 295 embryos were electroporated and 276 surviving embryos were transferred into 12 foster mothers. All foster mothers produced live litters with a total of 53 viable F0 pups. One F0 pup carried the correctly integrated HA tag. The founder animal was bred to C57BL/6J partner to establish the Nrx3-HA mouse line.

Cell Culture

HEK293T, Cos7 and Neuro2A cells were maintained in DMEM (Sigma D5796) containing glucose (4500mg/l) supplemented with 10% fetal calf serum (FCS) and Penicillin/Streptomycin at 37°C/5% CO_2. Transfections were done with Gibco™ Opti-MEM™ reduced serum medium and FuGENE® 6 transfection reagent according to the manufacturer instructions with a DNA to Fugene ratio of 1:3, amounts of DNA are specified in individual experiments.

Cortical cultures were prepared from E16.5 mouse embryos. Neocortices were dissociated by addition of papain (130 units, Worthington Biochemical LK003176) for 30 min at 37°C. Cells were maintained in neurobasal medium (Gibco 21103) containing 2% B27 supplement (Gibco 17504-044), 1% Glutamax (Gibco 35050-038), and 1% penicillin/streptomycin (Sigma P4333). Cortical cultures were treated for 4 hours on DIV12 with transcription and/or translation inhibitors (Actinomycin D (Sigma, A1410), Cycloheximide (Sigma, C1988) in a final concentration of 0.02%DMSO before lysis.

For hippocampal cultures, Hippocampi from P0 animals were dissected, trypsinized for 10 min in 0.05% trypsin (Gibco 25300) buffered with 10mM HEPES (Gibco 15630) at 37°C, washed 3x with HBSS (Gibco 14025) buffered with 10mM HEPES and titurated using a fire-polished glass Pasteur pipette. Cells were plated at a density of 10-12'000 cells per cm^2 on poly-D-lysine (Sigma P7886) coated glass coverslips in DMEM (Sigma D5796) containing 1% Penicillin/Streptomycin (Sigma P4333) and 10% fetal bovine serum (Gibco 10270). 4-6 h after plating, media was changed to serum-free Neurobasal media (Gibco 21103) supplemented with 2 mM GlutaMax (Gibco 35050), B27 supplement (Gibco 17504) and 1% penicillin/streptomycin (Sigma P4333). Cells were then grown at 37°C / 5% CO_2.

Western Blot HA mice

For detection of HA-tagged Nrxn3 different brain regions (Cortex, Hippocampus and Cerebellum) from P28 homozygous Nrxn3-AS5^{HA} mice or wildtype littermates were homogenized in 50mM Tris-HCL pH7.5, 150mM NaCl, 1% Triton-X100 and 1mM EDTA suppl. with protease inhibitors (Roche cOmplete™ mini) in a glass-teflon homogenizer. Lysates were centrifuged for 10 min, 16'000g at 4°C and supernatants analyzed by Western-Blot.

Membrane Fractionation HA mice

Tissue from different brain regions (Cortex, Hippocampus and Cerebellum) of P25-P30 mice was homogenized in 0.32M Sucrose, 50mM HEPES pH7.4 supplemented with protease inhibitors (Roche complete™ mini) using a glass-teflon homogenizer. Lysate was centrifuged for 5 min at 16'000g, supernatants (Input fractions) centrifuged for 60 min at 100'000g (TLA55 rotor, Optima™ MAX-XP Ultracentrifuge) and the pelleted membranes were re-suspended in high salt buffer (1M NaCl, 10mM EDTA suppl. with protease inhibitors). Membranes were centrifuged for 60 min at 100'000g and high-salt membranes were re-suspended in 150mM NaCl, 10mM EDTA. Proteins for all fractions were precipitated by methanol/chloroform method and analyzed by Western Blot.

Membrane Fractionation Alkaline Phosphatase Constructs

HEK293 cells were transfected with two different transcripts (AP-eGPI and AP-nGPI; 2µg DNA per 6-well dish), cells were washed once with PBS 24-hour after transfection and re-suspended in homogenization buffer (0.32M sucrose, 50mM HEPES, pH 7.4, supplemented with protease inhibitors (Roche complete™ mini protease inhibitors)). Cells were homogenized with a 28G syringe and centrifuged for 5 min at 15'000g. Generated supernatants were centrifuged for 60 min at 100'000g (TLA55 rotor, Optima™ MAX-XP Ultracentrifuge) and the pelleted membranes were re-suspended in high salt buffer (2M KCl, 10mM EDTA, supplemented with protease inhibitors) and centrifuged again for 60min

at 100'000g. High salt treated membranes were re-suspended in 10mM HEPES and proteins for all fractions were precipitated by methanol/chloroform method and analyzed by Western Blot.

Ethanolamine Labelling

For radioactive labeling, transfected HEK-cells (Nrxn3-GPI, Nrxn3-TM, AP-eGPI) were incubated 4 hours after transfection with 1.25% ^{3}H-Ethanolamine or non-radioactive Ethanolamine overnight at 37°C/5% CO_2. Cells were lysed in 1ml IP-Buffer (50mM Tris-HCl pH 7.5, 150mM NaCl, 10% Glycerol, 1% Triton-X100, 0.1% SDS, supplemented with protease inhibitors) and the cell lysate was centrifuged for 15 min at 16'000g, 4°C. The supernatant was transferred to a new tube and incubated overnight at 4°C with 20µl anti-HA coupled magnetic beads (Pierce, 88837). Samples were incubated overnight with end-over-end rotation at 4°C. Cell suspensions were washed 4x in IP-Buffer and resuspended after the last step in 30µl 1x Lämmli-Buffer. All samples were boiled for 10 min at 95°C and then loaded onto a SDS-PAGE gel, gels were run for 15 min at 80V and 90 min at 120V. Non-radioactive samples were processed by Western Blot and radioactive gels were incubated for 30 min in fixation solution (25% Isopropanol, 10% Acetic Acid) and 30 min in Amplify Fluorographic reagent (GE Healthcare Life Sciences). Gels were dried overnight with a vacuum pump at 60°C and exposed to X-ray film (Amersham Hyperfilm MP, GE Healthcare Life Sciences) up to 2 months.

Immunohistochemistry procedures

Mice from postnatal day 25 to 30 were deeply anesthetized and trans-cardially perfused with fixative (4% paraformaldehyde and 15% saturated picric acid in 100mM phosphate buffer, pH 7.4). Brains were post-fixed overnight in same fixative at 4°C. Fixed brains were washed 3 times with PBS and kept overnight at 4°C in 30% Sucrose in 100mM phosphate buffer before cryo-protection in OCT. Coronal brain slices were cut at 30µm with a Cryostat (Microm HM560, Thermo Scientific). For immunohistochemistry, brain sections were kept

in PBS before incubation for 0.5-1 hour with blocking solution containing 0.1% Triton X-100 and 10% normal donkey serum. Slices were incubated with primary antibodies in blocking solution at 4°C two times overnight and washed three times in PBS containing 0.05% Triton X-100, followed by incubation for 1-2 hours at room temperature with a secondary antibody. Sections were washed three times in PBS before mounting onto microscope slides with Fluoromount-G (SouthernBiotech, 0100-01). Hoechst dye was co-applied during washing at a final concentration of 0.5 µg/ml. Images were acquired at room temperature on a confocal microscope (Zeiss LSM700), using 20x, 40x and 63x Plan-Apochromat objectives (numerical aperture 0.45 and 1.40, respectively) and were then processed by using Fiji and Omero.

Hippocampal cells were fixed for 10 min using 4% PFA / 4% sucrose in 0.1M phosphate buffer pH 7.4 at room temperature (RT), washed 3x with 1x PBS, quenched 10 min with 0.1M glycine and blocked for 1h at RT with 10% normal donkey serum and 0.1% Triton-X100 in PBS. Primary antibodies were applied overnight at 4°C in blocking solution. After 4 washes with PBS, fluorophore-coupled secondary antibodies were applied 60 min at RT. Cells were then washed 3x with PBS, once with deionized water, mounted using Fluoromount G (Southern Biotech #0100-01), and dried at RT. Hoechst dye was co-applied during washes at a final concentration of 0.5 µg/ml. Stained cells were imaged on a Zeiss LSM 700 confocal microscope using a 63x Plan-Apochromat objectives (numerical aperture 1.40).

Transfected Cos7 cells grown on cover-slips (with AP-eGPI and AP-nGPI; 1µg DNA per 12-well dish) were fixed 24hrs after transfection with 4% PFA / 4% Sucrose in PBS for 10 min and stained with primary Antibodies in 1% BSA/PBS overnight at 4°C followed by Alexa-568 conjugated secondary antibodies. Nuclei were stained with Hoechst and coverslips were mounted on glass plates.

The following commercially available antibodies were used in this study: rat anti HA (Roche, Clone 3F10, 11867431001), rabbit anti β-actin (Abcam, ab8227), rabbit anti HA (Cell Signaling, 3724), mouse anti GAD67 (Millipore, MAB5406), goat anti parvalbumin

(Swant, PVG214), goat anti somatostatin (Santa Cruz, sc7618), guinea pig anti cholecystokinin (Synaptic Systems, 438004), mouse anti cannabinoid receptor 1 (Immunogene, IMG-CB1R-mAb001), guinea pig vGlut1 (Chemicon, AB5905), guinea pig anti vGAT (Synaptic Systems, 131004), mouse anti PSD95 (Santa Cruz, sc32290), mouse anti gephyrin (Synaptic Systems, 147011), mouse anti gephyrin (Synaptic Systems, 147021), mouse anti CamKII alpha (Thermo Fisher Scientific, Ma1-048), mouse anti calbindin (Swant, 300). The rabbit panNL antibody [74] and the pan-NRXN antibody [29] have been described previously.

Fluorophore-coupled secondary antibodies were from Life Technologies (Alexa Fluor 568 goat anti-rat A11077) and Jackson ImmunoResearch (Cy2 donkey anti-goat 705-225-147, Cy2 donkey anti-guinea pig 706-225-148, Cy3 donkey anti-rabbit 711-165-152, Cy3 donkey anti-mouse 715-165-151, Cy3 donkey anti-goat 705-165-147, Cy5 donkey anti-mouse 715-175-511, Cy5 donkey anti-rabbit 711-175-152). Hoechst 33342 dye (Sigma #B2261) was used for nuclear staining.

Secondary antibodies coupled to horse radish peroxidase (HRP) were from Jackson ImmunoResearch (goat anti-rabbit HRP 111-035-003; goat anti-rat HRP 112-035-143). For enhanced chemiluminescence detection, WesternBright ECL kit (Advansta K-12045-D20) and WesternBright Quantum (Advansta K-12042-D20) were used. Signals were acquired using an image analyzer (Bio-Rad, ChemiDoc MP Imaging System and Li-Cor, Odyssey) and images were analyzed using ImageJ.

RNA analysis

For RNA isolation, brain tissue or cultured cells were dissected or washed in ice-cold PBS respectively, homogenized in 1 ml TRI Reagent (Sigma T9424) and thoroughly mixed with 200 µl chloroform (Sigma 2432). Samples were centrifuged at 16’000 g, 4°C for 15 min. The aqueous phase was used for RNA purification with the RNeasy Plus Mini kit (Qiagen 74134) or RNeasy Micro kit (Qiagen 74034) following the manufacturer’s instructions, including on-column DNase-treatment to remove traces of genomic DNA. 0.5µg of total

RNA was reverse transcribed using random hexamers (Promega C1181) or Oligo(dT)$_{15}$ primer (Promega C1101) for flanking primer analysis and ImProm II reverse transcriptase (Promega A3802).

Sashimi plots were generated from published RNA-Seq data [19] using the MISO software package [75].

For qPCR assays, two technical replicates were run per experiment and the mean was calculated. The mRNA levels were normalized to *gapdh* mRNA. qPCR assays were analyzed with StepOne software. Flanking primer PCRs were run with FirePol Master mix (Solis BioDyne, 04-11-00125) on mRNA reverse transcribed with Oligo(dT)$_{15}$ Primer, PCR cycle numbers were carefully titrated to ensure correct amplification range and avoid signal saturation. DNA Oligonucleotides used with SYBR Green-based real-time PCR and for flanking primer PCRs are listed in Table S4.

Luciferase Assays

Nrxn3 3'UTR sequences were amplified from genomic DNA and inserted into the dual luciferase psiCHECK-2 vector (Promega) after the Renilla luciferase open reading frame. The resulting 3'UTR sequences are listed in Table S4. Neuro2a cells were plated at 20,000 cells/well in a 96 well plate. After 24h, cells were transfected with 50 ng dual luciferase construct containing different 3'UTRs of Nrxn 3. Empty vector ("no UTR" containing only Firefly luciferase and Renilla luciferase) was used as a control. Cells were collected after 24 hours for processing using the Dual-Luciferase reporter assay kit (Promega, E1910) or for purification of RNA. Renilla and firefly luciferase activity was measured using a Tecan Sparks plate reader and Renilla luciferase activity was normalized to firefly activity. mRNA levels were quantified by RT-qPCR using primers against Renilla and Firefly cDNA.

hRluc for: TCC AGA TTG TCC GCA ACT AC

hRluc rev: CTT CTT AGC TCC CTC GAC AAT AG

fluc for: CAT TCT TCG AGG CCA AGG T

fluc rev: TTC ACG TAG CCG GAC ATA ATC

Neurexin Immunopurification

Hippocampi from P28 animals (wild type or KI) were dissected, snap frozen and kept at -80°C until use. For immunoprecipitation hippocampi were homogenized by 30 strokes in glass-homogenizer in 2 mL per 2 x hippocampi of IP-buffer (50 mM Tris–HCl, pH7.5, 150 mM NaCl, 10% glycerol) completed with protease inhibitors (Roche), 1% Triton X-100, and 2 mM CaCl2. Homogenates were centrifuged at 16.000 x g for 15 min at 4°C. Supernatants were transferred in new tubes (ca. 1.8 mL per IP). For IPs of HA-tagged Nrx3-AS5 lysates from KI or WT animals were incubated for 2 h at 4°C with rotation and centrifuged again at 16.000 x g for 5 min at 4°C. Supernatants were transferred to new tubes and 18 μL of HA-magnetic beads (Pierce / Thermofisher) per 1.8 mL lysate. Samples were incubated for 6 h at 4°C with rotation before wash. For IPs with pan-NRX antibody 1 μg homemade affinity purified antibody or rabbit IgG per 1 mL lysate were added. Samples were incubated for 4 h at 4°C with rotation and then centrifuged at 16.000 x g for 5 min at 4°C. Supernatants were transferred into new tubes and 18 μL of Protein-A-dynabeads (Thermofisher) were added to the samples. Samples were incubated for additional 2 h at 4°C with rotation before wash. For both, HA- and pan-Nrx IPs, beads were washed 3 x with IP-buffer, transferred to new tubes and then washed 3 x with IP-wash buffer (50 mM Tris–HCl, pH7.5, 150 mM NaCl, 10% glycerol) completed with 0.1% Triton X-100, and 2 mM CaCl2. Bound proteins were eluted from beads by incubation in 50 μL elution buffer (1% SDS, 5 mM DTT) for mass spectrometry or 40 μL elution buffer for western blot analysis at 65°C for 10 min. Eluted proteins were transferred into new low-binding tubes and used for western blot or mass spectrometric analysis, respectively.

Preparation of samples for mass spectrometry: 8 μL of eluted proteins were transferred to a new tube and used for validation of IP by western blot. To the rest (42 μL) and to overexpressed splice insertion controls (Nrxn3α-AS3(+)-AS4(+)-AS6(+), expressed in

HEK-cells, reported before [29]) one volume of 2x MS-lysis buffer (200mM Triethyl-ammonium bicarbonate (TEAB / Sigma), 10% SDS, 20mM Tris-(2-carboxyethyl)-phosphin (TCEP / Sigma)) were added. Samples were incubated for 10 min at 95°C. Samples were cooled down to RT, 1.7 µL of 1M iodoacetamide (Sigma) were added and samples were incubated for 30 min (in dark) at RT. Subsequently samples were acidified by addition of 8.5 µL of 12% phosphoric acid and mixed 1:6 with S-trap buffer (90% methanol, 100 mM TEAB). Samples were loaded (3 x ca. 180 µL) on the S-trap micro columns (Protifi), spoon down for 15 sec at 4000 x g and washed 3 x with S-trap buffer. 20 µL of trypsin solution (2.5 µL trypsin (0.4 µg/ µL Promega) in 50 mM TEAB)) were added on the columns and samples incubated 47°C for 1h. Peptides were eluted from the columns 3 x times: 1x with 40 µL 50 mM TEAB, 1x with 40 µL 0.2% formic acid in H_2O and 1x with 40 µL 0.2% formic acid in 50% acetonitrile. Eluted peptides were vacuum dried and re-suspended in 20 µL LC/MS-buffer (2% acetonitrile 0.15% formic acid). For targeted proteomics, to each peptide sample an aliquot of a heavy reference peptide mix containing chemically synthesized proteotypic peptides (Spike-Tides, JPT, Berlin, Germany) was spiked into each sample at a concentration of 20 fmol of heavy reference peptides per sample.

Western blot analysis: 10 µL of 5x SDS-PAGE sample buffer were added to the 40 µL of the eluate. Samples were boiled for 5 min at 95°C. 50% (25 µL) of samples or 12 µL of input (corresponding to approximately 1 % of lysate) per lane were separated on the 4-20% gradient gel. After transfer to a nitrocellulose membrane and blocking with 5% milk in TBST samples were probed with primary antibodies.

Sample preparation targeted proteomics on *Nrxn3$^{\Delta Ex24}$* mice

Brain tissues were lysed and alkylated in lysis buffer (1% sodium deoxycholate (SDC), 0.1 M TRIS, 15mM chloroacetamide, 10 mM TCEP, pH = 8.5) by homogenization with a 21G syringe followed by strong ultra-sonication (10 cycles, Bioruptor, Diagnode). Samples were reduced for 10 min at 95 °C and digested by incubation with sequencing-grade modified

trypsin (1/50, w/w; Promega, Madison, Wisconsin) overnight at 37°C. Then, the peptides were cleaned up using iST cartridges (PreOmics, Munich) according to the manufacturer's instructions. Samples were dried under vacuum and stored at -80 °C until further use. Samples were resuspended in 0.15% Formic acid and 2% Acetonitrile. To each peptide sample an aliquot of a heavy reference peptide mix containing chemically synthesized proteotypic peptides (Spike-Tides, JPT, Berlin, Germany) was spiked into each sample at a concentration of 2 fmol of heavy reference peptides per 1µg of total endogenous protein mass.

Assays were validated by titrating recombinant proteins. A DNA construct for bacterial expression of the NRXN3 C-terminal fragment containing exons 25a,25b and 25c was generated as follows: Fragment encoding for exon 23-25a,b,c was PCR amplified from brain cDNA using following primers NRX3-Ex23-BspEI-FWD (5'-ACAAGTCCGGACCCACGTCAGATGATCTTGTTTC-3') and NRX3-Ex25-(w/o stop)-XhoI-REV (5'-ATACTCTCGAGCACATAATACTCCTTGTCCT TGTTTTTC-3'). Resulting PCR fragment was digested with BspEI and XhoI and ligated into pEGFP-C1 plasmid digested with the same restriction enzymes. 1 µL of ligation reaction was used as template to PCR amplify the GFP-Nrx3 fusion construct using following primers: GFP-NdeI-FWD (5'-ATATACATATGGTGAGCAAGGGCGAGGAG-3') and NRX3-Ex25-(w/o stop)-XhoI-REV. The resulting PCR product was digested with NdeI and XhoI and ligated into pET29b(+) plasmid digested with the same restriction enzymes.

GFP-constructs with added Nrxn3 Exon25 sequence were purified from transformed and induced E.coli (5µmol IPTG in 200ml medium). Cells were lysed with 50mM NaH_2PO_4, 300mM NaCl, pH 8.0 with 1mg/ml lysozyme, bound with cobalt beads (Talon Metal Affinity Resin, Clontech) and eluted in 50mM NaH_2PO_4, 300mM NaCl, 250mM imidazole with 6M Urea. For neutralization 3:1 0.1M Ammoniumbicarbonate was added, samples were reduced and alkylated for 60min at 37°C with 10mM TCEP and 15mM Chloroacetamide and digested by incubation with sequencing-grade modified trypsin (1/50, w/w; Promega, Madison, Wisconsin) overnight at 37°C. Then, the peptides were cleaned up using iST

cartridges (PreOmics, Munich) according to the manufacturer's instructions. Samples were dried under vacuum and stored at -80 °C until further use. Samples were resuspended in 0.15% Formic acid and 2% Acetonitrile and the dilution curve was prepared using HEK-lysate and heavy peptides.

Shotgun LC-MS analysis of Neurexin immunoprecipitates

1 ug of peptides of each sample were subjected to LC–MS analysis using a dual pressure LTQ-Orbitrap Elite mass spectrometer connected to an electrospray ion source (both Thermo Fisher Scientific) as described [76] with a few modifications. In brief, peptide separation was carried out using an EASY nLC-1000 system (Thermo Fisher Scientific) equipped with a RP-HPLC column (75 µm × 45 cm) packed in-house with C18 resin (ReproSil-Pur C18–AQ, 1.9 µm resin; Dr. Maisch GmbH, Ammerbuch-Entringen, Germany) using a linear gradient from 95% solvent A (0.15% formic acid, 2% acetonitrile) and 5% solvent B (98% acetonitrile, 0.15% formic acid) to 28% solvent B over 60 min at a flow rate of 0.2 µl/min. The data acquisition mode was set to obtain one high resolution MS scan in the FT part of the mass spectrometer at a resolution of 120,000 full width at half-maximum (at m/z 400) followed by MS/MS scans in the linear ion trap of the 20 most intense ions using rapid scan speed. The charged state screening modus was enabled to exclude unassigned and singly charged ions and the dynamic exclusion duration was set to 30s. The ion accumulation time was set to 300 ms (MS) and 25 ms (MS/MS).

The acquired raw-files were converted to the mascot generic file (mgf) format using the msconvert tool (part of ProteoWizard, version 3.0.4624 (2013-6-3)). Using the MASCOT algorithm (Matrix Science, Version 2.4.0), the mgf files were searched against a decoy database containing normal and reverse sequences of the predicted entries of *mus musculus* (SwissProt, www.uniprot.org, release date 26/09/2018) including all splice variants of interest plus commonly observed contaminants (in total 34,770 sequences) generated using the SequenceReverser tool from the MaxQuant software (Version 1.0.13.13). The precursor ion tolerance was set to 10 ppm and fragment ion tolerance was

set to 0.02 Da. The search criteria were set as follows: full tryptic specificity was required (cleavage after lysine or arginine residues unless followed by proline), 2 missed cleavages were allowed, carbamidomethylation (C), was set as fixed modification and oxidation (M) as a variable modification. Next, the database search results were imported to the Scaffold software (version 4.3.2, Proteome Software Inc., Portland, OR) and the protein false identification rate was set to 1% based on the number of decoy hits. Specifically, peptide identifications were accepted if they could achieve an FDR less than 1.0% by the scaffold local FDR algorithm. Protein identifications were accepted if they could achieve an FDR less than 1.0% and contained at least 1 identified peptide. Proteins that contained similar peptides and could not be differentiated based on MS/MS analysis alone were grouped to satisfy the principles of parsimony. Proteins sharing significant peptide evidence were grouped into clusters.

Targeted LC-MS analysis of Neurexin immunoprecipitates

In a first step, parallel reaction-monitoring (PRM) assays [77] were generated from a mixture containing 50 fmol of each proteotypic heavy reference peptide (Table S5, JPT Peptide Technologies GmbH). Here, the sample was subjected to LC–MS/MS analysis using a Orbitrap Fusion Lumos Mass Spectrometer fitted with an EASY-nLC 1200 (both Thermo Fisher Scientific) and a custom-made column heater set to 60°C. Peptides were resolved using a RP-HPLC column (75µm × 36cm) packed in-house with C18 resin (ReproSil-Pur C18–AQ, 1.9 µm resin; Dr. Maisch GmbH) at a flow rate of 0.2 µLmin-1. The following gradient was used for peptide separation: from 5% B to 50% B over 60 min o 95% B over 2 min followed by 18 min at 95% B. Buffer A was 0.1% formic acid in water and buffer B was 80% acetonitrile, 0.1% formic acid in water.

The mass spectrometer was operated in DDA mode with a cycle time of 3 seconds between master scans. Each master scan was acquired in the Orbitrap at a resolution of 120,000 FWHM (at 200 m/z) and a scan range from 300 to 1600 m/z followed by MS2

scans of the most intense precursors in the orbitrap at 30,000 FWHM (at 200 m/z) resolution with isolation width of the quadrupole set to 1.4 m/z. Maximum ion injection time was set to 50ms (MS1) and 50 ms (MS2) with an AGC target set to 1e6 and 1e5, respectively. Only peptides with charge state 2 – 5 were included in the analysis. Monoisotopic precursor selection (MIPS) was set to Peptide, and the Intensity Threshold was set to 5e3. Peptides were fragmented by HCD (Higher-energy collisional dissociation) with collision energy set to 35%, and one microscan was acquired for each spectrum. The dynamic exclusion duration was set to 30s.

The acquired raw-files were searched using the MaxQuant software (Version 1.6.2.3) against the same murine database mentioned above using default parameters except protein, peptide and site FDR were set to 1 and Lys8 and Arg10 were added as variable modifications. The best 6 transitions for each peptide were selected automatically using an in-house software tool and imported into SpectroDive (version 10, Biognosys, Schlieren). A unscheduled mass isolation list containing all peptide ion masses was exported form SpectroDive and imported into the Orbitrap Lumos operating software for PRM analysis.

Peptide samples for PRM analysis were resuspended in 0.1% aqueous formic acid, spiked with the heavy reference peptide mix at a concentration of 4 fmol of heavy reference peptides per 1 µg of total endogenous peptide mass and subjected to LC–MS/MS analysis on the same LC-MS system described above using the following settings: The resolution of the orbitrap was set to 30,000 FWHM (at 200 m/z), the fill time was set to 54 ms to reach an AGC target of 1e6, the normalized collision energy was set to 35%, ion isolation window was set to 0.4 m/z and the scan range was set to 150 – 1500 m/z. A MS1 scan at 120,000 resolution (at 200 m/z), AGC target 1e6 and fill time of 50 ms was included in each MS cycle. All raw-files were imported into SpectroDive for protein / peptide quantification. To control for variation in injected sample amounts, the total ion chromatogram (only comprising ions with two to five charges) of each sample was determined and used for normalization. To this end, the generated raw files were imported into the Progenesis QI

software (Nonlinear Dynamics (Waters), Version 2.0), together with one standard shotgun analysis of a pooled sample using the same MS1 and gradient setting. Then, the intensity of all identified precursor ions with a charge of 2+ - 5+ were extracted, summed for each sample and used for normalization. Normalized ratios were transformed from the linear to the log-scale, normalized relative to the control condition and the median ratio among peptides corresponding to one protein was reported.

Electrophysiology

Slice preparation for patch-clamp recordings. Electrophysiological experiments were performed using both male and female *Nrxn3*-AS5KO +/+ and -/- mice between 6 and 8 weeks of age. Animals were anesthetized with isoflurane (4% in O_2, Vapor, Draeger) and killed by decapitation. To increase cell viability, mice were exposed to oxygen-enriched atmosphere for 10 min before decapitation. Slices were obtained as previously described [78,79]. Briefly, the brain was dissected in ice-cold sucrose-based solution (approximately 4°C) which was equilibrated with carbogen (95% O_2/5% CO_2). Transverse 350 µm thick hippocampal slices were cut with an approximate 20° angle to the dorsal surface using a VT1200 vibratome (Leica Microsystems). The sucrose-based solution for cutting and storage contained the following (in mM): 87 NaCl, 25 $NaHCO_3$, 2.5 KCl, 1.25 NaH_2PO_4, 75 sucrose, 0.5 $CaCl_2$, 7 $MgCl_2$ and 10 glucose. Slices were incubated at 35°C for 30 min after cutting and subsequently stored at room temperature until experiments were performed.

Whole-cell voltage-clamp recordings. For electrophysiological recordings slices were transferred to a bath chamber and continuously perfused with oxygenated artificial cerebrospinal fluid (ACSF) containing (in mM): 125 NaCl, 25 $NaHCO_3$, 25 glucose, 2.5 KCl, 1.25 NaH_2PO_4, 2 $CaCl_2$, 1 $MgCl_2$. The ACSF was equilibrated with carbogen (95% O_2/5% CO_2) at room temperature (21-24 °C), resulting in pH 7.4. Dentate gyrus granule cells were visualized using an AxioExaminer.D1 (Zeiss) and infrared differential

interference contrast video microscopy. Patch pipettes were pulled from borosilicate glass tubing with a 2.0 mm outer diameter and 0.5 mm wall thickness (Hilgenberg) using a Flaming-Brown P-97 puller (Sutter Instruments). Patch pipettes had a resistance between 2.5 and 4 MΩ and were filled with an internal solution containing the following (in mM): 140 KCl, 10 EGTA, 10 HEPES, 2 $MgCl_2$, 2 Na_2ATP, 0.3 GTP, 1 phosphocreatine and adjusted to pH 7.3 with KOH. Recordings were obtained using a Multiclamp 700B amplifier (Molecular Devices), filtered at 10 kHz, and digitized at 20 kHz with a CED Power 1401 interface (Cambridge Electronic Design). Data acquisition was controlled using IGOR Pro 6.31 (Wave Metrics) and the CFS library support from Cambridge Electronic Design. Recordings were only included if the initial seal resistance was > 5 times higher than the input resistance of the cells typically ranging from 5-15 GΩ. In most recordings, series resistance (R_s = 10-25 MΩ) was compensated with a correction of 80%, and experiments were discarded if R_s changed by > 25%.

Extracellular synaptic stimulation. For electrical stimulation of synaptic inputs, pipettes (resistance: 5-7 MΩ) were filled with HEPES-buffered 3 M NaCl solution and used to apply brief negative current pulses (0.2 ms). GABAergic PSCs were evoked using low stimulation intensities ranging from 10 to 40 µA. To stimulate both proximal dendritic and perisomatic GABAergic synaptic inputs onto dentate gyrus granule cells, two stimulation pipettes were placed into the outer half of the inner molecular layer (IML) and into the granule cell layer (GCL) near the hilar border. Synapses were stimulated by either single stimuli or double pulses (inter-stimulus interval: 100 ms) to determine paired-pulse ratios for both stimulation sites. To identify possible crosstalk between stimulation electrodes (due to their physical proximity), GCL stimulation pulses and IML stimulation pulses were either applied independently or sequentially (inter-stimulus interval: 100 ms). Recordings were discarded if preceding GCL stimulation changed the amplitude of the IML-evoked postsynaptic current (PSC) by > 20%. To stimulate glutamatergic afferent perforant-path

synapses, the stimulation electrode was placed into the molecular layer. Glutamatergic PSCs were evoked by single pulses with stimulation intensities ranging from 10 to 80 µA.

Data Analysis. Patch-clamp data was analyzed offline using the open source analysis software Stimfit (https://neurodroid.github.io/stimfit; [80]) and customized scripts written in Python. Amplitudes, paired-pulse ratios and decay times of evoked GABAergic and glutamatergic PSCs were analysed using average traces of at least 5 repetitions. For the analysis of spontaneous GABAergic and glutamatergic PSCs a template-matching algorithm, implemented in Stimfit [81,82], was used as described previously [83]. Automatically detected events were visually controlled and false positive events were deleted. The remaining events were fitted with the sum of two exponential functions revealing the amplitude, rise time and decay time of the spontaneous PSCs. Standard electrophysiological parameters were determined using a negative voltage step of 5 mV. The input resistance was calculated measuring the plateau current in response to the voltage step, whereas the capacitance was determined by fitting a biexponential function to the capacitive current at the onset of the voltage step.

Pharmacology. Spontaneous and evoked GABAergic and glutamatergic PSCs were recorded in the presence of the following ionotropic receptor blockers: NBQX (10 µM) and D-AP5 (25 µM) for GABAergic currents and Picrotoxin (100 µM) for glutamatergic currents. All drugs were stored as aliquots at -20°C and diluted in ACSF within a maximum of 2 days prior to recording. NBQX (20 mM, Tocris Bioscience) was dissolved in DMSO. D-AP5 (50 mM; Tocris Bioscience) was dissolved in water. Picrotoxin (50 mM; Sigma-Aldrich) was dissolved in ethanol.

Acknowledgements

We are grateful to Ö. Genç and to R. Ortiz for comments on the manuscript and to members of the Scheiffele Lab for discussions. We thank Caroline Bornmann and Sabrina Innocenti for organizational and experimental support, Dr. Pawel Pelczar and staff of the Centre for Transgenic Models at University of Basel for outstanding gene editing services, and the Biozentrum Imaging Core Facility for support with image acquisition and analysis. **Funding:** This work was supported by funds to P.S. from the Canton Basel-Stadt/University of Basel, the Swiss National Science Foundation, a European Research Council Advanced Grant (SPLICECODE), and AIMS-2-TRIALS which are supported by the Innovative Medicines Initiatives from the European Commission.

Author contributions

This work was jointly conceived by D.H., J.B., and P.S., experimental procedures were performed by D.H., K.B., D.S., A.S., data analysis was conducted by D.H., K.B., D.S., A.S., J.B., P.S.. The manuscript was jointly written by D.H., K.B., and P.S., with editing provided by D.S., A.S., and K.B.

Competing Interests statement

The authors declare no competing interests.

References

1 Sudhof, T. C. Synaptic Neurexin Complexes: A Molecular Code for the Logic of Neural Circuits. *Cell* **171**, 745-769 (2017).

2 de Wit, J. & Ghosh, A. Specification of synaptic connectivity by cell surface interactions. *Nat Rev Neurosci* **17**, 22-35 (2016).

3 Gomez, A. M., Traunmuller, L. & Scheiffele, P. Neurexins: molecular codes for shaping neuronal synapses. *Nat Rev Neurosci* **22**, 137-151 (2021).

4 Chowdhury, D., Watters, K. & Biederer, T. Synaptic recognition molecules in development and disease. *Curr Top Dev Biol* **142**, 319-370 (2021).

5 Yuzaki, M. Two Classes of Secreted Synaptic Organizers in the Central Nervous System. *Annu Rev Physiol* **80**, 243-262 (2018).

6 Jang, S., Lee, H. & Kim, E. Synaptic adhesion molecules and excitatory synaptic transmission. *Curr Opin Neurobiol* **45**, 45-50 (2017).

7 Favuzzi, E. & Rico, B. Molecular diversity underlying cortical excitatory and inhibitory synapse development. *Curr Opin Neurobiol* **53**, 8-15 (2018).

8 Hobert, O. Terminal Selectors of Neuronal Identity. *Curr Top Dev Biol* **116**, 455-475 (2016).

9 Apostolo, N. *et al.* Synapse type-specific proteomic dissection identifies IgSF8 as a hippocampal CA3 microcircuit organizer. *Nat Commun* **11**, 5171 (2020).

10 Ribeiro, L. F. *et al.* SorCS1-mediated sorting in dendrites maintains neurexin axonal surface polarization required for synaptic function. *PLoS Biol* **17**, e3000466 (2019).

11 Savas, J. N. *et al.* The Sorting Receptor SorCS1 Regulates Trafficking of Neurexin and AMPA Receptors. *Neuron* **87**, 764-780 (2015).

12 Schreiner, D., Savas, J. N., Herzog, E., Brose, N. & de Wit, J. Synapse biology in the 'circuit-age'-paths toward molecular connectomics. *Curr Opin Neurobiol* **42**, 102-110 (2017).

13 Loh, K. H. *et al.* Proteomic Analysis of Unbounded Cellular Compartments: Synaptic Clefts. *Cell* **166**, 1295-1307 e1221 (2016).

14 Paul, A. *et al.* Transcriptional Architecture of Synaptic Communication Delineates GABAergic Neuron Identity. *Cell* **171**, 522-539 e520 (2017).

15 Favuzzi, E. *et al.* Distinct molecular programs regulate synapse specificity in cortical inhibitory circuits. *Science (New York, N.Y* **363**, 413-417 (2019).

16 Sanes, J. R. & Zipursky, S. L. Synaptic Specificity, Recognition Molecules, and Assembly of Neural Circuits. *Cell* **181**, 536-556 (2020).

17 Takano, T. *et al.* Chemico-genetic discovery of astrocytic control of inhibition in vivo. *Nature* **588**, 296-302 (2020).

18 Kurmangaliyev, Y. Z., Yoo, J., Valdes-Aleman, J., Sanfilippo, P. & Zipursky, S. L. Transcriptional Programs of Circuit Assembly in the Drosophila Visual System. *Neuron* **108**, 1045-1057 e1046 (2020).

19 Furlanis, E., Traunmuller, L., Fucile, G. & Scheiffele, P. Landscape of ribosome-engaged transcript isoforms reveals extensive neuronal-cell-class-specific alternative splicing programs. *Nature neuroscience* **22**, 1709-1717 (2019).

20 Wamsley, B. *et al.* Rbfox1 Mediates Cell-type-Specific Splicing in Cortical Interneurons. *Neuron* (2018).

21 Saito, Y. *et al.* Differential NOVA2-Mediated Splicing in Excitatory and Inhibitory Neurons Regulates Cortical Development and Cerebellar Function. *Neuron* **101**, 707-720 e705 (2019).

22 Traunmüller, L., Gomez, A. M., Nguyen, T.-M. & Scheiffele, P. Control of neuronal synapse specification by highly dedicated alternative splicing program. *Science (New York, N.Y* **352**, 982-986 (2016).

23 Vuong, C. K. *et al.* Rbfox1 Regulates Synaptic Transmission through the Inhibitory Neuron-Specific vSNARE Vamp1. *Neuron* **98**, 127-141 e127 (2018).

24 Zheng, S. *et al.* PSD-95 is post-transcriptionally repressed during early neural development by PTBP1 and PTBP2. *Nature neuroscience* **15**, 381-388, S381 (2012).

25 Ray, T. A. *et al.* Comprehensive identification of mRNA isoforms reveals the diversity of neural cell-surface molecules with roles in retinal development and disease. *Nat Commun* **11**, 3328 (2020).

26 Matsuda, K. *et al.* Transsynaptic Modulation of Kainate Receptor Functions by C1q-like Proteins. *Neuron* **90**, 752-767 (2016).

27 Merkin, J., Russell, C., Chen, P. & Burge, C. B. Evolutionary dynamics of gene and isoform regulation in Mammalian tissues. *Science (New York, N.Y* **338**, 1593-1599 (2012).

28 Barbosa-Morais, N. L., Irimia, M., Pan, Q., ... & Blencowe, B. J. The evolutionary landscape of alternative splicing in vertebrate species. *Science (New York, N.Y* **338**, 1587-1594 (2012).

29 Nguyen, T. M. *et al.* An alternative splicing switch shapes neurexin repertoires in principal neurons versus interneurons in the mouse hippocampus. *eLife* **5** (2016).

30 Aoto, J., Foldy, C., Ilcus, S. M., Tabuchi, K. & Sudhof, T. C. Distinct circuit-dependent functions of presynaptic neurexin-3 at GABAergic and glutamatergic synapses. *Nature neuroscience* **18**, 997-1007 (2015).

31 Aoto, J., Martinelli, D. C., Malenka, R. C., Tabuchi, K. & Südhof, T. C. Presynaptic neurexin-3 alternative splicing trans-synaptically controls postsynaptic AMPA receptor trafficking. *Cell* **154**, 75-88 (2013).

32 Yap, K., Xiao, Y., Friedman, B. A., Je, H. S. & Makeyev, E. V. Polarizing the Neuron through Sustained Co-expression of Alternatively Spliced Isoforms. *Cell reports* **15**, 1316-1328 (2016).

33 Thalhammer, A. *et al.* Alternative Splicing of P/Q-Type Ca(2+) Channels Shapes Presynaptic Plasticity. *Cell reports* **20**, 333-343 (2017).

34 Reissner, C. *et al.* Dystroglycan binding to alpha-neurexin competes with neurexophilin-1 and neuroligin in the brain. *J Biol Chem* **289**, 27585-27603 (2014).

35 Park, H. *et al.* Splice-dependent trans-synaptic PTPdelta-IL1RAPL1 interaction regulates synapse formation and non-REM sleep. *EMBO J* **39**, e104150 (2020).

36 Uchigashima, M. *et al.* Specific Neuroligin3-alphaNeurexin1 signaling regulates GABAergic synaptic function in mouse hippocampus. *eLife* **9** (2020).

37 Quesnel-Vallieres, M., Irimia, M., Cordes, S. P. & Blencowe, B. J. Essential roles for the splicing regulator nSR100/SRRM4 during nervous system development. *Genes Dev* **29**, 746-759 (2015).

38 Feng, H. *et al.* Complexity and graded regulation of neuronal cell-type-specific alternative splicing revealed by single-cell RNA sequencing. *Proc Natl Acad Sci U S A* **118** (2021).

39 Miura, S. K., Martins, A., Zhang, K. X., Graveley, B. R. & Zipursky, S. L. Probabilistic splicing of Dscam1 establishes identity at the level of single neurons. *Cell* **155**, 1166-1177 (2013).

40 Vogel, C. & Marcotte, E. M. Insights into the regulation of protein abundance from proteomic and transcriptomic analyses. *Nature reviews. Genetics* **13**, 227-232 (2012).

41 Liu, Y., Beyer, A. & Aebersold, R. On the Dependency of Cellular Protein Levels on mRNA Abundance. *Cell* **165**, 535-550 (2016).

42 Smith, L. M., Kelleher, N. L. & Consortium for Top Down, P. Proteoform: a single term describing protein complexity. *Nat Methods* **10**, 186-187 (2013).

43 Aebersold, R. *et al.* How many human proteoforms are there? *Nat Chem Biol* **14**, 206-214 (2018).

44 Mayr, C. Regulation by 3'-Untranslated Regions. *Annu Rev Genet* **51**, 171-194 (2017).

45 Tushev, G. *et al.* Alternative 3' UTRs Modify the Localization, Regulatory Potential, Stability, and Plasticity of mRNAs in Neuronal Compartments. *Neuron* **98**, 495-511 e496 (2018).

46 Holt, C. E., Martin, K. C. & Schuman, E. M. Local translation in neurons: visualization and function. *Nat Struct Mol Biol* **26**, 557-566 (2019).

47 Keum, S. *et al.* A Missense Variant at the Nrxn3 Locus Enhances Empathy Fear in the Mouse. *Neuron* **98**, 588-601 e585 (2018).

48 Vaags, A. K. *et al.* Rare deletions at the neurexin 3 locus in autism spectrum disorder. *Am J Hum Genet* **90**, 133-141 (2012).

49 Schreiner, D. *et al.* Targeted Combinatorial Alternative Splicing Generates Brain Region-Specific Repertoires of Neurexins. *Neuron* (2014).

50 Treutlein, B., Gokce, O., Quake, S. R. & Südhof, T. C. Cartography of neurexin alternative splicing mapped by single-molecule long-read mRNA sequencing. *Proceedings of the National Academy of Sciences of the United States of America* **111**, E1291-1299 (2014).

51 Ushkaryov, Y. A. & Sudhof, T. C. Neurexin III alpha: extensive alternative splicing generates membrane- bound and soluble forms. *Proc Natl Acad Sci U S A* **90**, 6410-6414 (1993).

52 Giorgi, C. *et al.* The EJC Factor eIF4AIII Modulates Synaptic Strength and Neuronal Protein Expression. *Cell* **130**, 179-191 (2007).

53 Richardson, C. D., Ray, G. J., DeWitt, M. A., Curie, G. L. & Corn, J. E. Enhancing homology-directed genome editing by catalytically active and inactive CRISPR-Cas9 using asymmetric donor DNA. *Nat Biotechnol* **34**, 339-344 (2016).

54 Fuccillo, M. V. *et al.* Single-Cell mRNA Profiling Reveals Cell-Type-Specific Expression of Neurexin Isoforms. *Neuron* **87**, 326-340 (2015).

55 Lukacsovich, D. *et al.* Single-Cell RNA-Seq Reveals Developmental Origins and Ontogenetic Stability of Neurexin Alternative Splicing Profiles. *Cell reports* **27**, 3752-3759 e3754 (2019).

56 Halasy, K. & Somogyi, P. Subdivisions in the multiple GABAergic innervation of granule cells in the dentate gyrus of the rat hippocampus. *Eur J Neurosci* **5**, 411-429 (1993).

57 Hosp, J. A. *et al.* Morpho-physiological criteria divide dentate gyrus interneurons into classes. *Hippocampus* **24**, 189-203 (2014).

58 Hefft, S. & Jonas, P. Asynchronous GABA release generates long-lasting inhibition at a hippocampal interneuron-principal neuron synapse. *Nature neuroscience* **8**, 1319-1328 (2005).

59 Khalaj, A. J. *et al.* Deorphanizing FAM19A proteins as pan-neurexin ligands with an unusual biosynthetic binding mechanism. *The Journal of cell biology* **219** (2020).

60 Sugita, S. *et al.* A stoichiometric complex of neurexins and dystroglycan in brain. *The Journal of cell biology* **154**, 435-445. (2001).

61 Born, G. *et al.* Modulation of synaptic function through the alpha-neurexin-specific ligand neurexophilin-1. *Proc Natl Acad Sci U S A* **111**, E1274-1283 (2014).

62 Missler, M. & Sudhof, T. C. Neurexophilins form a conserved family of neuropeptide-like glycoproteins. *J Neurosci* **18**, 3630-3638 (1998).

63 de Wit, J. *et al.* LRRTM2 interacts with Neurexin1 and regulates excitatory synapse formation. *Neuron* **64**, 799-806 (2009).

64 Linhoff, M. W. *et al.* An unbiased expression screen for synaptogenic proteins identifies the LRRTM protein family as synaptic organizers. *Neuron* **61**, 734-749 (2009).

65 Maiolica, A., Junger, M. A., Ezkurdia, I. & Aebersold, R. Targeted proteome investigation via selected reaction monitoring mass spectrometry. *Journal of proteomics* **75**, 3495-3513 (2012).

66 Schreiner, D., Simicevic, J., Ahrné, E., Schmidt, A. & Scheiffele, P. Quantitative isoform-profiling of highly diversified recognition molecules. *eLife* **4**, 1-17 (2015).

67 Trotter, J. H. *et al.* Synaptic neurexin-1 assembles into dynamically regulated active zone nanoclusters. *The Journal of cell biology* **218**, 2677-2698 (2019).

68 Li, J. *et al.* Cell-Surface Proteomic Profiling in the Fly Brain Uncovers Wiring Regulators. *Cell* **180**, 373-386 e315 (2020).

69 Whiteaker, J. R. *et al.* CPTAC Assay Portal: a repository of targeted proteomic assays. *Nat Methods* **11**, 703-704 (2014).

70 Kusebauch, U. *et al.* Human SRMAtlas: A Resource of Targeted Assays to Quantify the Complete Human Proteome. *Cell* **166**, 766-778 (2016).

71 Bhowmick, P., Roome, S., Borchers, C. H., Goodlett, D. R. & Mohammed, Y. An Update on MRMAssayDB: A Comprehensive Resource for Targeted Proteomics Assays in the Community. *Journal of proteome research* **20**, 2105-2115 (2021).

72 Haueter, S. *et al.* Genetic vasectomy-overexpression of Prm1-EGFP fusion protein in elongating spermatids causes dominant male sterility in mice. *Genesis* **48**, 151-160 (2010).

73 Chen, S., Lee, B., Lee, A. Y., Modzelewski, A. J. & He, L. Highly Efficient Mouse Genome Editing by CRISPR Ribonucleoprotein Electroporation of Zygotes. *J Biol Chem* **291**, 14457-14467 (2016).

74 Taniguchi, H. *et al.* Silencing of neuroligin function by postsynaptic neurexins. *J Neurosci* **27**, 2815-2824 (2007).

75 Katz, Y., Wang, E. T., Airoldi, E. M. & Burge, C. B. Analysis and design of RNA sequencing experiments for identifying isoform regulation. *Nat Methods* **7**, 1009-1015 (2010).

76 Glatter, T. *et al.* Large-scale quantitative assessment of different in-solution protein digestion protocols reveals superior cleavage efficiency of tandem Lys-C/trypsin proteolysis over trypsin digestion. *Journal of proteome research* **11**, 5145-5156 (2012).

77 Peterson, A. C., Russell, J. D., Bailey, D. J., Westphall, M. S. & Coon, J. J. Parallel reaction monitoring for high resolution and high mass accuracy quantitative, targeted proteomics. *Mol Cell Proteomics* **11**, 1475-1488 (2012).

78 Bischofberger, J., Engel, D., Frotscher, M. & Jonas, P. Timing and efficacy of transmitter release at mossy fiber synapses in the hippocampal network. *Pflugers Arch* **453**, 361-372 (2006).

79 Heigele, S., Sultan, S., Toni, N. & Bischofberger, J. Bidirectional GABAergic control of action potential firing in newborn hippocampal granule cells. *Nature neuroscience* **19**, 263-270 (2016).

80 Guzman, S. J., Schlogl, A. & Schmidt-Hieber, C. Stimfit: quantifying electrophysiological data with Python. *Front Neuroinform* **8**, 16 (2014).

81 Jonas, P., Major, G. & Sakmann, B. Quantal components of unitary EPSCs at the mossy fibre synapse on CA3 pyramidal cells of rat hippocampus. *The Journal of physiology* **472**, 615-663 (1993).

82 Clements, J. D. & Bekkers, J. M. Detection of spontaneous synaptic events with an optimally scaled template. *Biophys J* **73**, 220-229 (1997).

83 Schmidt-Salzmann, C., Li, L. & Bischofberger, J. Functional properties of extrasynaptic AMPA and NMDA receptors during postnatal hippocampal neurogenesis. *The Journal of physiology* **592**, 125-140 (2014).

Figure 1

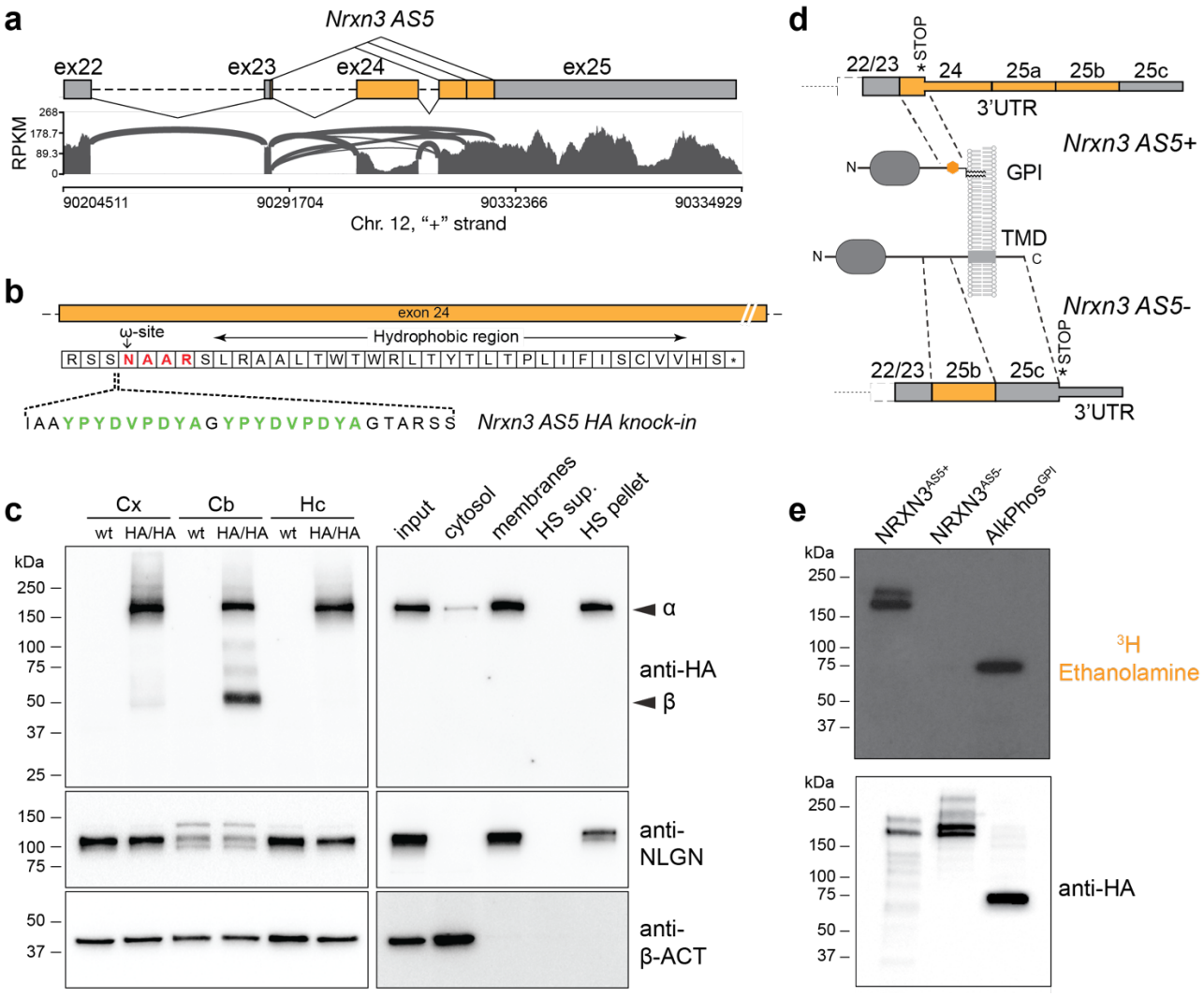
a
Nrxn3 AS5
ex22
ex23
ex24
ex25
RPKM
268
178.7
89.3
0
90204511
90291704
90332366
90334929
Chr. 12, "+" strand
b
exon 24
ω-site
Hydrophobic region
R S S N A A R S L R A A L T W T W R L T Y T L T P L I F I S C V V H S *
I A A Y P Y D V P D Y A G Y P Y D V P D Y A G T A R S S
Nrxn3 AS5 HA knock-in
d
22/23
*STOP
24
25a
25b
25c
3'UTR
Nrxn3 AS5+
N
GPI
TMD
C
Nrxn3 AS5-
22/23
25b
25c
*STOP
3'UTR
c
Cx
Cb
Hc
wt
HA/HA
wt
HA/HA
wt
HA/HA
input
cytosol
membranes
HS sup.
HS pellet
kDa
250
150
100
75
50
37
25
α
anti-HA
β
150
100
75
anti-
NLGN
50
37
anti-
β-ACT
e
NRXN3AS5+
NRXN3AS5-
AlkPhosGPI
kDa
250
150
100
75
50
37
3H
Ethanolamine
kDa
250
150
100
75
50
37
anti-HA

Figure 1. Expression and detection of NRXN3 AS5+ proteoforms in mice

a, Sashimi plots illustrating read distribution and splice junctions arising from mouse *Nrxn3 AS5*. Exons are depicted as boxes, introns as dashed lines. Alternative exons and alternative acceptor sites are marked in orange, constitutive exons in grey. **b**, Amino acids of exon 24 protein coding sequence in *Nrxn3-AS5*^{HA} knock-in mice. The HA epitopes (green), ω-site (red) and hydrophobic stretch conferring GPI-anchoring are indicated. **c**, Western blot of whole neocortex (Cx), cerebellum (Cb), and hippocampal (Hc) extract from P28 wild-type and *Nrxn3-AS5*$^{HA/HA}$ knock-in mice probed with anti-HA, anti-Neuroligin (NLGN), and anti-beta-actin (β-ACT) antibodies. The right panel shows hippocampal subcellular fractionation of cytosolic, membrane, and high-salt (HS) washed membrane fractions (equal percentage of total sample loaded in all lanes). Position of α- and β-Neurexin proteoforms is indicated. **d**, Schematic diagram illustrating introduction of a translational stop codon in AS5+ (exon 24-containing mRNAs). This results in production of shortened, GPI-anchored NRXN3 proteoforms encoded by mRNAs with a long 3'UTR encoded by exons 25a, 25b, 25c. AS5- mRNA isoforms encode canonical transmembrane NRXN3 proteins. **e**, HA-tagged NRXN3-AS5+, NRXN3 AS5-, and placental alkaline phosphatase proteins immunoprecipitated from transfected HEK293 cells after radiolabelling with ^{3}H-ethanolamine. Immunoprecipitates were probed by western blotting with anti-HA antibodies or analyzed by autoradiography.

Figure 2

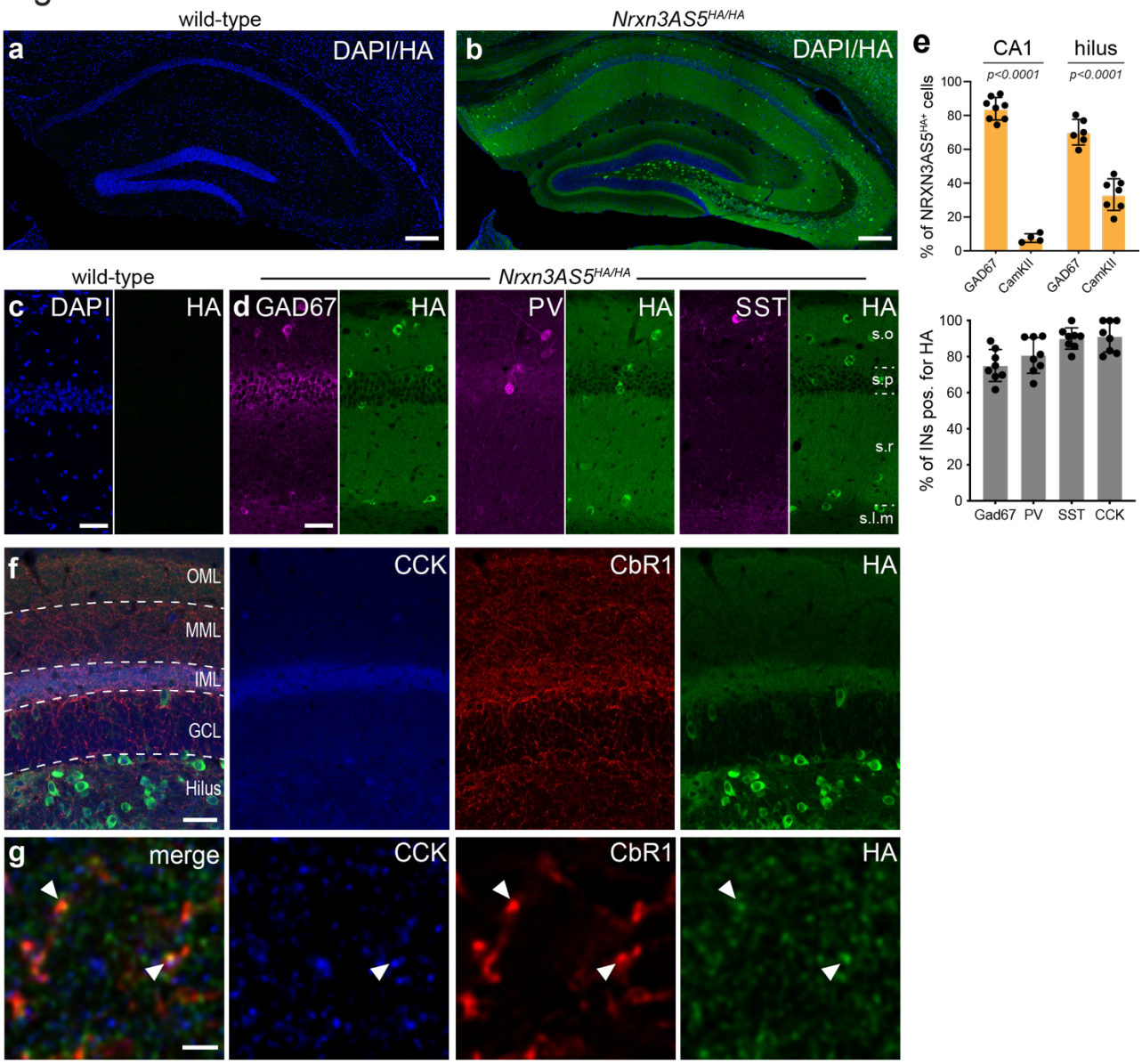
wild-type
Nrxn3AS5HA/HA
a
DAPI/HA
b
DAPI/HA
e
CA1
hilus
p<0.0001
p<0.0001
% of NRXN3AS5HA+ cells
GAD67
CamKII
GAD67
CamKII
wild-type
Nrxn3AS5HA/HA
c DAPI
HA
d GAD67
HA
PV
HA
SST
HA
s.o
s.p
s.r
s.l.m
% of INs pos. for HA
Gad67
PV
SST
CCK
f
OML
MML
IML
GCL
Hilus
CCK
CbR1
HA
g
merge
CCK
CbR1
HA

Figure 2. Selective expression and synaptic localization of NRXN3 AS5+ proteoforms

a, **b**, Immunochemical detection of HA-tagged proteins in hippocampus from wild-type mice (a) and homozygous knock-in mice (b) **c**-**e**, Co-expression analysis of NRXN3-AS5^{HA} protein with interneuron markers GAD67, parvalbumin (PV), and somatostatin (SST) in CA1. **e-g**, Co-expression and co-localization analysis of NRXN3-AS5^{HA} and cholecystokinin (CCK) and cannabinoid receptor 1 (CbR1) in the hilus of the dentate gyrus, OML=outer molecular layer, MML=middle molecular layer, IML=inner molecular layer, GCL=granule cell layer. **e**, Quantification of co-expression analysis, the top panel shows the amount of GAD67/CamKII positive NRXN3-AS5^{HA} protein expressing cells in the hilus of the dentate gyrus, the bottom panel the amount of NRXN3-AS5^{HA} positive cells in different interneuron populations in CA1, N=2 mice, n=2-4 brain slices, P25-30, p-values were calculated using two-way anova followed by Bonferroni's test. Scale bar is 200 μm in a/b, 50 μm in c/d, 50 μm in f, 2 μm in g.

Figure 3

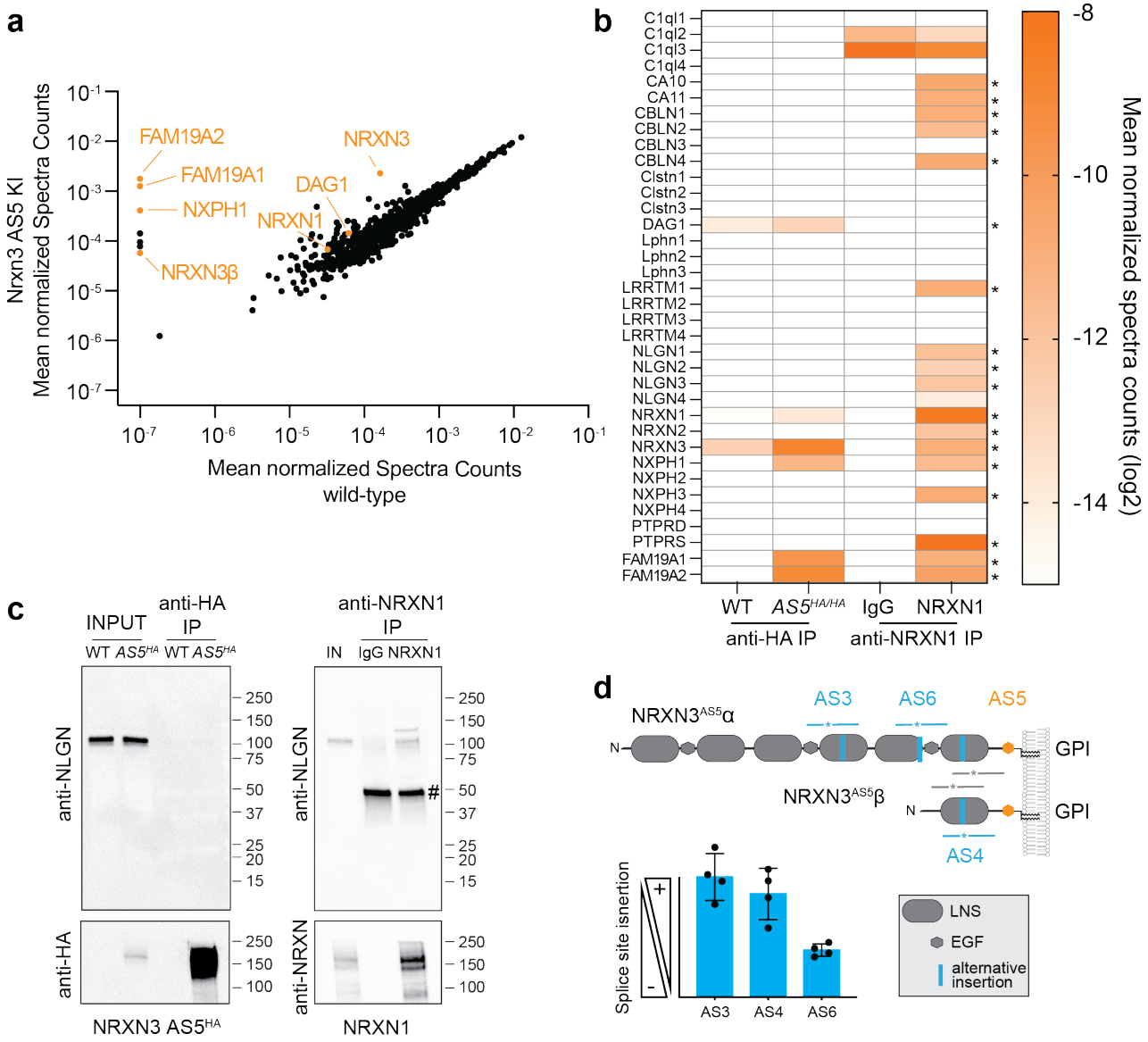
a
Nrxn3 AS5 KI
Mean normalized Spectra Counts
FAM19A2
FAM19A1
NXPH1
NRXN3β
NRXN3
DAG1
NRXN1
Mean normalized Spectra Counts
wild-type
b
C1ql1
C1ql2
C1ql3
C1ql4
CA10
CA11
CBLN1
CBLN2
CBLN3
CBLN4
Clstn1
Clstn2
Clstn3
DAG1
Lphn1
Lphn2
Lphn3
LRRTM1
LRRTM2
LRRTM3
LRRTM4
NLGN1
NLGN2
NLGN3
NLGN4
NRXN1
NRXN2
NRXN3
NXPH1
NXPH2
NXPH3
NXPH4
PTPRD
PTPRS
FAM19A1
FAM19A2
WT
AS5HA/HA
IgG
NRXN1
anti-HA IP
anti-NRXN1 IP
Mean normalized spectra counts (log2)
c
INPUT
anti-HA IP
WT AS5HA WT AS5HA
anti-NRXN1 IP
IN IgG NRXN1
anti-NLGN
anti-HA
anti-NRXN
NRXN3 AS5HA
NRXN1
d
NRXN3AS5α
AS3
AS6
AS5
N
GPI
NRXN3AS5β
AS4
Splice site isnertion
AS3
AS4
AS6
LNS
EGF
alternative insertion

Figure 3. NRXN3 AS5+ proteoforms recruit specific synaptic ligands

a, Scatter plot of normalized spectra counts (log10 scale) in anti-HA immunoprecipitates from hippocampi from *Nrxn3-AS5*$^{HA/HA}$ and wild-type (negative control) P25-30 mice (N=5 mice per genotype). Identified known Neurexin ligands are marked in orange. See Table S1 for detailed data. **b**, Heatmap of mean normalized spectral counts (log2 scale) of known Neurexin ligands recovered from wild-type and *Nrxn3-AS5*$^{HA/HA}$ mice in anti-HA immunoprecipitates and recovered from wild-type mice in control IgG and anti-NRXN1 immunoprecipitates, respectively. Ligands significantly enriched in the precipitate as compared to negative controls are marked with an asterisk (multiple T-TEST with Benjamini, Krieger, and Yekutieli correction). AS5HA/HA vs. wild-type: $q < 0.001$ for NRXN3, NXPH1, FAM19A1 and A2; $q < 0.04$ for NRXN1 and DAG1. Anti-NRXN1 vs. control IgG: $q< 0.001$ for all except PTPRS ($q=0.0021$). See Table S2 for details on selected ligands and Table S3 for NRXN1 immunoprecipitates. **c**, Confirmation of differential ligand interactions by western blotting. Input (1%) and immunoprecipitates with anti-HA (left) or control IgG and anti-NRXN1 antibodies (right) probed with anti-NLGN (top) and anti-HA or anti-NRXN antibodies (bottom). Molecular weight markers indicated in kDa. # indicates heavy IgG-chains. **d**, Schematic of NRXN3 AS5 domain organization, alternatively spliced segments (blue), and proteotypic peptides reporting on constitutive/common (gray) and alternative splice proteoform-specific (blue) amino acids, which are quantified for AS3, AS4 and AS6, normalized to recombinant protein expressing all splice isoforms (100% splice site inclusion) and to constitutive exons.

Figure 4

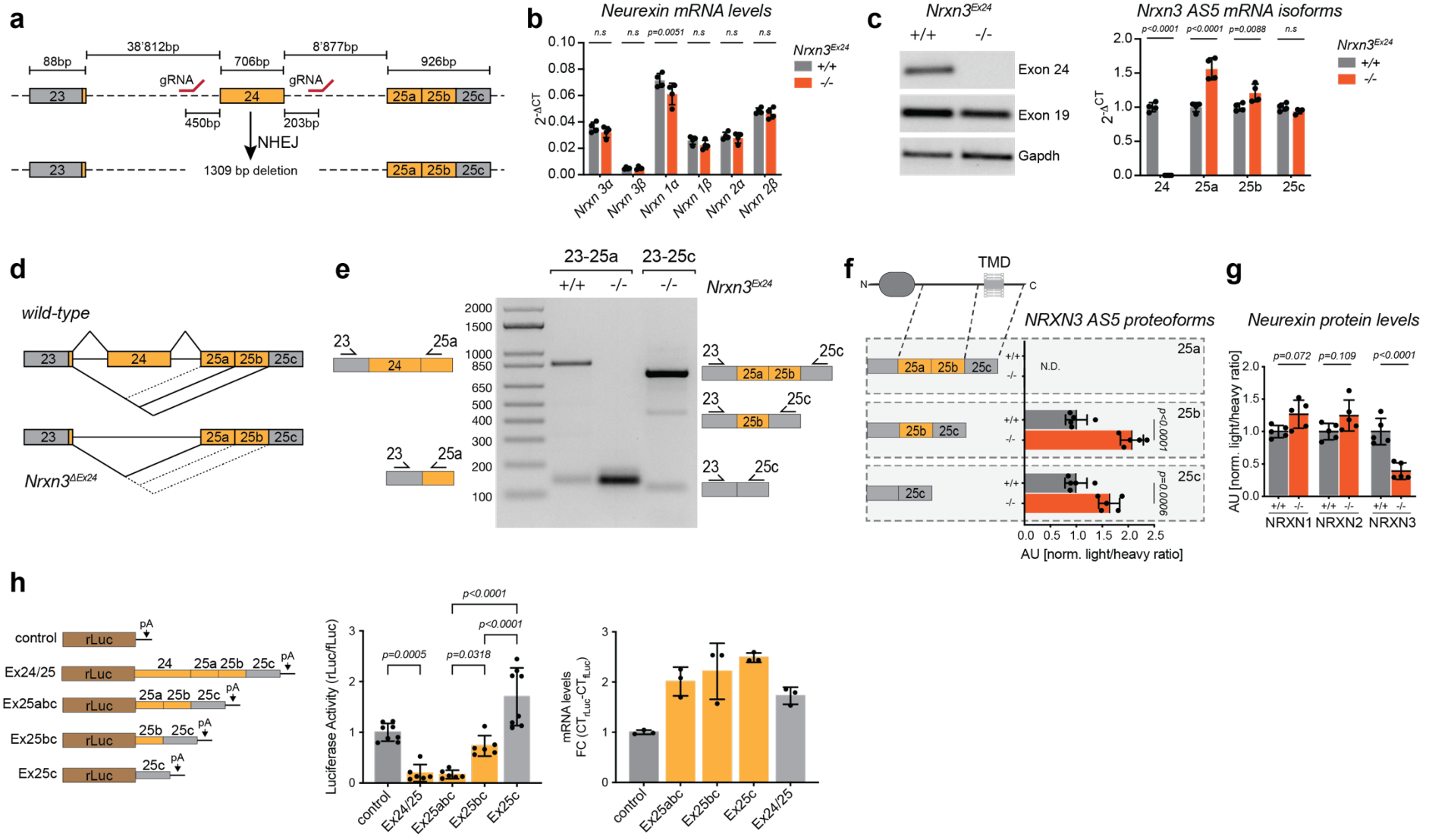
a
38'812bp
88bp
706bp
8'877bp
926bp
gRNA
gRNA
23
24
25a 25b 25c
450bp
203bp
NHEJ
1309 bp deletion
b
Neurexin mRNA levels
Nrxn3Ex24
+/+
-/-
Nrxn 3α
Nrxn 3β
Nrxn 1α
Nrxn 1β
Nrxn 2α
Nrxn 2β
c
Nrxn3Ex24
Exon 24
Exon 19
Gapdh
Nrxn3 AS5 mRNA isoforms
d
wild-type
Nrxn3ΔEx24
e
23-25a
23-25c
Nrxn3Ex24
f
TMD
NRXN3 AS5 proteoforms
N.D.
AU [norm. light/heavy ratio]
g
Neurexin protein levels
AU [norm. light/heavy ratio]
NRXN1 NRXN2 NRXN3
h
control
Ex24/25
Ex25abc
Ex25bc
Ex25c
Luciferase Activity (rLuc/fLuc)
mRNA levels

Figure 4. Translational silencing gates NRXN3 protein expression

a, Schematic diagram illustrating the generation of *Nrxn3*$^{\Delta Ex24}$ mice by Crispr/Cas9 gene editing with two gRNAs targeting introns upstream and downstream of exon 24. Sizes of exons (boxes) and introns (dashed lines), and position of gRNA recognition sites are indicated. **b**, quantitative PCRs of major *Nrxn* transcript isoforms for wildtype and *Nrxn3*$^{\Delta Ex24}$ mice, normalized to *Gapdh*, hippocampus, P25-30, N=4 mice per genotype. **c**, Semi-quantitative PCR amplifying *Nrxn3* transcript regions containing alternative exon 24 or the constitutive exon 19 from mouse hippocampus and quantitative PCR probing abundance of mRNAs containing exon 24, alternative acceptors 25a, 25b, and the constitutive exon 25c, normalized to *Gapdh*, hippocampus, P25-30, N=4 mice per genotype. **d**, Schematic diagram illustrating alternative splicing events in wild-type and *Nrxn3*$^{\Delta Ex24}$ hippocampus. **e**, semi-quantitative PCR visualizing *Nrxn3* transcript variants arising from alternative splicing at AS5 in wild-type and *Nrxn3*$^{\Delta Ex24}$ mice. Position of primer binding sites on alternative exon segments is illustrated. See methods for details. **f**, **g**, Detection of AS5 proteoforms by targeted proteomics with heavy peptides targeting alternative acceptors 25a, 25b and constitutive exon 25c or targeting all NRXN1, NRXN2 and NRXN3 proteoforms, ratios of light to heavy peptide detection are displayed in reference to wild-type samples of each peptide individually, one representative peptide shown (See Table S5 for all peptide values), hippocampus, P25-20, N=5 mice per genotype. **h,** Luciferase Assay of dual-promoter plasmids expressing firefly (fLuc) and renilla (rLuc) luciferase, left panel: Schematic representation of different *Nrxn3* exonic sequences fused to renilla, middle panel: Measurement of luciferase activity from renilla luciferase constructs normalized to firefly luciferase activity, N=2-3 cell cultures, n=2-3 replicates per culture. right panel: mRNA levels determined by RT-qPCR of renilla luciferase constructs normalized to firelfly luciferase, N=3 cell cultures. p-values were calculated using two-way or one-way anova followed by Bonferroni's test for both qPCR and proteomic analysis or luciferase assay, respectively.

Figure 5

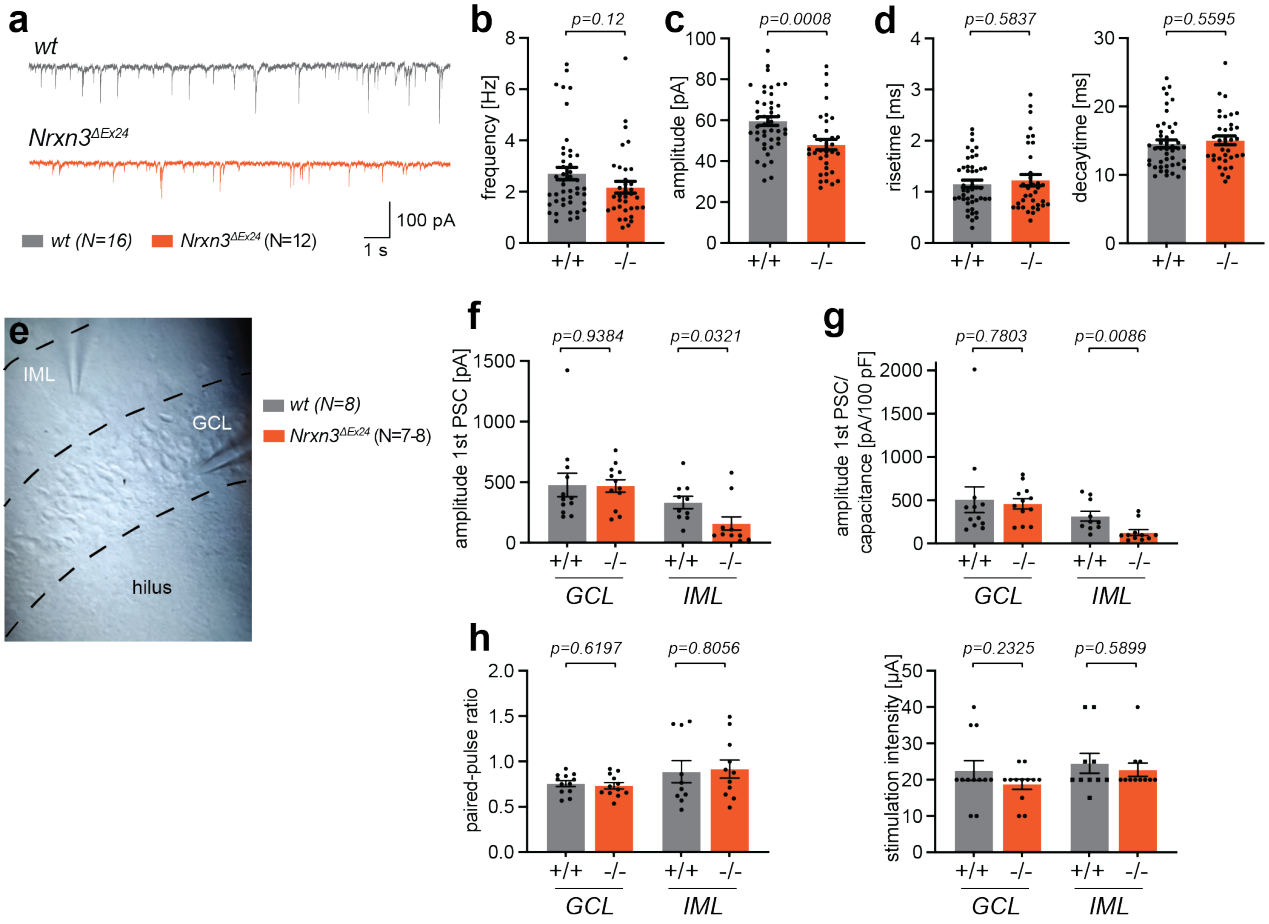
a
wt
Nrxn3ΔEx24
wt (N=16)
Nrxn3ΔEx24 (N=12)
100 pA
1 s
b
p=0.12
frequency [Hz]
c
p=0.0008
amplitude [pA]
d
p=0.5837
risetime [ms]
p=0.5595
decaytime [ms]
+/+
-/-
e
IML
GCL
hilus
wt (N=8)
Nrxn3ΔEx24 (N=7-8)
f
p=0.9384
p=0.0321
amplitude 1st PSC [pA]
g
p=0.7803
p=0.0086
amplitude 1st PSC/ capacitance [pA/100 pF]
h
p=0.6197
p=0.8056
paired-pulse ratio
p=0.2325
p=0.5899
stimulation intensity [µA]
GCL
IML

Figure 5. Impaired synaptic transmission in *Nrxn3*$^{\Delta Ex24}$ mice

a, Representative traces of sIPSCs from 6-8 week-old wildtype and homozygous *NRXN3*$^{\Delta Ex24}$ mice. **b**-**d**, Quantification of sIPSC in wildtype and homozygous *NRXN3*$^{\Delta Ex24}$ mice (N=12-16 animals, n=35 cells), with frequency (b), amplitude (c) and kinetics (d) quantified. **e,** Positioning of electrodes for evoked transmission measurements, inner molecular layer (IML), granule cell layer (GCL) and hilar region of the dentate gyrus indicated. **f**, **g**, Amplitude of post-synaptic currents when evoked in GCL for PV-specific an in IML for CCK-specific inputs onto granule cells, not normalized (f) and normalized to the capacitance of individual cells (g), N=7-8 animals, n=12 cells. **h**, Paired-pulse ratio (left panel) and stimulation intensities (right panel) of GCL and IML stimulations. P-values were calculated with student's t-test.

Figure S1

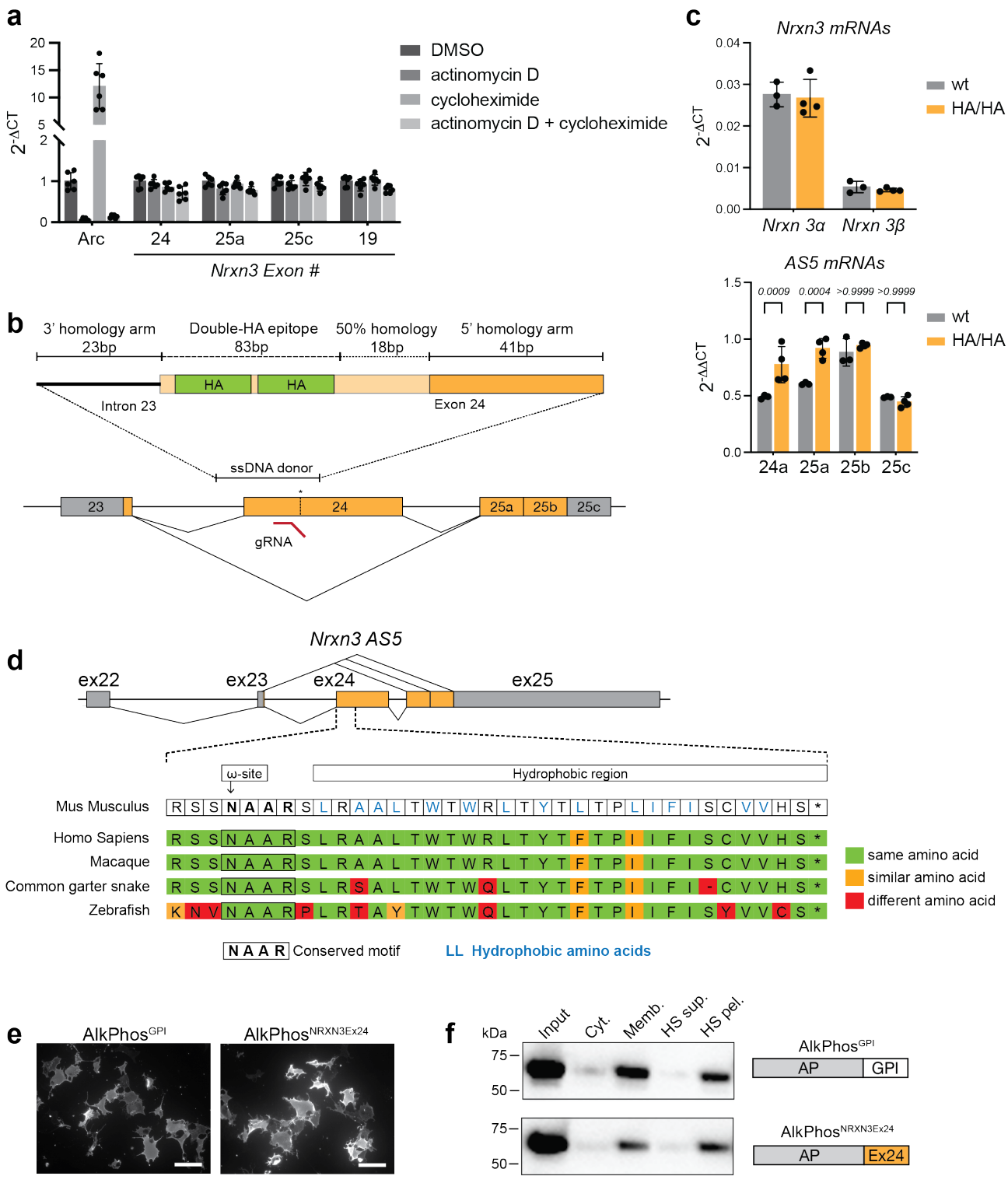
a
DMSO
actinomycin D
cycloheximide
actinomycin D + cycloheximide
2-ΔCT
Arc
24
25a
25c
19
Nrxn3 Exon #
b
3' homology arm 23bp
Double-HA epitope 83bp
50% homology 18bp
5' homology arm 41bp
HA
HA
Intron 23
Exon 24
ssDNA donor
23
24
25a
25b
25c
gRNA
c
Nrxn3 mRNAs
wt
HA/HA
Nrxn 3α
Nrxn 3β
AS5 mRNAs
0.0009
0.0004
>0.9999
>0.9999
24a
25a
25b
25c
d
Nrxn3 AS5
ex22
ex23
ex24
ex25
ω-site
Hydrophobic region
Mus Musculus
Homo Sapiens
Macaque
Common garter snake
Zebrafish
same amino acid
similar amino acid
different amino acid
N A A R Conserved motif
LL Hydrophobic amino acids
e
AlkPhos^GPI
AlkPhos^NRXN3Ex24
f
kDa
Input
Cyt.
Memb.
HS sup.
HS pel.
75
50
AlkPhos^GPI
AP
GPI
AlkPhos^NRXN3Ex24
AP
Ex24

Figure S1.

a, Quantitative RT-PCRs of mRNA from cortical cultures treated with actinomycin D, cycloheximide or both and DMSO only control, normalized to *Gapdh*, N=2 cortical cultures, n=3 replicates, DIV12. **b**, Schematic of double-HA tag insertion strategy into exon 24 of *Nrxn3*. Splice site 5 with alternative donor- and acceptor site or alternative exon (yellow) and constitutive exon (grey) indicated below, single stranded DNA donor and homology regions indicated on top, with homology arms and insert labelled. **c**, quantitative PCRs of wildtype and homozygous NRXN3AS5HA knock-in mice, for both major *Nrxn3* (top panel) and splice site (bottom panel) targets, normalized to *Gapdh* (top) or *Gapdh and PAN-Nrxn3* (bottom), hippocampus, N=3-4 mice per genotype, p-values were calculated using two-way anova followed by Bonferroni's test. **d**, Schematic representation of splice segment 5 of *Nrxn3* and evolutionary conservation between species of the coding region of exon 24. Same amino acids are highlighted green, amino acids with similar side charges and pK_a in orange, different amino acids in red. **e**, Immunostainings of Cos-cells with overexpressed HA-tagged alkaline phosphatase constructs with endogenous GPI-anchor triggering sequence (left) or fused to the coding sequence of *Nrxn3* exon 24, scale bar is 100 μm. **f**, Western Blot of subcellular fractionation of cytosolic, membrane, and high-salt (HS) washed membrane fractions (equal percentage of total sample loaded in all lanes) from HEK-cells expressing HA-tagged alkaline phosphatase constructs.

Figure S2

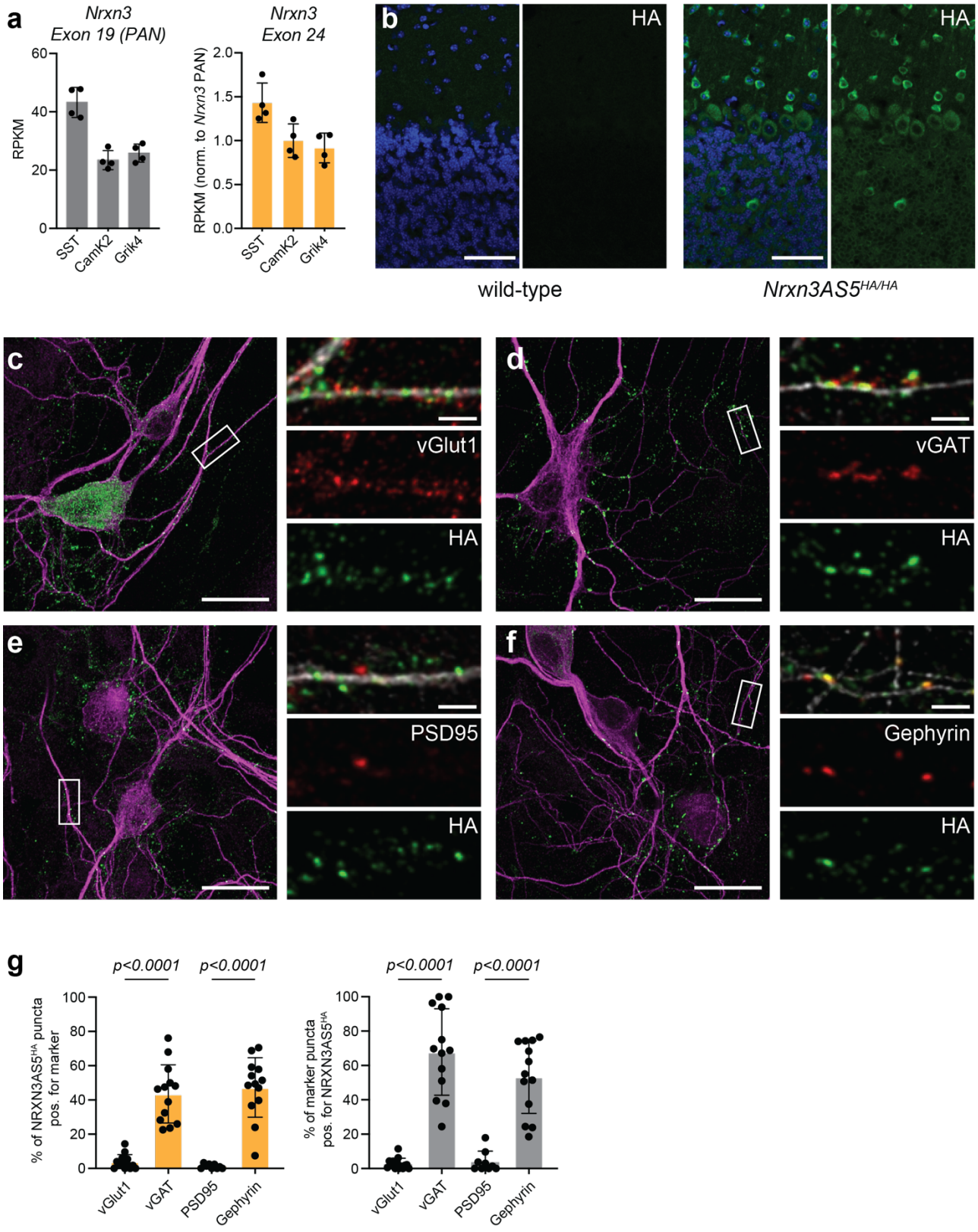
a
Nrxn3
Exon 19 (PAN)
RPKM
SST
CamK2
Grik4
Nrxn3
Exon 24
RPKM (norm. to Nrxn3 PAN)
b
HA
wild-type
Nrxn3AS5HA/HA
c
vGlut1
HA
d
vGAT
HA
e
PSD95
HA
f
Gephyrin
HA
g
p<0.0001
p<0.0001
% of NRXN3AS5HA puncta pos. for marker
vGlut1
vGAT
PSD95
Gephyrin
p<0.0001
p<0.0001
% of marker puncta pos. for NRXN3AS5HA

Figure S2.

a, RNA sequencing reads for constitutive (exon 19) and alternative exon 24 of *Nrxn3*, from RiboTag isolated SST, CamKII or Grik4 positive cells. **b**, Immunochemical detection of HA-tagged proteins in cerebellum from wild-type mice (left panel) and homozygous knock-in mice (right panel). **c-f**, Immunocytochemistry of hippocampal cultures from NRXN3AS5HA homozygous knock-in mice, DIV10, with co-labelling of pre-synaptic markers vGlut1 (c), vGAT (d), post-synaptic markers PSD95 (e), Gephyrin (f). **g**, Quantification of c-f with SynapseCounter Plug-in for Fiji, with the percentage of HA-positive synapses co-labelled with pre- and post-synaptic marker (left panel) and percentage of pre- and post-synaptic markers co-labelled with HA-positive synapses indicated. P-values were calculated using one-way anova followed by Bonferroni's test, N=2 hippocampal cultures, n=6-8 ROI per condition, 60-100 puncta per ROI. Scale bar is 50 μm in b, 20 μm in c-f, 2 μm in c-f ROIs.

Figure S3

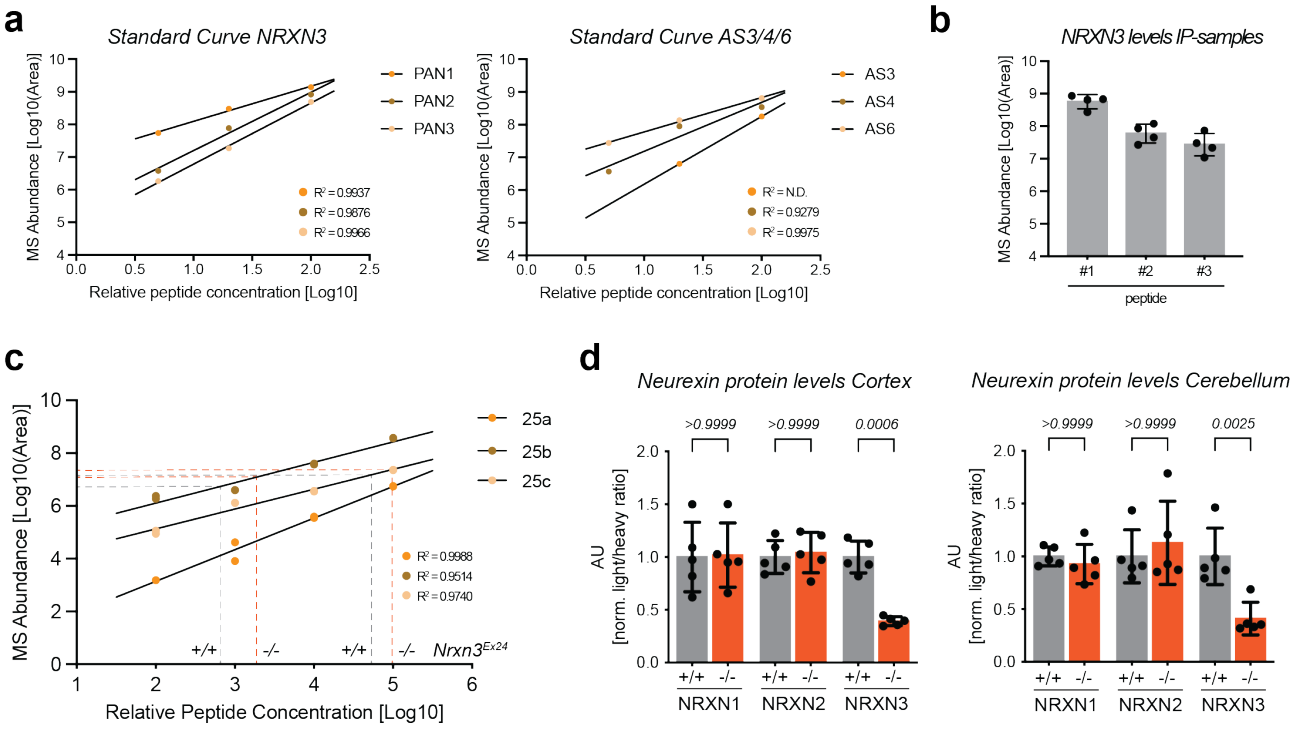
a
Standard Curve NRXN3
MS Abundance [Log10(Area)]
Relative peptide concentration [Log10]
PAN1
PAN2
PAN3
R² = 0.9937
R² = 0.9876
R² = 0.9966
Standard Curve AS3/4/6
AS3
AS4
AS6
R² = N.D.
R² = 0.9279
R² = 0.9975
b
NRXN3 levels IP-samples
#1
#2
#3
peptide
c
25a
25b
25c
R² = 0.9988
R² = 0.9514
R² = 0.9740
+/+
-/-
+/+
-/-
Nrxn3Ex24
Relative Peptide Concentration [Log10]
d
Neurexin protein levels Cortex
Neurexin protein levels Cerebellum
>0.9999
>0.9999
0.0006
0.0025
AU
[norm. light/heavy ratio]
NRXN1
NRXN2
NRXN3

Figure S3.

a, Peptide abundance of NRXN3 PAN peptides (left panel) and splice insertion peptides for AS3, AS4 and AS6 (right panel) showing a linear detection range for all peptides for constructs including all splice insertions and which were overexpressed in HEK-cells. **b**, NRXN3 protein levels of co-immunoprecipitated NRXN3AS5$^{HA/HA}$ pull-downs, as determined by three different PAN peptides, N=4 IP samples. **c**, Peptide abundance of alternative acceptor sites 25a and 25b and constitutive exon 25c from recombinant protein expressing equimolar amounts of all splice sites. Detection range of endogenous peptides for wildtype and *NRXN3*$^{\Delta Ex24}$ mice indicated with dashed lines (average N=5 mice per genotype, hippocampus) for 25b and 25c, detection of endogenous 25a peptides was not possible. **d**, Detection of NRXN1-3 by targeted proteomics with heavy peptides targeting all NRXN1, NRXN2 and NRXN3 proteoforms, ratios of light to heavy peptide detection are displayed in reference to wild-type samples of each peptide individually, one representative peptide shown for cerebellum and cortical samples, P25-30, N=5 mice per genotype / brain area, p-values were calculated using a two-way anova followed by Bonferroni's test.

Figure S4

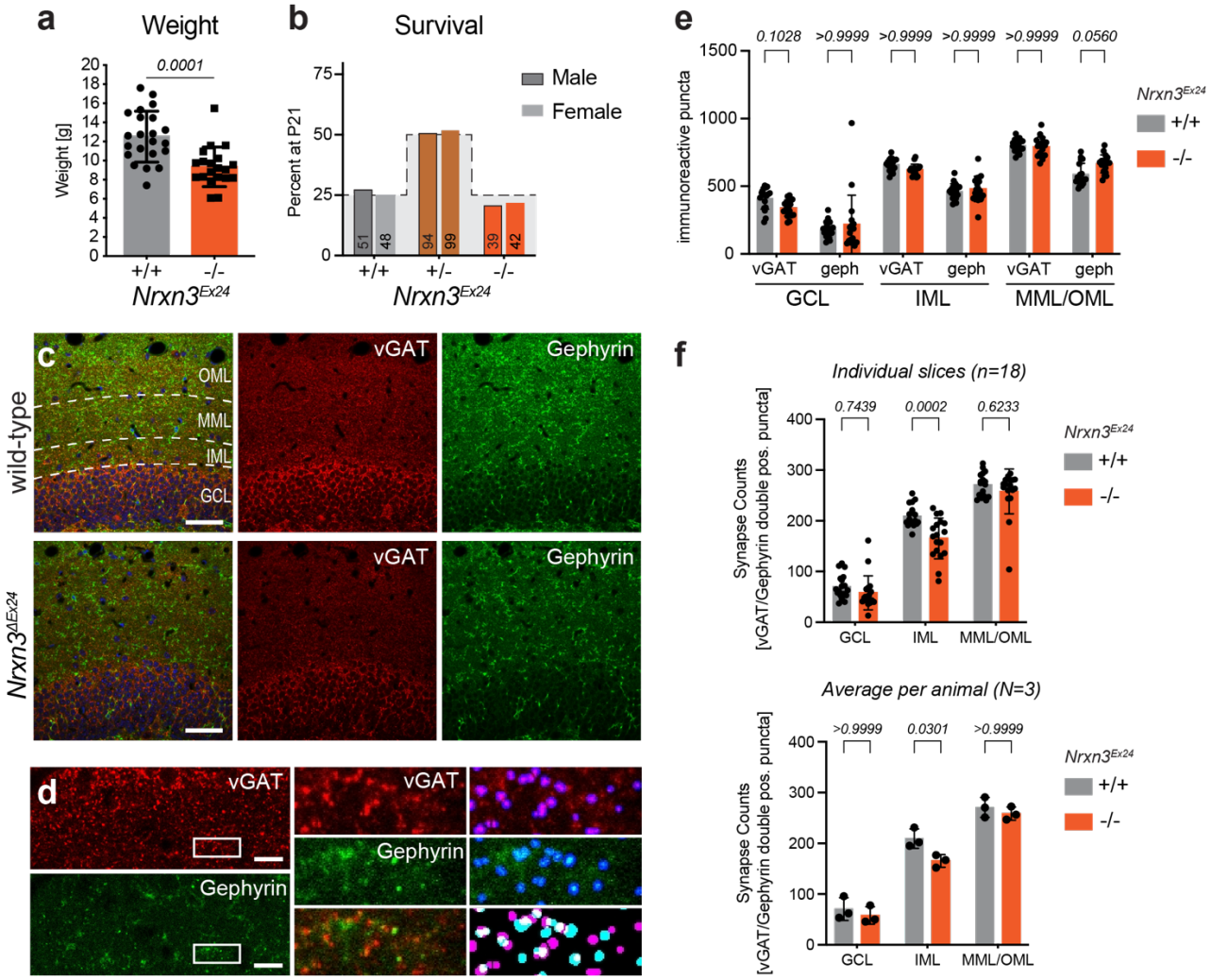
a
Weight
0.0001
Weight [g]
+/+
-/-
Nrxn3Ex24
b
Survival
Male
Female
Percent at P21
51
48
94
99
39
42
+/+
+/-
-/-
Nrxn3Ex24
c
wild-type
Nrxn3ΔEx24
OML
MML
IML
GCL
vGAT
Gephyrin
d
vGAT
Gephyrin
e
0.1028
>0.9999
>0.9999
>0.9999
>0.9999
0.0560
immunoreactive puncta
vGAT
geph
GCL
IML
MML/OML
Nrxn3Ex24
+/+
-/-
f
Individual slices (n=18)
0.7439
0.0002
0.6233
Synapse Counts
[vGAT/Gephyrin double pos. puncta]
GCL
IML
MML/OML
Nrxn3Ex24
+/+
-/-
Average per animal (N=3)
>0.9999
0.0301
>0.9999
Synapse Counts
[vGAT/Gephyrin double pos. puncta]
GCL
IML
MML/OML
Nrxn3Ex24
+/+
-/-

Figure S4.

a, Weight of wildtype and *NRXN3*$^{\Delta Ex24}$ littermates, P25-30, Student's t-test. **b**, Survival of wildtype, heterozygous and homozygous *NRXN3*$^{\Delta Ex24}$ mice in relation to expected mendelian ratios for male and female mice, after P21, numbers of mice indicated within columns. **c**, Immunochemical detection of synaptic markers in dentate gyrus of hippocampus from wild-type mice (top panel) and homozygous knock-in mice (bottom panel), OML=outer molecular layer, MML=middle molecular layer, IML=inner molecular layer, GCL=granule cell layer. **d**, Representative image of IML of the dentate gyrus, with individual synaptic markers, co-labelling of synaptic markers (middle panel) and overlay of SynapseCounter Plug-in in Fiji with individual and co-labelling detection (right panel). **e**, **f**, Immunoreactive puncta for pre- (vGAT) and post- (gephyrin) synaptic markers (e) and synapse counts for individual slices (left panel) and animal average (right panel)(f) in granule cell (GCL), inner molecular (IML) and middle/outer molecular (MML/OML) layers of wildtype and homozygous *NRXN3*$^{\Delta Ex24}$ mice, N=3 mice per genotype, n=6 brain slices per animal. P-values were calculated using two-way anova followed by Bonferroni's test. Scale bar is 50 μm in c, 10 μm in d.

Supplementary Information

Supplementary Table 1. Normalized Spectral Counts Proteins recovered in anti-HA immuno-precipitates from hippocampal tissue lysates from wild-type and NRXN3 AS5 HA/HA mice. Proteins were considered reliably detected if they were recovered in at least 3 of the 5 replicates for the precipitations from NRXN3 AS5 HA/HA hippocampi. Common contaminants (keratins, histones, 40S and 60S ribosomal core proteins, excluded from the plot in Figure 3) are marked in red. Note that for plotting on a log scale, mean values were set to 10^{-7} (just below level of lowest "detected" protein) when the actual detection in wild-type control precipitates was zero (7 values marked in blue).

Supplementary Table 2. Normalized Spectral Counts Proteins for a hand-curated list of known extracellular Neurexin ligands and their detection in anti-HA immunoprecipitates from hippocampal tissue lysates of wild-type and NRXN3 AS5 HA/HA mice or detection in anti-NRXN1 and control IgG immunoprecipitates from hippocampal tissue lysates of wild-type mice, respectively.

Supplementary Table 3. Normalized Spectral Counts of Proteins recovered in anti-NRXN1 and control IgG immunoprecipitates from hippocampal tissue lysates of wild-type mice. Proteins were considered reliably detected if they were recovered in at least 3 of the 5 replicates for the precipitations with the NRXN1 antibodies. Common contaminants (keratins, histones, 40S and 60S ribosomal core proteins) are marked in red. Note that for plotting, mean values were set to 10^{-6} when the actual detection in the control IgG sample was zero (marked in blue).

Supplementary Table 4. Method supplement, with oligonucleotide primer used for flanking primer PCRs or qPCR assays and 3'UTR sequences which were cloned into dual-promotor luciferase plasmids.

Supplementary Table 5. List of heavy peptides used for targeted proteomic assays.

General statistical methods. Statistical analysis was conducted with GraphPad Prism 7 (San Diego, CA, USA). Sample sizes were chosen based on previous experiments and literature surveys. No statistical methods were used to pre-determine sample sizes. Exclusion criteria used throughout this manuscript were pre-defined. There are detailed descriptions in the respective sections of the methods. Group assignment was defined by genotype, thus, no randomization was necessary. During initial pilot experiments, investigators were not blinded to genotype during data collection and/or analysis. Subsequent acquisition and analysis of larger datasets for quantification of synaptic markers and electrophysiological recordings were done by an investigator blinded to genotype. Appropriate statistical tests were chosen based on sample size.

Data availability. All renewable reagents, detailed protocols, and transgenic mice will be made available on request. Proteomic data will be deposited at PRIDE and will be made available upon acceptance of the manuscript.

3. Discussion and future directions

3.1 Nrxn3 AS5+ contribution to the molecular code

In my PhD thesis my main focus lied on the characterization of the alternative splice segment 5 of Neurexin 3 and its role in shaping a molecular code responsible for synapse specificity. My work thereby adds to a better understanding of an important synaptic contributor, the family of Neurexin, in generating this code. Moreover, analysis of *Nrxn3-AS5+* isoforms highlight the importance of studying synaptic diversity in combining transcriptome, translatome and further proteome studies.

To characterize the little studied NRXN3-AS5+ isoform on the protein level, we specifically tagged the endogenous protein and generated a knock-in mouse model using CRISPR-Cas9. AS5+ proteoforms were previously reported to be GPI-anchored and not secreted (Schreiner et al., 2014). Indeed, membrane fractionation experiments confirmed HA-tagged NRXN3-AS5+ isoforms to be enriched at the cell membrane. Radioactive labelling of a core GPI-anchor molecule further showed that NRXN-AS5+ is membrane tethered via a GPI-anchor. It could thus exhibit similar functions as the transmembrane NRXN3 in organizing an extracellular scaffold, as loss of intracellular domains was shown to not interfere with heterologous synapse formation (Gokce and Sudhof, 2013). Subsequently, artificial membrane tethered Neurexins could rescue loss of synapse formation, demonstrating that the extracellular part of Neurexins is sufficient for its synaptogenic function when membrane bound (Gokce and Sudhof, 2013).

Even though membrane bound Nrxn3 is sufficient for synapse formation, the release of GABA at inhibitory synapses in the olfactory bulb is dependent on intracellular domains of *Nrxn3* (Aoto et al., 2015). Conditional deletion of *Nrxn3α* and *Nrxn3β* thereby leads to a decrease in evoked IPSCs amplitude, which was further characterized to be a pre-synaptic phenotype based on altered paired-pulse ratios, consistent with lower release probability. This phenotype could not be rescued by the expression of artificially GPI-anchored NRXN3 but needed the intracellular domains via the transmembrane domain (Aoto et al., 2015). In my PhD thesis, we report a decreased amplitude of IPSCs in a specific subset of GABAergic synapses in the hippocampus when deleting GPI-anchored *Nrxn3,* which suggests differential roles for transmembrane and GPI-anchored Nrxns based on brain region and cell class.

Thus, *Nrxn3 AS5+* could act in different *trans*-synaptic recognition modules, which concept was introduced in using defined “sender” and “reader” modules consisting of variable proteoforms of synaptic molecules (Gomez et al., 2021). Our immunoprecipitation experiments add further evidence supporting this concept of synaptic modules, here in the

case of CCK inhibitory synapses enriched in the inner molecular layer of the DG represented by one “sender”, Nrxn3-AS5+.
Pre-synaptically, NRXN3 AS5+ might interact with NRXN1 and linking the extracellular “sender” module to the intracellular scaffold, as shown by co-immunoprecipitates of HA-tagged NRXN3 AS5+. Interestingly, when we look at our data comparing the post-synaptic interactome or the “reader” module of PAN-NRXN1 and HA-tagged NRXN3-AS5, we can see a huge difference in specificity. While pulling down all NRXN1 protein isoforms, we identify many binding partners, thereby pulling down a variety of individual “sender” modules. HA-tagged NRXN3 AS5+ on the other hand only interact with a subset of binding partners, thereby representing a more defined synaptic module. This shows the importance of analyzing binding partners of Neurexins in a more isoform driven way.

Advantages of GPI-anchored proteins in representing “sender” modules when compared to their trans-membrane counterparts could be based on higher mobility or the association with lipid rafts, which are known to segregate constituents of membranes (Lingwood and Simons, 2010). NRXN3 AS5+ could therefore be nucleated at sub-cellular domains of the synapse. On this account, dynamics of such synaptic nanomodules were shown to be essential for synaptic plasticity or play important roles in clustering pre- and post-synaptic binding partners (Crosby et al., 2019; Egawa et al., 2018; Hruska et al., 2018). Thus, differential tethering either via GPI-anchors or transmembrane domains might influence not only cell-type specific but further sub-cellular distribution of Neurexins. GPI-anchored Nrxn could help in the formation or control of nanodomains at the synapse, therefore not only contributing to a molecular synaptic code but further in shaping sub-synaptic domains.

One possibility of how NRXN3 AS5+ protein isoforms shape the molecular code would be the regulation of CCK-terminals via α-dystroglycan (*Dag1*). *Dag1* was shown to be essential for proper CCK innervation of pyramidal cells in the CA1 region of the hippocampus. Deletion of *Dag1* leads to the loss of CCK basket cell synapses and altered levels of *Dag1* in adult mice influence synaptic maintenance (Früh et al., 2016). Although the authors argued that these mechanisms are not dependent on Neurexin interactions, binding of Nrxns was analyzed with non-specific *Nrxn1* fusion proteins (Hara et al., 2011; Sugita et al., 2001). This overlaps with our immunoprecipitation data, where we did not find *Dag1* binding to *Nrxn1.* Specific expression of NRXN3 AS5+ at CCK positive terminals, and the proposed binding to *Dag1*, could thus be one newly characterized nanomodule. Specific expression of NRXN3-AS5+ might thereby be regulated by mRNA translational regulation, which will be discussed in the following chapter.

3.2 Regulation of Nrxn3 expression

The expression of either GPI-anchored or transmembrane *Nrxn3* is dependent on the inclusion of alternative exon 24. While our study did not address the question of which *trans*-acting factors could influence co- or post-transcriptional regulation of *Nrxn3-AS5*$^{+}$, we can draw some conclusions from our knock-in and knock-out mouse models.

Already the small insertion of a double HA-tag of ~70nt in the 5' region of exon 24 leads to a minor splice shift. Although splice site strength and possible splice regulator binding sites where maintained, this demonstrates how vulnerable splice sites are to small changes. The higher inclusion of exon 24 and the downregulation of transmembrane *Nrxn3* as examined by qPCRs is also visible on the protein level as determined by targeted proteomics (Appendix Figure 1). NRXN3-PAN and NRXN3α protein levels are slightly down-regulated, while splice forms NRXN3-25b and NRXN3-25c are more than two-fold downregulated. This means that there is a minimal over-expression of GPI-anchored NRXN3 in our knock-in mice.

In the NRXN3-AS5KO mouse model, this effect is greatly enhanced. Deletion of the alternative Exon 24 leads to major downstream splicing changes, most notably a higher direct splicing to Exon 25a. The underlying mechanisms could be two-fold: Elements directing splicing by either enhancing or repressing inclusion could reside within the sequence of exon 24, or the splicing of exon 24 and exon 25a could be coupled. This coupling might thereby regulate that all transcripts that incorporate exon 24 also include exon 25a, making them co-dependent, leading to a drastic change when deleting exon 24. The consequence of higher exon 25a inclusion is evident if we look at the protein levels of Nrxn3 in our AS5KO model. While the overall proteome of *NRXN3*$^{\Delta Ex24}$ mice shows only minor changes (Appendix Figure 2), PAN-NRXN3 is down-regulated by 60% even though we do not detect any differences in mRNA levels of *Nrxn3*. This leads to two interesting observations. First, as overall NRXN protein levels are dropping, transmembrane or *Nrxn3-AS5-* are higher expressed in AS5KO mice when compared to wild-type mice. This means that the majority of NRXN3 protein is GPI-anchored, which stands in stark contrast to transcriptomic studies, where the dominant isoforms were thought to encode transmembrane NRXN3 (Ray et al., 2020; Schreiner et al., 2014; Sudhof, 2017; Treutlein et al., 2014).

As nearly every study on *Nrxn3* function is done on transmembrane isoforms or artificially anchored proteins, those studies might therefore not represent an accurate model on the influence of *Nrxn3* on its function at the synapse.

Moreover, we found that incorporation of exon 25a leads to strong translational repression, as validated with targeted proteomics on hippocampal tissue and luciferase assays in heterologous cells. This could also be observed in cortical neuronal cell culture and does not seem to be different between excitatory and inhibitory cells in a reduced cellular system. When expressing the luciferase constructs with the 3'UTR of *Nrxn3* with Synapsin (all neurons) or mDLX (inhibitory specific) promoters in cortical neurons, translational repression mirrors the results from heterologous cells (Appendix Figure 3). Repression of translation is furthermore also regulating transcripts incorporating exon 24 and exon 25, raising the question how these transcripts can be expressed. To address this, we first tested activity dependent translational changes, but did not detect significant differences (Appendix Figure 3). Another possibility of circumventing translational repression would be the usage of an early poly(A)-site residing in the alternative exon 24. Importantly, we could verify this proximal poly(A)-site using a reductionist reporter system and by qPCRs on endogenous transcripts (Appendix Figure 4). Studies from other groups support these findings as they reported a proximal poly(A)-site *in silico* or by transcriptomics (Gruber et al., 2016; Herrmann et al., 2020; Ray et al., 2020).

Confirmation of an early poly(A)-site usage came from RNA-sequencing coverage of exon 24 in different cell types, in which we can see a clear drop after the early poly(A)-site (Furlanis et al., 2019). Usage of this early or proximal poly(A)-site could thereby evade translational repression, as longer 3'UTRs are known to have more *trans*-acting interactors (Miura et al., 2014).

Another possibility to evade translational control would be cleavage and thereby release of translational repression of the 3'UTR of *Nrxn3.* Examples for this phenomenon are now emerging, based on the possibility that 3'UTRs and CDS are differentially expressed (Kocabas et al., 2015). Moreover, post-transcriptional 3'UTR cleavage was shown to be widespread and can alter miRNA mediated regulation (Malka et al., 2017). Finally, cleaved 3'UTRs could not only release transcripts from translational regulation but act as an additional class of 3'UTR-derived RNAs (Andreassi et al., 2021).

One next step in characterizing 3'UTR regulation of *Nrxn3* would be to identify possible *trans*-acting factors. An interesting candidate, which emerged through sequence analysis of exon 24 – exon 25 was Musashi (Msi), as this revealed binding recognition elements of this RBP family consisting of *Msi1* and *Msi2*. MSI1 binds to poly(A)-binding protein (PABP) and acts as a translational repressor of target mRNAs by competing with the eukaryotic initiation factor 4 complex (eIF4G) for the binding of PABP (Kawahara et al., 2008). Using GFP-reporters fused to exon 24 and exon 25 of *Nrxn3,* we could demonstrate that mutating Musashi binding sites partially releases transcripts from translational repression (Appendix Figure 5). As this effect was only minimal, further experiments would be needed to

investigate regulators of *Nrxn3* translation. This could include probing of different miRNAs based on seed regions in the *Nrxn3* 3'UTR, and further inactivating predicted miRNAs by antisense oligos or miRNA sponges (Ebert and Sharp, 2010).
Taken together, these results highlight the importance of applying and combining multiple approaches to study synaptic diversity. To understand the proposed molecular code underlying synapse function we need to specifically probe synaptic proteins and their proteoforms.

3.3 Necessity of proteomic studies for studying synaptic diversity

In-depth transcriptome and translatome studies gave us a huge leap forward in analyzing the basic function of the nervous system and its underlying cell-types. We therefore could characterize the importance of co- and post-transcriptional mechanisms as for example alternative splicing and the localization of transcripts by mRNA transport.
One caveat therein is the limited amount of mRNA that can be isolated from single cells or from small cell populations. This leads to a biased analysis, as those mRNA pools need to be reverse transcribed and amplified from the 3' end to be detected. More abundant transcripts and splice isoforms can thereby cloud the detection of low abundant mRNA. Thus, we need more in-depth sequencing studies, which are able to detect less abundant isoforms with more confidence. In addition to more precise transcriptome studies, it is evident that there is a substantial need to study the synaptic proteome, for which we need to combine different techniques. One promising route are new high-resolution imaging techniques that can help us studying the sub-cellular and even sub-synaptic localization of proteins. However, we are facing the challenge that antibodies against specific synaptic proteins are not isoform specific, limiting us in separating individual isoforms. As demonstrated in our study and as shown in multiple examples when analyzing AS4 of Nrxns this would be necessary to decipher the function of not only Neurexins in general but other synaptogenic proteins as well. We overcame this limitation by genetically introducing a small tag and thus labelling a specific slice isoform of Neurexin for the first time.

To get a handle on proteins, more and more effort was put into developing ways of efficiently labeling proteins, which in a second step then can be detected by a reporter. This can be achieved by a wide range of possibilities, including affinity tags, enzymatic modules or directly adding a fluorophore to a protein. As all of these labels and reporters have their limitations, either in large sizes and steric hindrance or limited combinatorial use, effective labelling remains a big challenge in studying synaptic proteins (Choquet et al., 2021). For reporters such as antibodies, which are quite large, fragments including nanobodies and short-chain variable fragments (scFv), which are smaller by a factor of 10 (Helma et al., 2015), are promising options and emerging to tag specific synaptic proteins (Dong et al., 2019).

In addition to conventional confocal microscopy, which was our method of choice to elucidate co-labelling of NRXN3-AS5^{+} protein isoforms with GABAergic synaptic markers, high resolution imaging techniques would enable us to analyze sub-cellular localization of NRXN3-AS5+. These techniques are able to reveal the localization of single molecules and were successfully used in a variety of studies, as for example in understanding the dynamics of specific post-synaptic receptors in both normal and disease state (Groc and Choquet, 2020).

Next to fluorescent based imaging techniques, electron-microscopy (EM) is used to analyze the subcellular localization of proteins. EM has the highest resolution, and recent efforts managed to reconstruct 3D images of the complex wiring of the brain (Motta 2019). Immuno-EM, meaning the labelling of proteins with antibodies linked to heavy particles, is one option to get an accurate measurement where certain proteins are localized. In an ongoing collaboration we are now trying to decipher sub-cellular localization of NRXN3-AS5+ specifically at CCK synaptic terminals in the IML of the DG using immuno-EM on NRXN3AS5$^{HA/HA}$ knock-in mice.

A clear emerging trend is the necessity of combining multiple strategies to overcome the limitations of individual ones. Another approach which we believe has enormous potential, is the analysis of different proteoforms by targeted proteomics. Using heavy reference peptides to detect low abundant peptides is a fast and streamlined process after individual reference peptides are validated (Schreiner et al., 2015). In addition to analyzing Neurexin splice isoforms, we also applied this targeted assay on a splice target of SAM68, a member of the STAR family of RBP's. There we could assist in demonstrating that a splice shift due to SAM68 function alters *Il1rap* (Interleukin 1 receptor accessory protein) from a membrane-bound to a secreted protein isoform (Iijima et al., 2019), again demonstrating the specificity of this assay. To further promote and to collect already validated and successfully used heavy peptides, we put together a database for heavy reference peptides. This database, which will be publicly available (https://scheiffele-

SYNCODE.scicore.unibas.ch/), incorporates all mass-spectronomy data already collected and can be completed with additional peptides. Combining targeted mass-spec analysis with other approaches including sophisticated imaging techniques and loss-of-function studies on individual isoforms will help us make another step into understanding brain function.

3.4 Conclusion

Taken together, the work done in the scope of my PhD thesis highlights the importance of a profound and in-depth analysis combining both transcriptomic and proteomic studies to get a better insight in synaptic diversity. In using a specific splice-isoform knock-in, and the targeted proteomics on splice site knock-out mice we could delineate an uncharacterized splice isoform and a part of its role in shaping synapse specificity. Its selective expression at GABAergic terminals and the lack of expression at glutamatergic terminals propose a cell class dependent function. Additionally, the selective functional effect on a subset of GABAergic terminals further uncovers a more finetuned role of Neurexins in the brain. Moreover, the divergence from predicted mRNA levels, which are controlled by translational regulatory elements, adds another layer of control.
Alternative splicing and the regulation of mRNA therefore play an important role in shaping synaptic wiring. Our study supports novel strategies to further understand the comprehensive mosaic of signaling molecules dependent and independent of Neurexins. The dissection of synaptic proteoforms will help us to not only understand the development and maintenance of brain circuitry, but furthermore will enable us to get more insight in brain malfunctions.

4. Appendix

4.1 Additional Data

Figure 1

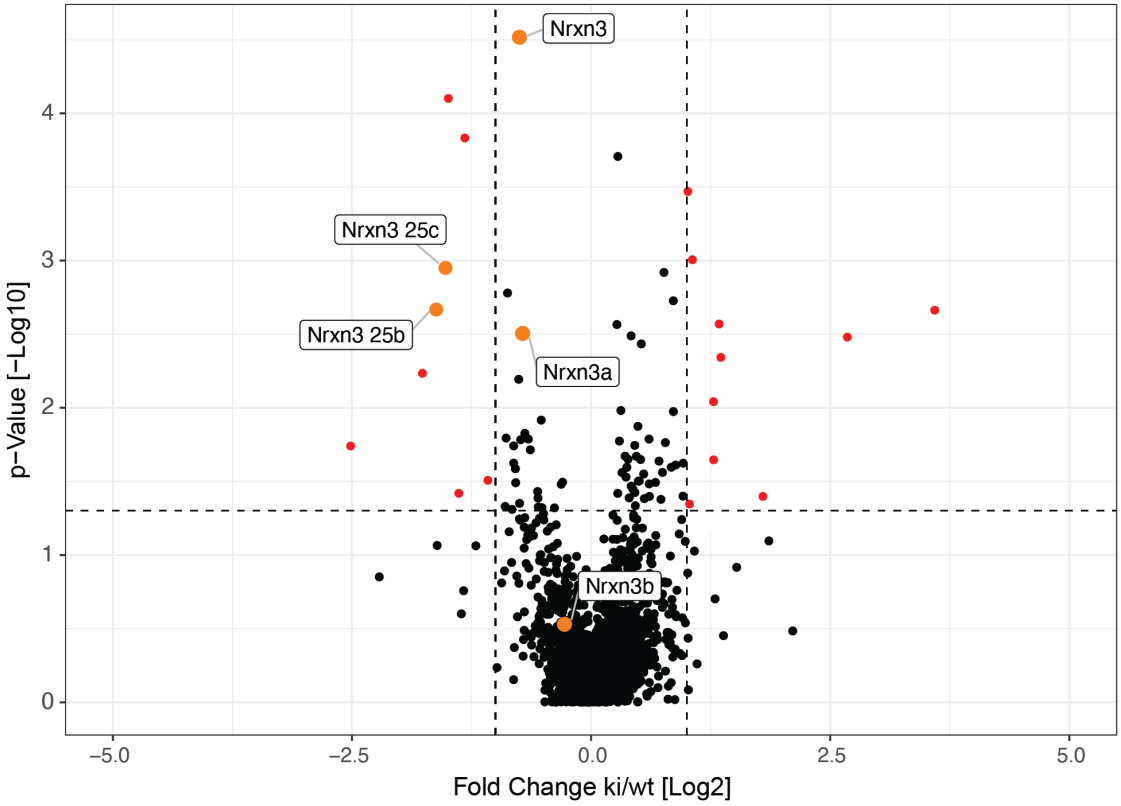

Figure 1. Proteome analysis *Nrxn3-AS5^{HA}* knock-in mice

Combined plot of targeted and shotgun proteomic analysis of *Nrxn3-AS5^{HA}* knock-in mice, with heavy peptides representing PAN-NRXN3, NRXN3α, NRXN3β, NRXN3-25b and NRXN3-25c as reference (highlighted in orange). X-axis shows fold change (Log2) of homozygous knock-in mice when compared to wildtype, y-axis represents p-values (Log2). N=5 hippocampi from wild-type and homozygous knock-in mice, proteins with p-values <0.05 (horizontal dotted line) and fold change >2, <-2 (vertical dotted lines) are highlighted in red.

Figure 2

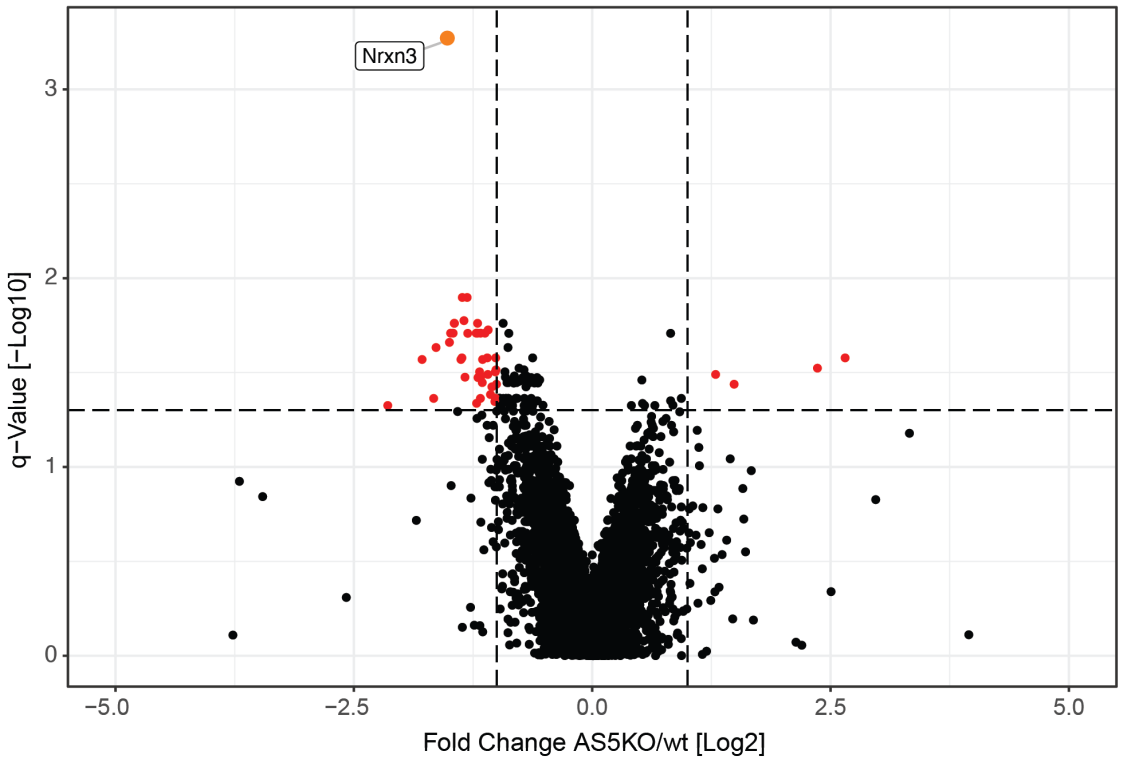

Figure 2. Proteome analysis *Nrxn3$^{\Delta Ex24}$* mice

Tandem-mass-tag Mass Spectronomy of wildtype and homozygous *Nrxn3$^{\Delta Ex24}$* isolated hippocampal tissue (N=5 per genotype), Nrxn3 is highlighted. X-axis shows fold change (Log2) of homozygous knock-out mice when compared to wildtype, y-axis represents q-values (p-values corrected for sample size, Log2). Proteins with q-values <0.05 (horizontal dotted line) and fold change >2, <-2 (vertical dotted lines) are highlighted in red.

Figure 3

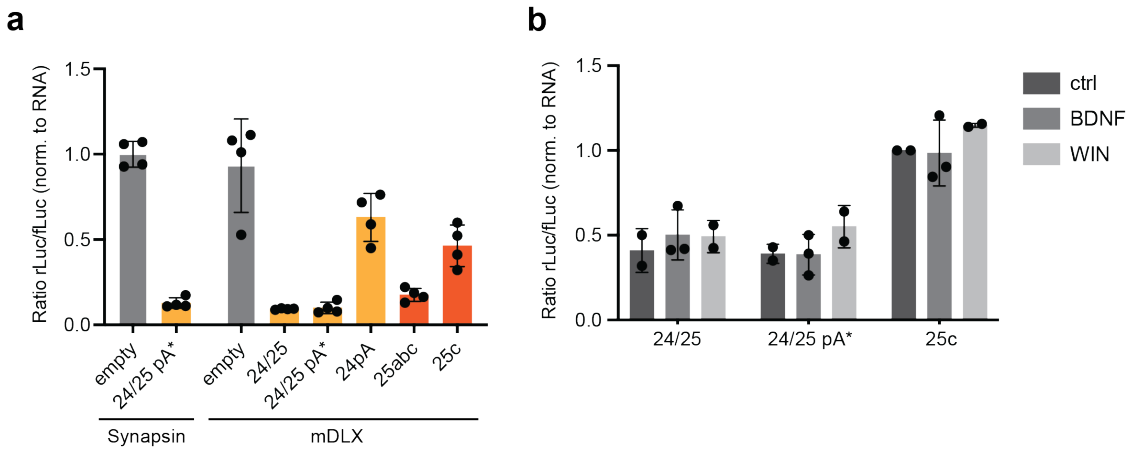

Figure 3. Translational regulation of *Nrxn3 AS5+* in neuronal cell culture

a, Luciferase Assay of cortical cultures, DIV14, with Synapsin or mDLX driven alternative 3'UTRs of *Nrxn3* (exon numbers indicated), ratios of renilla to firefly luciferase are normalized to respective mRNA levels, N=4 cortical cultures. **b**, Stimulation (3hrs) and subsequent luciferase assay of cortical cultures, DIV14, with BDNF (50ng/ml) or WIN-55,212 (5µM) to stimulate TrkB or CbR1/2 mediated signaling, with mDLX driven alternative 3'UTRs of *Nrxn3*, ratios of renilla to firefly luciferase are normalized to respective mRNA levels, N=2-3 cortical cultures.

Figure 4

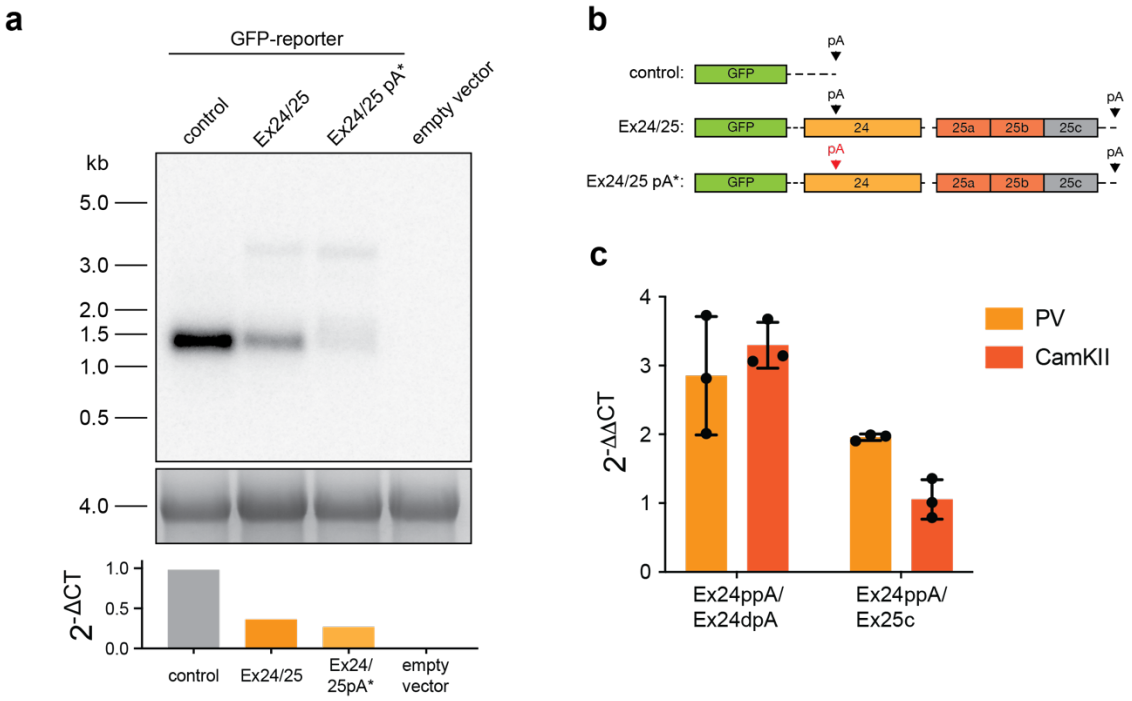

Figure 4. Alternative polyadenylation validation of *Nrxn3*

a, Northern Blot of overexpressed GFP-reporter (GFP-control, GFP-Ex24/25, GFP-Ex24/25pA*) or empty vector in HEK293T-cells. Hybridized membrane was exposed for 2 days to an intensifying screen, loading control (28S ribosomal subunit) is visible below northern blot, RNA ladder labeled on the left. qPCR levels of all constructs relative to co-transfected RFP and measured with GFP specific forward and reverse primers indicated below. **b**, Schematic of GFP-reporter fused to Exon24/25 with and without mutation of the proximal / early poly(A)-site, exon numbers indicated. **c**, Quantitative PCRs of exonic regions before and after the proximal poly(A)-site of Nrxn3-AS5 (ppA=proximal poly(A)-site, dpA=distal poly(A)-site), normalized to standard as determined by linearized Plasmid DNA, samples from PV or CamKII RiboTag pulldowns.

Figure 5

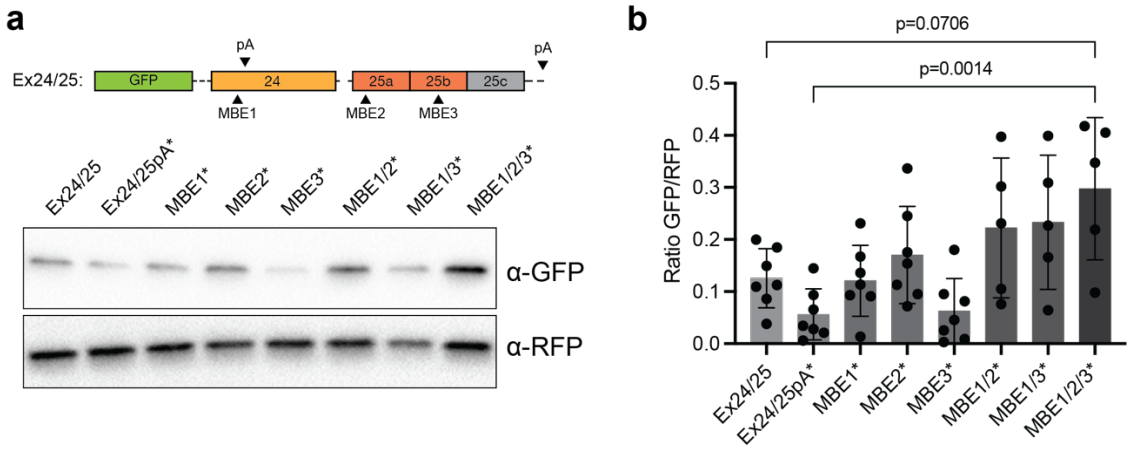

Figure 5. Influence of Musashi on *Nrxn3-AS5+* translational regulation

a, Top: Schematic of GFP-reporter fused to Exon24/25 of *Nrxn3*, Musashi binding elements (MBEs) and poly(A)-sites indicated. Bottom: Western Blot of overexpressed GFP constructs co-transfected with RFP in HEK293T-cells and probed with α-GFP and α-RFP antibodies, individual and combined mutations of MBE indicated. **b**, Quantification of five individual transfections, normalized to RFP-levels, intensities of Western Blot signal measured and quantified in Fiji, p-value calculated with one-way anova, Bonferroni's test.

4.2 Methods Additional Data

Methods for qPCR analysis, targeted and normal shotgun mass-spectronomy, luciferase assays and cell cultures were done as described in the manuscript, RiboTag Samples from Cre-driver lines crossed with floxed RiboTag-HA mice were a kind gift from Elisabetta Furlanis.

Global proteome analysis using tandem mass tags

Sample aliquots containing 25 ug of peptides were dried and labeled with tandem mass isobaric tags (TMT 10-plex, Thermo Fisher Scientific) according to the manufacturer's instructions. To control for ratio distortion during quantification, a peptide calibration mixture consisting of six digested standard proteins mixed in different amounts were added to each sample before TMT labeling as recently described (Ahrne et al., 2016). After pooling the differentially TMT labeled peptide samples, peptides were again desalted on C18 reversed-phase spin columns according to the manufacturer's instructions (Macrospin, Harvard Apparatus) and dried under vacuum. TMT-labeled peptides were fractionated by high-pH reversed phase separation using a XBridge Peptide BEH C18 column (3,5 µm, 130 Å, 1 mm x 150 mm, Waters) on an Agilent 1260 Infinity HPLC system. Peptides were loaded on column in buffer A (ammonium formate (20 mM, pH 10) in water) and eluted using a two-step linear gradient starting from 2% to 10% in 5 minutes and then to 50% (v/v) buffer B (90% acetonitrile / 10% ammonium formate (20 mM, pH 10) over 55 minutes at a flow rate of 42 µl/min. Elution of peptides was monitored with a UV detector (215 nm, 254 nm). A total of 36 fractions were collected, pooled into 12 fractions using a post-concatenation strategy as previously described (Wang et al., 2011), dried under vacuum.

1µg of peptides were LC-MS analyzed as described previously (Ahrne et al., 2016). Chromatographic separation of peptides was carried out using an EASY nano-LC 1000 system (Thermo Fisher Scientific), equipped with a heated RP-HPLC column (75 µm x 37 cm) packed in-house with 1.9 µm C18 resin (Reprosil-AQ Pur, Dr. Maisch). Aliquots of 1 µg total peptides were analyzed per LC-MS/MS run using a linear gradient ranging from 95% solvent A (0.15% formic acid, 2% acetonitrile) and 5% solvent B (98% acetonitrile, 2% water, 0.15% formic acid) to 30% solvent B over 90 minutes at a flow rate of 200 nl/min. Mass spectrometry analysis was performed on Q-Exactive HF mass spectrometer equipped with a nanoelectrospray ion source (both Thermo Fisher Scientific). Each MS1 scan was followed by high-collision-dissociation (HCD) of the 10 most abundant precursor ions with dynamic exclusion for 20 seconds. Total cycle time was approximately 1 s. For

MS1, 3e6 ions were accumulated in the Orbitrap cell over a maximum time of 100 ms and scanned at a resolution of 120,000 FWHM (at 200 m/z). MS2 scans were acquired at a target setting of 1e5 ions, accumulation time of 100 ms and a resolution of 30,000 FWHM (at 200 m/z). Singly charged ions and ions with unassigned charge state were excluded from triggering MS2 events. The normalized collision energy was set to 35%, the mass isolation window was set to 1.1 m/z and one microscan was acquired for each spectrum.
The acquired raw-files were converted to the mascot generic file (mgf) format using the msconvert tool (part of ProteoWizard, version 3.0.4624 (2013-6-3)). Using the MASCOT algorithm (Matrix Science, Version 2.4.1), the mgf files were searched against the same murine database mentioned above containing the six calibration mix proteins (Ahrne et al., 2016) this time for protein ratio correction. The precursor ion tolerance was set to 10 ppm and fragment ion tolerance was set to 0.02 Da. The search criteria were set as follows: full tryptic specificity was required (cleavage after lysine or arginine residues unless followed by proline), 3 missed cleavages were allowed, carbamidomethylation (C), TMT6plex (K and peptide n-terminus) were set as fixed modification and oxidation (M) as a variable modification. Next, the database search results were imported to the Scaffold Q+ software (version 4.3.2, Proteome Software Inc., Portland, OR) and the protein false identification rate was set to 1% based on the number of decoy hits. Proteins that contained similar peptides and could not be differentiated based on MS/MS analysis alone were grouped to satisfy the principles of parsimony. Proteins sharing significant peptide evidence were grouped into clusters. Acquired reporter ion intensities in the experiments were employed for automated quantification and statically analysis using a modified version of our in-house developed SafeQuant R script (v2.3, (Ahrne et al., 2016)). This analysis included adjustment of reporter ion intensities, global data normalization by equalizing the total reporter ion intensity across all channels, summation of reporter ion intensities per protein and channel, calculation of protein abundance ratios and testing for differential abundance using empirical Bayes moderated t-statistics. Finally, the calculated p-values were corrected for multiple testing using the Benjamini−Hochberg method.

Mutagenesis of GFP-Ex24/25

QuikChange site directed mutagenesis kit (Agilent technologies) was used to insert 2bp mutations into GFP-Ex24/25 reporter plasmids, in combination with using PCR amplification of Nrxn 3 exon 24 and 25 with gene specific and mutagenesis primers followed by overlapping PCR and insertion into GFP-AA using BglII and EcoRI restriction sites.

#	*Primer Name*	*Sequence*
1	N3-MBE1-for	CTT CAT CTC CTG TGT CCT ACA CTCA TAG AC
2	N3-MBE1-rev	GTC TAT GAG TGT AGG ACA CAG GAG ATG AAG
3	N3-MBE2-for	GTT GAT GAG GTG AAT TCC TTA TTC CTC TTC
4	N3-MBE2-rev	GAA GAG GAA TAA GGA ATT CAC CTC ATC AAC
5	N3-MBE3-for	CCA GCC TGA TAT CCT CTT GCT TCC GTT GCC
6	N3-MBE3-rev	GGC AAC GGA AGC AAG AGG ATA TCA GGC TGG
7	N3-pA-mut-for	AAA GAT ACT AGA AGT ATA AAT ATA TAT TGA GAA
8	N3-pA-mut-rev	TTC CAA TAT ATA TTT ATA CTT CTA GTA TCT TT

Northern Blot

RNA from transfected HEK293T-cells was mixed with 2x RNA loading dye (Gel loading buffer II (Invitrogen)) and 1µl ethidium bromide, denatured at 75°C for 10min and separated by gel electrophoresis (0.6g Agarose in 45ml DEPC H_2O + 5ml 10x Northern Max Denaturing Gel Buffer (Thermo Fisher)). Before transfer the gel was soaked in 20x SSC (Ambion) for 15min and the overnight transfer was set up as described by (Streit et al., 2008). After transfer RNA was crosslinked to the membrane at 120 mJ cm^{-2} and baked at 60°C for 45min. Pre-hybridization was done overnight at 42°C in 50% formamide, 0.2% SDS, 5x Denhardt's solution, 5x SSC, 100µg ml^{-1} salmon sperm (Invitrogen) and 50mM sodium phosphate buffer (pH 6.5). Radiolabelled probe was prepared by PCR with Phusion HF Polymerase according to the manufacturer instructions in addition of 10µCi [alpha-^{32}P]dCTP (3000 Ci $mmol^{-1}$). PCR product was cleaned up by size-exclusion Chroma Spin TE-400 Columns and then added for overnight incubation at 42°C to the pre-hybridization solution. The membrane was then washed in 1x SSPE (Sigma) / 0.5% SDS at 65°C for 10 min and twice in 0.1x SSPE / 0.5% SDS at 68°C for 10min. Membrane was dried on blotting paper and incubated with Phospho-imager intensifying screen for 2 days before imaging.

4.3 Index of figures

Introduction:

Results:

Appendix:

4.4 Index of abbreviations

AMPA = α-amino-3-hydroxy-5-methyl-4-isoxazolepropionic acid

APA = alternative polyadenylation

AS = alternative splice segment

BDNF = brain-derived neurotrophic factor

bp = basepair

C1ql = C1q-like

CA = cornu ammonis

CAM = cell adhesion molecule

CASK = calcium/calmodulin-activated serine/threonine kinase

Cbln = Cerebellin

CCK = cholecystokinin

CDS = coding sequence

CGE = caudal ganglionic eminence

CPSF = cleavage and polyadenylation specificity factor

CR = calretinin

CSTF = cleavage stimulation factor

DG = dentate gyrus

DSE = downstream sequence element

EGF = epidermal growth factor

eIF4g = eukaryotic initiation factor 4 complex

EJC = exon junction complex

EM = electron microscopy

ESE = exonic splice enhancer

ESS = exonic splice silencer

GABA = γ-aminobutyric acid

GCL = granule cell layer

GFP = green fluorescent protein

GPI-anchor = glycosylphosphatidylinositol-anchor

HA = Human influenza hemagglutinin

HIL = hilus

hnRNP = heterogenous nuclear ribonucleoprotein

HS = heparan sulfate

HSGP = heparan sulfate glycoprotein

IgM = Immunoglobulin M

IML = inner molecular layer

IP = immuno-purification

IPSC = inhibitory post-synaptic current

IPSP = inhibitory post-synaptic potential

ISE = intronic splice enhancer

ISS = intronic splice silencer

KI = knock-in

KO = knock-out

LNS domain = Laminin-Neurexin-Sex hormone-binding globulin domain

LRRTM = leucine-rich repeat transmembrane protein

LTP = long-term potentiation

MF = mossy fiber

MGE = medial ganglionic eminence

miRNA = microRNA

MML = middle molecular layer

mRNA = messenger RNA

Msi = Musashi

Nlgn = Neuroligin

NMD = nonsense mediated mRNA decay

NMDA = N-Methyl-D-aspartic acid

Nrxn = Neurexin

nt = nucleotide

Nxph = Neurexophilin

OML = outer molecular layer

PABP = poly(A)-binding protein

PacBio = pacific biosciences

PI-PLC = phosphatidylinositol-specific phospholipase C

PP = perforant path

PTC = premature translation termination codon

PV = parvalbumin

RBP = RNA-binding protein

RT = reverse transcription

SC = schaffer collateral

scFv = short-chain variable fragments

SGZ = subgranular zone

SLM = Sam68-like mammalian protein

SST = somatostatin

STAR = signal transduction activator of RNA

TMD = transmembrane domain

TMT = tandem-mass-tag

USE = upstream sequence element

UTR = untranslated region

VIP = vasoactive intestinal peptide

5. References

Ahrne, E., Glatter, T., Vigano, C., Schubert, C., Nigg, E.A., and Schmidt, A. (2016). Evaluation and Improvement of Quantification Accuracy in Isobaric Mass Tag-Based Protein Quantification Experiments. J Proteome Res *15*, 2537-2547.

Alt, F.W., Bothwell, A.L., Knapp, M., Siden, E., Mather, E., Koshland, M., and Baltimore, D. (1980). Synthesis of secreted and membrane-bound immunoglobulin mu heavy chains is directed by mRNAs that differ at their 3' ends. Cell *20*, 293-301.

Amara, S.G., Jonas, V., Rosenfeld, M.G., Ong, E.S., and Evans, R.M. (1982). Alternative RNA processing in calcitonin gene expression generates mRNAs encoding different polypeptide products. Nature *298*, 240-244.

An, J.J., Gharami, K., Liao, G.-Y., Woo, N.H., Lau, A.G., Vanevski, F., Torre, E.R., Jones, K.R., Feng, Y., Lu, B.*, et al.* (2008). Distinct Role of Long 3' UTR BDNF mRNA in Spine Morphology and Synaptic Plasticity in Hippocampal Neurons. Cell *134*, 175-187.

Andersen, P. (2007). The hippocampus book (Oxford ; New York: Oxford University Press).

Andreassi, C., Luisier, R., Crerar, H., Darsinou, M., Blokzijl-Franke, S., Lenn, T., Luscombe, N.M., Cuda, G., Gaspari, M., Saiardi, A.*, et al.* (2021). Cytoplasmic cleavage of IMPA1 3' UTR is necessary for maintaining axon integrity. Cell Rep *34*, 108778.

Aoto, J., Foldy, C., Ilcus, S.M.C., Tabuchi, K., and Sudhof, T.C. (2015). Distinct circuit-dependent functions of presynaptic neurexin-3 at GABAergic and glutamatergic synapses. Nature neuroscience *18*, 997-1007.

Aoto, J., Martinelli, D.C., Malenka, R.C., Tabuchi, K., and Sudhof, T.C. (2013). Presynaptic neurexin-3 alternative splicing trans-synaptically controls postsynaptic AMPA receptor trafficking. Cell *154*, 75-88.

Autism Genome Project, C., Szatmari, P., Paterson, A.D., Zwaigenbaum, L., Roberts, W., Brian, J., Liu, X.Q., Vincent, J.B., Skaug, J.L., Thompson, A.P.*, et al.* (2007). Mapping autism risk loci using genetic linkage and chromosomal rearrangements. Nat Genet *39*, 319-328.

Barbosa-Morais, N.L., Irimia, M., Pan, Q., ..., and Blencowe, B.J. (2012). The evolutionary landscape of alternative splicing in vertebrate species. science *338*, 1587-1594.

Bartel, D.P. (2009). MicroRNAs: target recognition and regulatory functions. Cell *136*, 215-233.

Biederer, T., and Sudhof, T.C. (2001). CASK and protein 4.1 support F-actin nucleation on neurexins. J Biol Chem *276*, 47869-47876.

Black, D.L. (2003). Mechanisms of Alternative Pre-Messenger RNA Splicing. Annual Review of Biochemistry *72*, 291-336.

Brogna, S., McLeod, T., and Petric, M. (2016). The Meaning of NMD: Translate or Perish. Trends Genet *32*, 395-407.

Brown, K.N., Chen, S., Han, Z., Lu, C.H., Tan, X., Zhang, X.J., Ding, L., Lopez-Cruz, A., Saur, D., Anderson, S.A.*, et al.* (2011). Clonal production and organization of inhibitory interneurons in the neocortex. Science *334*, 480-486.

Cajigas, I.J., Tushev, G., Will, T.J., tom Dieck, S., Fuerst, N., and Schuman, E.M. (2012). The local transcriptome in the synaptic neuropil revealed by deep sequencing and high-resolution imaging. Neuron *74*, 453-466.

Castle, J.C., Zhang, C., Shah, J.K., Kulkarni, A.V., Kalsotra, A., Cooper, T.A., and Johnson, J.M. (2008). Expression of 24,426 human alternative splicing events and predicted cis regulation in 48 tissues and cell lines. Nat Genet *40*, 1416-1425.

Chen, L.Y., Jiang, M., Zhang, B., Gokce, O., and Südhof, T.C. (2017). Conditional Deletion of All Neurexins Defines Diversity of Essential Synaptic Organizer Functions for Neurexins. Neuron *94*, 611-625.e614.

Chen, M., and Manley, J.L. (2009). Mechanisms of alternative splicing regulation: insights from molecular and genomics approaches. Nat Rev Mol Cell Biol *10*, 741-754.

Chen, S., Lee, B., Lee, A.Y., Modzelewski, A.J., and He, L. (2016). Highly Efficient Mouse Genome Editing by CRISPR Ribonucleoprotein Electroporation of Zygotes. J Biol Chem *291*, 14457-14467.

Chen, Z., Cooper, B., Kalla, S., Varoqueaux, F., and Young, S.M., Jr. (2013). The Munc13 proteins differentially regulate readily releasable pool dynamics and calcium-dependent recovery at a central synapse. J Neurosci *33*, 8336-8351.

Chih, B., Engelman, H., and Scheiffele, P. (2005). Control of excitatory and inhibitory synapse formation by neuroligins. Science *307*, 1324-1328.

Chih, B., Gollan, L., and Scheiffele, P. (2006). Alternative splicing controls selective trans-synaptic interactions of the neuroligin-neurexin complex. Neuron *51*, 171-178.

Choquet, D., Sainlos, M., and Sibarita, J.B. (2021). Advanced imaging and labelling methods to decipher brain cell organization and function. Nature reviews Neuroscience *22*, 237-255.

Colgan, D.F., and Manley, J.L. (1997). Mechanism and regulation of mRNA polyadenylation. Genes & development *11*, 2755-2766.

Conti, E., and Izaurralde, E. (2005). Nonsense-mediated mRNA decay: molecular insights and mechanistic variations across species. Curr Opin Cell Biol *17*, 316-325.

Crosby, K.C., Gookin, S.E., Garcia, J.D., Hahm, K.M., Dell'Acqua, M.L., and Smith, K.R. (2019). Nanoscale Subsynaptic Domains Underlie the Organization of the Inhibitory Synapse. Cell Rep *26*, 3284-3297.e3283.

Dai, J., Aoto, J., and Südhof, T.C. (2019). Alternative Splicing of Presynaptic Neurexins Differentially Controls Postsynaptic NMDA and AMPA Receptor Responses. Neuron *102*, 993-1008.e1005.

Danckwardt, S., Hentze, M.W., and Kulozik, A.E. (2008). 3' end mRNA processing: molecular mechanisms and implications for health and disease. The EMBO journal *27*, 482-498.

Danckwardt, S., Kaufmann, I., Gentzel, M., Foerstner, K.U., Gantzert, A.S., Gehring, N.H., Neu-Yilik, G., Bork, P., Keller, W., Wilm, M.*, et al.* (2007). Splicing factors stimulate polyadenylation via USEs at non-canonical 3' end formation signals. The EMBO journal *26*, 2658-2669.

David, C.J., and Manley, J.L. (2010). Alternative pre-mRNA splicing regulation in cancer: pathways and programs unhinged. Genes & development *24*, 2343-2364.

Davis, M.J., Hanson, K.A., Clark, F., Fink, J.L., Zhang, F., Kasukawa, T., Kai, C., Kawai, J., Carninci, P., Hayashizaki, Y.*, et al.* (2006). Differential Use of Signal Peptides and Membrane Domains Is a Common Occurrence in the Protein Output of Transcriptional Units. PLoS Genet *2*, e46.

de Wit, J., and Ghosh, A. (2016). Specification of synaptic connectivity by cell surface interactions. Nature reviews Neuroscience *17*, 22-35.

de Wit, J., Sylwestrak, E., O'Sullivan, M.L., Otto, S., Tiglio, K., Savas, J.N., Yates, J.R., Comoletti, D., Taylor, P., and Ghosh, A. (2009). LRRTM2 interacts with Neurexin1 and regulates excitatory synapse formation. Neuron *64*, 799-806.

Dean, C., Scholl, F.G., Choih, J., DeMaria, S., Berger, J., Isacoff, E., and Scheiffele, P. (2003). Neurexin mediates the assembly of presynaptic terminals. Nature neuroscience *6*, 708-716.

Di Giammartino, D.C., Li, W., Ogami, K., Yashinskie, J.J., Hoque, M., Tian, B., and Manley, J.L. (2014). RBBP6 isoforms regulate the human polyadenylation machinery and modulate expression of mRNAs with AU-rich 3' UTRs. Genes & development *28*, 2248-2260.

Dong, J.X., Lee, Y., Kirmiz, M., Palacio, S., Dumitras, C., Moreno, C.M., Sando, R., Santana, L.F., Südhof, T.C., Gong, B.*, et al.* (2019). A toolbox of nanobodies developed and validated for use as intrabodies and nanoscale immunolabels in mammalian brain neurons. Elife *8*.

Dredge, B.K., and Darnell, R.B. (2003). Nova regulates GABA(A) receptor gamma2 alternative splicing via a distal downstream UCAU-rich intronic splicing enhancer. Mol Cell Biol *23*, 4687-4700.

Dredge, B.K., Stefani, G., Engelhard, C.C., and Darnell, R.B. (2005). Nova autoregulation reveals dual functions in neuronal splicing. The EMBO journal *24*, 1608-1620.

Ebert, M.S., and Sharp, P.A. (2010). MicroRNA sponges: progress and possibilities. RNA *16*, 2043-2050.

Egawa, J., Zemljic-Harpf, A., Mandyam, C.D., Niesman, I.R., Lysenko, L.V., Kleschevnikov, A.M., Roth, D.M., Patel, H.H., Patel, P.M., and Head, B.P. (2018). Neuron-Targeted Caveolin-1 Promotes Ultrastructural and Functional Hippocampal Synaptic Plasticity. Cereb Cortex *28*, 3255-3266.

Elkon, R., Drost, J., van Haaften, G., Jenal, M., Schrier, M., Oude Vrielink, J.A., and Agami, R. (2012). E2F mediates enhanced alternative polyadenylation in proliferation. Genome Biol *13*, R59.

Elkon, R., Ugalde, A.P., and Agami, R. (2013). Alternative cleavage and polyadenylation: extent, regulation and function. Nat Rev Genet *14*, 496-506.

Etherton, M.R., Blaiss, C.A., Powell, C.M., and Sudhof, T.C. (2009). Mouse neurexin-1alpha deletion causes correlated electrophysiological and behavioral changes consistent with cognitive impairments. Proc Natl Acad Sci U S A *106*, 17998-18003.

Favuzzi, E., Deogracias, R., Marques-Smith, A., Maeso, P., Jezequel, J., Exposito-Alonso, D., Balia, M., Kroon, T., Hinojosa, A.J., E, F.M.*, et al.* (2019). Distinct molecular programs regulate synapse specificity in cortical inhibitory circuits. Science *363*, 413-417.

Flaherty, E., Zhu, S., Barretto, N., Cheng, E., Deans, P.J.M., Fernando, M.B., Schrode, N., Francoeur, N., Antoine, A., Alganem, K.*, et al.* (2019). Neuronal impact of patient-specific aberrant NRXN1α splicing. Nat Genet *51*, 1679-1690.

Flavell, S.W., Kim, T.K., Gray, J.M., Harmin, D.A., Hemberg, M., Hong, E.J., Markenscoff-Papadimitriou, E., Bear, D.M., and Greenberg, M.E. (2008). Genome-wide analysis of MEF2 transcriptional program reveals synaptic target genes and neuronal activity-dependent polyadenylation site selection. Neuron *60*, 1022-1038.

Früh, S., Romanos, J., Panzanelli, P., Bürgisser, D., Tyagarajan, S.K., Campbell, K.P., Santello, M., and Fritschy, J.M. (2016). Neuronal Dystroglycan Is Necessary for Formation and Maintenance of Functional CCK-Positive Basket Cell Terminals on Pyramidal Cells. J Neurosci *36*, 10296-10313.

Fuccillo, M.V., Foldy, C., Gokce, O., Rothwell, P.E., Sun, G.L., Malenka, R.C., and Sudhof, T.C. (2015). Single-Cell mRNA Profiling Reveals Cell-Type-Specific Expression of Neurexin Isoforms. Neuron *87*, 326-340.

Furlanis, E., Traunmuller, L., Fucile, G., and Scheiffele, P. (2019). Landscape of ribosome-engaged transcript isoforms reveals extensive neuronal-cell-class-specific alternative splicing programs. Nature neuroscience *22*, 1709-1717.

Garneau, N.L., Wilusz, J., and Wilusz, C.J. (2007). The highways and byways of mRNA decay. Nat Rev Mol Cell Biol *8*, 113-126.

Geschwind, D.H., and State, M.W. (2015). Gene hunting in autism spectrum disorder: on the path to precision medicine. Lancet Neurol *14*, 1109-1120.

Giorgi, C., Yeo, G.W., Stone, M.E., Katz, D.B., Burge, C., Turrigiano, G., and Moore, M.J. (2007). The EJC factor eIF4AIII modulates synaptic strength and neuronal protein expression. Cell *130*, 179-191.

Glock, C., Heumüller, M., and Schuman, E.M. (2017). mRNA transport & local translation in neurons. Curr Opin Neurobiol *45*, 169-177.

Gokce, O., and Sudhof, T.C. (2013). Membrane-tethered monomeric neurexin LNS-domain triggers synapse formation. J Neurosci *33*, 14617-14628.

Gomez, A.M., Traunmuller, L., and Scheiffele, P. (2021). Neurexins: molecular codes for shaping neuronal synapses. Nature reviews Neuroscience *22*, 137-151.

Graf, E.R., Zhang, X., Jin, S.X., Linhoff, M.W., and Craig, A.M. (2004). Neurexins induce differentiation of GABA and glutamate postsynaptic specializations via neuroligins. Cell *119*, 1013-1026.

Groc, L., and Choquet, D. (2020). Linking glutamate receptor movements and synapse function. Science *368*.

Gruber, A.J., Schmidt, R., Gruber, A.R., Martin, G., Ghosh, S., Belmadani, M., Keller, W., and Zavolan, M. (2016). A comprehensive analysis of 3' end sequencing data sets reveals novel polyadenylation signals and the repressive role of heterogeneous ribonucleoprotein C on cleavage and polyadenylation. Genome Res *26*, 1145-1159.

Hara, Y., Balci-Hayta, B., Yoshida-Moriguchi, T., Kanagawa, M., Beltrán-Valero de Bernabé, D., Gündeşli, H., Willer, T., Satz, J.S., Crawford, R.W., Burden, S.J.*, et al.* (2011). A dystroglycan mutation associated with limb-girdle muscular dystrophy. N Engl J Med *364*, 939-946.

Hassan, B.A., and Hiesinger, P.R. (2015). Beyond Molecular Codes: Simple Rules to Wire Complex Brains. Cell *163*, 285-291.

Hata, Y., Butz, S., and Sudhof, T.C. (1996). CASK: a novel dlg/PSD95 homolog with an N-terminal calmodulin-dependent protein kinase domain identified by interaction with neurexins. J Neurosci *16*, 2488-2494.

Haueter, S., Kawasumi, M., Asner, I., Brykczynska, U., Cinelli, P., Moisyadi, S., Bürki, K., Peters, A.H., and Pelczar, P. (2010). Genetic vasectomy-overexpression of Prm1-EGFP fusion protein in elongating spermatids causes dominant male sterility in mice. Genesis *48*, 151-160.

He, F., and Jacobson, A. (2015). Nonsense-Mediated mRNA Decay: Degradation of Defective Transcripts Is Only Part of the Story. Annual review of genetics *49*, 339-366.

Helma, J., Cardoso, M.C., Muyldermans, S., and Leonhardt, H. (2015). Nanobodies and recombinant binders in cell biology. J Cell Biol *209*, 633-644.

Herrmann, C.J., Schmidt, R., Kanitz, A., Artimo, P., Gruber, A.J., and Zavolan, M. (2020). PolyASite 2.0: a consolidated atlas of polyadenylation sites from 3' end sequencing. Nucleic Acids Res *48*, D174-D179.

Hobert, O. (2016). Terminal Selectors of Neuronal Identity. Curr Top Dev Biol *116*, 455-475.

Hofer, S.B., Mrsic-Flogel, T.D., Bonhoeffer, T., and Hubener, M. (2009). Experience leaves a lasting structural trace in cortical circuits. Nature *457*, 313-317.

Hogg, J.R., and Goff, S.P. (2010). Upf1 senses 3'UTR length to potentiate mRNA decay. Cell *143*, 379-389.

Holt, C.E., Martin, K.C., and Schuman, E.M. (2019). Local translation in neurons: visualization and function. Nat Struct Mol Biol *26*, 557-566.

Holt, C.E., and Schuman, E.M. (2013). The central dogma decentralized: new perspectives on RNA function and local translation in neurons. Neuron *80*, 648-657.

Honig, B., and Shapiro, L. (2020). Adhesion Protein Structure, Molecular Affinities, and Principles of Cell-Cell Recognition. Cell *181*, 520-535.

Hoque, M., Ji, Z., Zheng, D., Luo, W., Li, W., You, B., Park, J.Y., Yehia, G., and Tian, B. (2013). Analysis of alternative cleavage and polyadenylation by 3' region extraction and deep sequencing. Nat Methods *10*, 133-139.

Houseley, J., LaCava, J., and Tollervey, D. (2006). RNA-quality control by the exosome. Nat Rev Mol Cell Biol *7*, 529-539.

Hruska, M., Henderson, N., Le Marchand, S.J., Jafri, H., and Dalva, M.B. (2018). Synaptic nanomodules underlie the organization and plasticity of spine synapses. Nature neuroscience *21*, 671-682.

Hrvatin, S., Hochbaum, D.R., Nagy, M.A., Cicconet, M., Robertson, K., Cheadle, L., Zilionis, R., Ratner, A., Borges-Monroy, R., Klein, A.M*., et al.* (2018). Single-cell analysis of experience-dependent transcriptomic states in the mouse visual cortex. Nature neuroscience *21*, 120-129.

Ichtchenko, K., Hata, Y., Nguyen, T., Ullrich, B., Missler, M., Moomaw, C., and Südhof, T.C. (1995). Neuroligin 1: a splice site-specific ligand for beta-neurexins. Cell *81*, 435-443.

Iijima, T., Iijima, Y., Witte, H., and Scheiffele, P. (2014). Neuronal cell type-specific alternative splicing is regulated by the KH domain protein SLM1. J Cell Biol *204*, 331-342.

Iijima, Y., Tanaka, M., Suzuki, S., Hauser, D., Tanaka, M., Okada, C., Ito, M., Ayukawa, N., Sato, Y., Ohtsuka, M.*, et al.* (2019). SAM68-Specific Splicing Is Required for Proper Selection of Alternative 3' UTR Isoforms in the Nervous System. iScience *22*, 318-335.

Jereb, S., Hwang, H.W., Van Otterloo, E., Govek, E.E., Fak, J.J., Yuan, Y., Hatten, M.E., and Darnell, R.B. (2018). Differential 3' Processing of Specific Transcripts Expands Regulatory and Protein Diversity Across Neuronal Cell Types. Elife *7*.

Ji, Z., Lee, J.Y., Pan, Z., Jiang, B., and Tian, B. (2009). Progressive lengthening of 3' untranslated regions of mRNAs by alternative polyadenylation during mouse embryonic development. Proc Natl Acad Sci U S A *106*, 7028-7033.

Kawahara, H., Imai, T., Imataka, H., Tsujimoto, M., Matsumoto, K., and Okano, H. (2008). Neural RNA-binding protein Musashi1 inhibits translation initiation by competing with eIF4G for PABP. J Cell Biol *181*, 639-653.

Kepecs, A., and Fishell, G. (2014). Interneuron cell types are fit to function. Nature *505*, 318-326.

Klausberger, T., and Somogyi, P. (2008). Neuronal diversity and temporal dynamics: the unity of hippocampal circuit operations. Science *321*, 53-57.

Kleiman, R., Banker, G., and Steward, O. (1990). Differential subcellular localization of particular mRNAs in hippocampal neurons in culture. Neuron *5*, 821-830.

Ko, J., Fuccillo, M.V., Malenka, R.C., and Sudhof, T.C. (2009). LRRTM2 functions as a neurexin ligand in promoting excitatory synapse formation. Neuron *64*, 791-798.

Kocabas, A., Duarte, T., Kumar, S., and Hynes, M.A. (2015). Widespread Differential Expression of Coding Region and 3' UTR Sequences in Neurons and Other Tissues. Neuron *88*, 1149-1156.

Kwon, H.B., and Sabatini, B.L. (2011). Glutamate induces de novo growth of functional spines in developing cortex. Nature *474*, 100-104.

Le Hir, H., Izaurralde, E., Maquat, L.E., and Moore, M.J. (2000). The spliceosome deposits multiple proteins 20-24 nucleotides upstream of mRNA exon-exon junctions. The EMBO journal *19*, 6860-6869.

Lee, Y., and Rio, D.C. (2015). Mechanisms and Regulation of Alternative Pre-mRNA Splicing. Annu Rev Biochem *84*, 291-323.

Leonoudakis, D., Conti, L.R., Radeke, C.M., McGuire, L.M., and Vandenberg, C.A. (2004). A multiprotein trafficking complex composed of SAP97, CASK, Veli, and Mint1 is associated with inward rectifier Kir2 potassium channels. J Biol Chem *279*, 19051-19063.

Licatalosi, D.D., and Darnell, R.B. (2010). RNA processing and its regulation: global insights into biological networks. Nat Rev Genet *11*, 75-87.

Lingwood, D., and Simons, K. (2010). Lipid rafts as a membrane-organizing principle. Science *327*, 46-50.

Liu, Y., Beyer, A., and Aebersold, R. (2016). On the Dependency of Cellular Protein Levels on mRNA Abundance. Cell *165*, 535-550.

Lu, W., Bushong, E.A., Shih, T.P., Ellisman, M.H., and Nicoll, R.A. (2013). The cell-autonomous role of excitatory synaptic transmission in the regulation of neuronal structure and function. Neuron *78*, 433-439.

Lukacsovich, D., Winterer, J., Que, L., Luo, W., Lukacsovich, T., and Földy, C. (2019). Single-Cell RNA-Seq Reveals Developmental Origins and Ontogenetic Stability of Neurexin Alternative Splicing Profiles. Cell Rep *27*, 3752-3759.e3754.

Malka, Y., Steiman-Shimony, A., Rosenthal, E., Argaman, L., Cohen-Daniel, L., Arbib, E., Margalit, H., Kaplan, T., and Berger, M. (2017). Post-transcriptional 3´-UTR cleavage of mRNA transcripts generates thousands of stable uncapped autonomous RNA fragments. Nat Commun *8*, 2029.

Mandel, C.R., Bai, Y., and Tong, L. (2008). Protein factors in pre-mRNA 3′-end processing. Cellular and Molecular Life Sciences *65*, 1099-1122.

Matsuda, K., Budisantoso, T., Mitakidis, N., Sugaya, Y., Miura, E., Kakegawa, W., Yamasaki, M., Konno, K., Uchigashima, M., Abe, M.*, et al.* (2016). Transsynaptic Modulation of Kainate Receptor Functions by C1q-like Proteins. Neuron *90*, 752-767.

Matsuda, K., and Yuzaki, M. (2011). Cbln family proteins promote synapse formation by regulating distinct neurexin signaling pathways in various brain regions. Eur J Neurosci *33*, 1447-1461.

Maximov, A., Sudhof, T.C., and Bezprozvanny, I. (1999). Association of neuronal calcium channels with modular adaptor proteins. J Biol Chem *274*, 24453-24456.

Mayer, C., Hafemeister, C., Bandler, R.C., Machold, R., Batista Brito, R., Jaglin, X., Allaway, K., Butler, A., Fishell, G., and Satija, R. (2018). Developmental diversification of cortical inhibitory interneurons. Nature *555*, 457-462.

Merkin, J., Russell, C., Chen, P., and Burge, C.B. (2012). Evolutionary dynamics of gene and isoform regulation in Mammalian tissues. Science *338*, 1593-1599.

Meyer, H.S., Schwarz, D., Wimmer, V.C., Schmitt, A.C., Kerr, J.N., Sakmann, B., and Helmstaedter, M. (2011). Inhibitory interneurons in a cortical column form hot zones of inhibition in layers 2 and 5A. Proc Natl Acad Sci U S A *108*, 16807-16812.

Mi, D., Li, Z., Lim, L., Li, M., Moissidis, M., Yang, Y., Gao, T., Hu, T.X., Pratt, T., Price, D.J.*, et al.* (2018). Early emergence of cortical interneuron diversity in the mouse embryo. Science *360*, 81-85.

Miller, M.T., Mileni, M., Comoletti, D., Stevens, R.C., Harel, M., and Taylor, P. (2011). The crystal structure of the α-neurexin-1 extracellular region reveals a hinge point for mediating synaptic adhesion and function. Structure *19*, 767-778.

Missler, M., Hammer, R.E., and Südhof, T.C. (1998). Neurexophilin binding to alpha-neurexins. A single LNS domain functions as an independently folding ligand-binding unit. J Biol Chem *273*, 34716-34723.

Missler, M., Zhang, W., Rohlmann, A., Kattenstroth, G., Hammer, R.E., Gottmann, K., and Sudhof, T.C. (2003). Alpha-neurexins couple Ca2+ channels to synaptic vesicle exocytosis. Nature *423*, 939-948.

Miura, P., Sanfilippo, P., Shenker, S., and Lai, E.C. (2014). Alternative polyadenylation in the nervous system: To what lengths will 3′ UTR extensions take us? BioEssays *36*, 766-777.

Miura, P., Shenker, S., Andreu-Agullo, C., Westholm, J.O., and Lai, E.C. (2013). Widespread and extensive lengthening of 3' UTRs in the mammalian brain. Genome Res *23*, 812-825.

Motta, A., Berning, M., Boergens, K.M., Staffler, B., Beining, M., Loomba, S., Hennig, P., Wissler, H., and Helmstaedter, M. (2019). Dense connectomic reconstruction in layer 4 of the somatosensory cortex. Science *366*.

Nguyen, T.M., Schreiner, D., Xiao, L., Traunmuller, L., Bornmann, C., and Scheiffele, P. (2016). An alternative splicing switch shapes neurexin repertoires in principal neurons versus interneurons in the mouse hippocampus. Elife *5*.

Pan, Q., Shai, O., Lee, L.J., Frey, B.J., and Blencowe, B.J. (2008). Deep surveying of alternative splicing complexity in the human transcriptome by high-throughput sequencing. Nat Genet *40*, 1413-1415.

Parikshak, N.N., Swarup, V., Belgard, T.G., Irimia, M., Ramaswami, G., Gandal, M.J., Hartl, C., Leppa, V., Ubieta, L.T., Huang, J.*, et al.* (2016). Genome-wide changes in lncRNA, splicing, and regional gene expression patterns in autism. Nature *540*, 423-427.

Paul, A., Crow, M., Raudales, R., He, M., Gillis, J., and Huang, Z.J. (2017). Transcriptional Architecture of Synaptic Communication Delineates GABAergic Neuron Identity. Cell *171*, 522-539 e520.

Petrenko, A.G., Ullrich, B., Missler, M., Krasnoperov, V., Rosahl, T.W., and Südhof, T.C. (1996). Structure and evolution of neurexophilin. J Neurosci *16*, 4360-4369.

Poon, M.M., Choi, S.H., Jamieson, C.A., Geschwind, D.H., and Martin, K.C. (2006). Identification of process-localized mRNAs from cultured rodent hippocampal neurons. J Neurosci *26*, 13390-13399.

Quesnel-Vallieres, M., Dargaei, Z., Irimia, M., Gonatopoulos-Pournatzis, T., Ip, J.Y., Wu, M., Sterne-Weiler, T., Nakagawa, S., Woodin, M.A., Blencowe, B.J.*, et al.* (2016). Misregulation of an Activity-Dependent Splicing Network as a Common Mechanism Underlying Autism Spectrum Disorders. Mol Cell *64*, 1023-1034.

Ray, T.A., Cochran, K., Kozlowski, C., Wang, J., Alexander, G., Cady, M.A., Spencer, W.J., Ruzycki, P.A., Clark, B.S., Laeremans, A.*, et al.* (2020). Comprehensive identification of mRNA isoforms reveals the diversity of neural cell-surface molecules with roles in retinal development and disease. Nat Commun *11*, 3328.

Reissner, C., Runkel, F., and Missler, M. (2013). Neurexins. Genome Biol *14*, 213.

Reissner, C., Stahn, J., Breuer, D., Klose, M., Pohlentz, G., Mormann, M., and Missler, M. (2014). Dystroglycan binding to α-neurexin competes with neurexophilin-1 and neuroligin in the brain. J Biol Chem *289*, 27585-27603.

Roppongi, R.T., Dhume, S.H., Padmanabhan, N., Silwal, P., Zahra, N., Karimi, B., Bomkamp, C., Patil, C.S., Champagne-Jorgensen, K., Twilley, R.E.*, et al.* (2020). LRRTMs Organize Synapses through Differential Engagement of Neurexin and PTPσ. Neuron *106*, 108-125.e112.

Saito, Y., Yuan, Y., Zucker-Scharff, I., Fak, J.J., Jereb, S., Tajima, Y., Licatalosi, D.D., and Darnell, R.B. (2019). Differential NOVA2-Mediated Splicing in Excitatory and Inhibitory Neurons Regulates Cortical Development and Cerebellar Function. Neuron *101*, 707-720.e705.

Sando, R., Bushong, E., Zhu, Y., Huang, M., Considine, C., Phan, S., Ju, S., Uytiepo, M., Ellisman, M., and Maximov, A. (2017). Assembly of Excitatory Synapses in the Absence of Glutamatergic Neurotransmission. Neuron *94*, 312-321 e313.

Sanes, J.R., and Zipursky, S.L. (2020). Synaptic Specificity, Recognition Molecules, and Assembly of Neural Circuits. Cell *181*, 1434-1435.

Sanz, E., Yang, L., Su, T., Morris, D.R., McKnight, G.S., and Amieux, P.S. (2009). Cell-type-specific isolation of ribosome-associated mRNA from complex tissues. Proc Natl Acad Sci U S A *106*, 13939-13944.

Saura, C.A., Servián-Morilla, E., and Scholl, F.G. (2011). Presenilin/γ-secretase regulates neurexin processing at synapses. PLoS One *6*, e19430.

Scharfman, H.E. (2016). The enigmatic mossy cell of the dentate gyrus. Nature reviews Neuroscience *17*, 562-575.

Scheiffele, P., Fan, J., Choih, J., Fetter, R., and Serafini, T. (2000). Neuroligin expressed in nonneuronal cells triggers presynaptic development in contacting axons. Cell *101*, 657-669.

Schmucker, D., Clemens, J.C., Shu, H., Worby, C.A., Xiao, J., Muda, M., Dixon, J.E., and Zipursky, S.L. (2000). Drosophila Dscam Is an Axon Guidance Receptor Exhibiting Extraordinary Molecular Diversity. Cell *101*, 671-684.

Schreiner, D., Nguyen, T.M., Russo, G., Heber, S., Patrignani, A., Ahrne, E., and Scheiffele, P. (2014). Targeted combinatorial alternative splicing generates brain region-specific repertoires of neurexins. Neuron *84*, 386-398.

Schreiner, D., Simicevic, J., Ahrne, E., Schmidt, A., and Scheiffele, P. (2015). Quantitative isoform-profiling of highly diversified recognition molecules. Elife *4*, e07794.

Schroeder, A., Vanderlinden, J., Vints, K., Ribeiro, L.F., Vennekens, K.M., Gounko, N.V., Wierda, K.D., and de Wit, J. (2018). A Modular Organization of LRR Protein-Mediated Synaptic Adhesion Defines Synapse Identity. Neuron *99*, 329-344.e327.

Servián-Morilla, E., Robles-Lanuza, E., Sánchez-Hidalgo, A.C., Camacho-Garcia, R.J., Paez-Gomez, J.A., Mavillard, F., Saura, C.A., Martinez-Mir, A., and Scholl, F.G. (2018). Proteolytic Processing of Neurexins by Presenilins Sustains Synaptic Vesicle Release. J Neurosci *38*, 901-917.

Sheckler, L.R., Henry, L., Sugita, S., Südhof, T.C., and Rudenko, G. (2006). Crystal structure of the second LNS/LG domain from neurexin 1alpha: Ca2+ binding and the effects of alternative splicing. J Biol Chem *281*, 22896-22905.

Shen, K., and Scheiffele, P. (2010). Genetics and cell biology of building specific synaptic connectivity. Annu Rev Neurosci *33*, 473-507.

Sheth, U., and Parker, R. (2003). Decapping and decay of messenger RNA occur in cytoplasmic processing bodies. Science *300*, 805-808.

Shigeoka, T., Jung, H., Jung, J., Turner-Bridger, B., Ohk, J., Lin, Julie Q., Amieux, Paul S., and Holt, Christine E. (2016). Dynamic Axonal Translation in Developing and Mature Visual Circuits. Cell *166*, 181-192.

Siddiqui, T.J., Pancaroglu, R., Kang, Y., Rooyakkers, A., and Craig, A.M. (2010). LRRTMs and neuroligins bind neurexins with a differential code to cooperate in glutamate synapse development. J Neurosci *30*, 7495-7506.

Sigler, A., Oh, W.C., Imig, C., Altas, B., Kawabe, H., Cooper, B.H., Kwon, H.B., Rhee, J.S., and Brose, N. (2017). Formation and Maintenance of Functional Spines in the Absence of Presynaptic Glutamate Release. Neuron *94*, 304-311 e304.

Smith, C.W., and Valcarcel, J. (2000). Alternative pre-mRNA splicing: the logic of combinatorial control. Trends Biochem Sci *25*, 381-388.

Streit, S., Michalski, C.W., Erkan, M., Kleeff, J., and Friess, H. (2008). Northern blot analysis for detection and quantification of RNA in pancreatic cancer cells and tissues. Nat Protocols *4*, 37-43.

Sudhof, T.C. (2008). Neuroligins and neurexins link synaptic function to cognitive disease. Nature *455*, 903-911.

Sudhof, T.C. (2017). Synaptic Neurexin Complexes: A Molecular Code for the Logic of Neural Circuits. Cell *171*, 745-769.

Sudhof, T.C. (2018). Towards an Understanding of Synapse Formation. Neuron *100*, 276-293.

Sugita, S., Saito, F., Tang, J., Satz, J., Campbell, K., and Sudhof, T.C. (2001). A stoichiometric complex of neurexins and dystroglycan in brain. J Cell Biol *154*, 435-445.

Tabuchi, K., and Sudhof, T.C. (2002). Structure and evolution of neurexin genes: insight into the mechanism of alternative splicing. Genomics *79*, 849-859.

Taliaferro, J.M., Vidaki, M., Oliveira, R., Olson, S., Zhan, L., Saxena, T., Wang, E.T., Graveley, B.R., Gertler, F.B., Swanson, M.S.*, et al.* (2016). Distal Alternative Last Exons Localize mRNAs to Neural Projections. Mol Cell *61*, 821-833.

Taniguchi, H., Gollan, L., Scholl, F.G., Mahadomrongkul, V., Dobler, E., Limthong, N., Peck, M., Aoki, C., and Scheiffele, P. (2007). Silencing of neuroligin function by postsynaptic neurexins. J Neurosci *27*, 2815-2824.

Tasic, B., Menon, V., Nguyen, T.N., Kim, T.K., Jarsky, T., Yao, Z., Levi, B., Gray, L.T., Sorensen, S.A., Dolbeare, T.*, et al.* (2016). Adult mouse cortical cell taxonomy revealed by single cell transcriptomics. Nature neuroscience *19*, 335-346.

Tasic, B., Yao, Z., Graybuck, L.T., Smith, K.A., Nguyen, T.N., Bertagnolli, D., Goldy, J., Garren, E., Economo, M.N., Viswanathan, S.*, et al.* (2018). Shared and distinct transcriptomic cell types across neocortical areas. Nature *563*, 72-78.

Tian, B., and Manley, J.L. (2017). Alternative polyadenylation of mRNA precursors. Nat Rev Mol Cell Biol *18*, 18-30.

Trachtenberg, J.T., Chen, B.E., Knott, G.W., Feng, G., Sanes, J.R., Welker, E., and Svoboda, K. (2002). Long-term in vivo imaging of experience-dependent synaptic plasticity in adult cortex. Nature *420*, 788-794.

Traunmuller, L., Bornmann, C., and Scheiffele, P. (2014). Alternative splicing coupled nonsense-mediated decay generates neuronal cell type-specific expression of SLM proteins. J Neurosci *34*, 16755-16761.

Traunmuller, L., Gomez, A.M., Nguyen, T.M., and Scheiffele, P. (2016). Control of neuronal synapse specification by a highly dedicated alternative splicing program. Science *352*, 982-986.

Treutlein, B., Gokce, O., Quake, S.R., and Sudhof, T.C. (2014). Cartography of neurexin alternative splicing mapped by single-molecule long-read mRNA sequencing. Proc Natl Acad Sci U S A *111*, E1291-1299.

Tushev, G., Glock, C., Heumuller, M., Biever, A., Jovanovic, M., and Schuman, E.M. (2018). Alternative 3' UTRs Modify the Localization, Regulatory Potential, Stability, and Plasticity of mRNAs in Neuronal Compartments. Neuron *98*, 495-511 e496.

Uemura, T., Lee, S.J., Yasumura, M., Takeuchi, T., Yoshida, T., Ra, M., Taguchi, R., Sakimura, K., and Mishina, M. (2010). Trans-synaptic interaction of GluRdelta2 and Neurexin through Cbln1 mediates synapse formation in the cerebellum. Cell *141*, 1068-1079.

Ule, J., and Darnell, R.B. (2006). RNA binding proteins and the regulation of neuronal synaptic plasticity. Curr Opin Neurobiol *16*, 102-110.

Ule, J., Ule, A., Spencer, J., Williams, A., Hu, J.S., Cline, M., Wang, H., Clark, T., Fraser, C., Ruggiu, M.*, et al.* (2005). Nova regulates brain-specific splicing to shape the synapse. Nat Genet *37*, 844-852.

Ushkaryov, Y.A., Petrenko, A.G., Geppert, M., and Sudhof, T.C. (1992). Neurexins: synaptic cell surface proteins related to the alpha-latrotoxin receptor and laminin. Science *257*, 50-56.

Ushkaryov, Y.A., and Sudhof, T.C. (1993). Neurexin III alpha: extensive alternative splicing generates membrane-bound and soluble forms. Proc Natl Acad Sci U S A *90*, 6410-6414.

Verhage, M., Maia, A.S., Plomp, J.J., Brussaard, A.B., Heeroma, J.H., Vermeer, H., Toonen, R.F., Hammer, R.E., van den Berg, T.K., Missler, M.*, et al.* (2000). Synaptic assembly of the brain in the absence of neurotransmitter secretion. Science *287*, 864-869.

Vernet, C., and Artzt, K. (1997). STAR, a gene family involved in signal transduction and activation of RNA. Trends Genet *13*, 479-484.

Vogel, C., and Marcotte, E.M. (2012). Insights into the regulation of protein abundance from proteomic and transcriptomic analyses. Nat Rev Genet *13*, 227-232.

Vuong, C.K., Black, D.L., and Zheng, S. (2016). The neurogenetics of alternative splicing. Nature reviews Neuroscience *17*, 265-281.

Wamsley, B., Jaglin, X.H., Favuzzi, E., Quattrocolo, G., Nigro, M.J., Yusuf, N., Khodadadi-Jamayran, A., Rudy, B., and Fishell, G. (2018). Rbfox1 Mediates Cell-type-Specific Splicing in Cortical Interneurons. Neuron *100*, 846-859 e847.

Wang, E.T., Sandberg, R., Luo, S., Khrebtukova, I., Zhang, L., Mayr, C., Kingsmore, S.F., Schroth, G.P., and Burge, C.B. (2008). Alternative isoform regulation in human tissue transcriptomes. Nature *456*, 470-476.

Wang, L., Dowell, R.D., and Yi, R. (2013). Genome-wide maps of polyadenylation reveal dynamic mRNA 3'-end formation in mammalian cell lineages. RNA *19*, 413-425.

Wang, Y., Yang, F., Gritsenko, M.A., Wang, Y.,Clauss, T., Liu, T., Shen, Y., Monroe, M.E., Lopez-Ferrer, D., Reno, T., Moore, R.J., Klemke, R.L., Camp, D.G., 2nd, and Smith, R.D. (2011). Reversed-phase chromatography with multiple fraction concatenation strategy for proteome profiling of human MCF10A cells. Proteomics *11*(10), 2019–2026.

Wilson, S.C., White, K.I., Zhou, Q., Pfuetzner, R.A., Choi, U.B., Südhof, T.C., and Brunger, A.T. (2019). Structures of neurexophilin-neurexin complexes reveal a regulatory mechanism of alternative splicing. The EMBO journal *38*, e101603.

Yan, Q., Weyn-Vanhentenryck, S.M., Wu, J., Sloan, S.A., Zhang, Y., Chen, K., Wu, J.Q., Barres, B.A., and Zhang, C. (2015). Systematic discovery of regulated and conserved alternative exons in the mammalian brain reveals NMD modulating chromatin regulators. Proc Natl Acad Sci U S A *112*, 3445-3450.

Zeng, H., and Sanes, J.R. (2017). Neuronal cell-type classification: challenges, opportunities and the path forward. Nature reviews Neuroscience *18*, 530-546.

Zhang, C., Atasoy, D., Arac, D., Yang, X., Fucillo, M.V., Robison, A.J., Ko, J., Brunger, A.T., and Sudhof, T.C. (2010). Neurexins physically and functionally interact with GABA(A) receptors. Neuron *66*, 403-416.

Zhang, H., Lee, J.Y., and Tian, B. (2005). Biased alternative polyadenylation in human tissues. Genome Biology *6*, 1-13.

Zhang, P., Lu, H., Peixoto, R.T., Pines, M.K., Ge, Y., Oku, S., Siddiqui, T.J., Xie, Y., Wu, W., Archer-Hartmann, S.*, et al.* (2018). Heparan Sulfate Organizes Neuronal Synapses through Neurexin Partnerships. Cell *174*, 1450-1464.e1423.

Zhang, Z., Lotti, F., Dittmar, K., Younis, I., Wan, L., Kasim, M., and Dreyfuss, G. (2008). SMN deficiency causes tissue-specific perturbations in the repertoire of snRNAs and widespread defects in splicing. Cell *133*, 585-600.

Zhong, J., Zhang, T., and Bloch, L.M. (2006). Dendritic mRNAs encode diversified functionalities in hippocampal pyramidal neurons. BMC Neurosci *7*, 17.

Acknowledgements

I would first like to express my gratitude to Peter Scheiffele for giving me the chance to work on this project, but even more for constantly helping me improving my skills and in always pushing me to achieve more. The constant support and all the meetings discussing my project were a tremendous help in asking the right questions and to get a head start where to find answers. Thank you for guiding the lab in working together and help each other in striving for the best results.

I am thankful to my committee members, Markus Rüegg and Helge Grosshans, for their feedback on my thesis project through the years and for their guidance in how to proceed within my project.

I am grateful to all members of the Scheiffele Lab, current and past, for their support. You all helped me in long discussions, experimental support and furthermore in generally making the time in- and also outside of the lab enjoyable. I would like to say thanks especially to Lisa and Elisabetta for all the discussions and support and even more for your friendship. I'd like to further say thanks to Dietmar, not only did you introduce me to my project and helped getting started, but you were a tremendous help in tying the story together.

A big thanks goes to Alexander Schmidt, without your help and always welcoming me in the facility finishing the project could not have been achieved in this way.

I am really lucky to have an amazing family and friends, without you this work would not have been possible. Thanks to my parents, who always supported me in everything I do and always listened to me talking about my passion for biology, you helped me in keeping this excitement from the moment I choose this path. I want to say thanks also to my friends, who always cheered for me and to my oldest scientific colleague, whose curiosity about the scientific world inspired me since I was little.

Last but not least, I want to say thanks to Fabienne, for always being there for me, for lifting me up when my energy was low and for letting me believe in myself. Thank you so much for your continuous support, you help me more than you can imagine.